Disease modelling of diabetic retinopathy using hiPSC-derived endothelial cells and pericytes in 3D cell culture chip

Dissertation
zur Erlangung des Grades eines
Doktors der Naturwissenschaften
der Mathematisch-Naturwissenschaftlichen Fakultät und
der Medizinischen Fakultät

der Eberhard-Karls-Universität Tübingen

vorgelegt von

Selin Pars
aus Izmir, Türkei

2023

Tag der mündlichen Prüfung: 24. Mai 2023

Dekan der Math.-Nat. Fakultät: Prof. Dr. Thilo Stehle
Dekan der Medizinischen Fakultät: Prof. Dr. Bernd Pichler

1. Berichterstatter: Prof. Dr. Stefan Liebau

2. Berichterstatter: Prof. Dr. Peter Loskill

Prüfungskommission:

Prof. Dr. Stefan Liebau

Prof. Dr. Ulrich Schraermeyer

Prof. Dr. Peter Loskill

PD Dr. Andrea Wizenmann

Erklärung / Declaration:

Ich erkläre, dass ich die zur Promotion eingereichte Arbeit mit dem Titel:

„ Disease modelling of diabetic retinopathy using hiPSC-derived endothelial cells and pericytes in 3D cell culture chip “

selbständig verfasst, nur die angegebenen Quellen und Hilfsmittel benutzt und wörtlich oder inhaltlich übernommene Stellen als solche gekennzeichnet habe. Ich versichere an Eides statt, dass diese Angaben wahr sind und dass ich nichts verschwiegen habe. Mir ist bekannt, dass die falsche Abgabe einer Versicherung an Eides statt mit Freiheitsstrafe bis zu drei Jahren oder mit Geldstrafe bestraft wird.

*I hereby declare that I have produced the work entitled "**Disease modelling of diabetic retinopathy using hiPSC-derived endothelial cells and pericytes in 3D cell culture chip**", submitted for the award of a doctorate, on my own (without external help), have used only the sources and aids indicated and have marked passages included from other works, whether verbatim or in content, as such. I swear upon oath that these statements are true and that I have not concealed anything. I am aware that making a false declaration under oath is punishable by a term of imprisonment of up to three years or by a fine.*

Australien, den ....

Datum / Date Unterschrift /Signature

Acknowledgements

I would like to express my gratitude to the Principal Investigator of our laboratory, Prof. Dr. Stefan Liebau for accepting me in his lab, and made it possible for me to carry out my project. Dr. Natalia Pashkovskaia has been guiding me through my project as my research supervisor, and her advise and constructive critism added great value to my scientific thinking and planning. Without her help and enthusiasm, this work would have not been possible. I am also grateful for the help of Dr. Kevin Acherberger, who shared his knowledge with me whenever I needed help.

My advisory board members Prof. Dr. Ulrich Schraermeyer and Dr. Andrea Wizenmann, along with Prof. Liebau supported me during the annual Advisory Board Meetings and I am grateful for that.

Additionally, I would like to express my appreciation to all former and current members of Liebau Lab, with whom I have had great scientific discussions and a great team spirit.

Table of Contents

Erklärung / Declaration: *3*

Acknowledgements *4*

Table of Contents *5*

Abbreviations *8*

List of Figures *12*

List of Tables *14*

Summary *15*

Zusammenfassung *18*

1. Introduction *21*

1.1. Neural Retina – development and function **21**

1.2. Retinal blood vessels **26**

1.3. Retinal barriers **30**

1.3.1. Outer blood-retinal barrier (oBRB) 31

1.3.2. Inner blood-retinal barrier (iBRB) 32

1.4. Diabetic retinopathy (DR) **38**

1.4.1. Disease etiology and clinical manifestations 38

1.4.2. Pathophysiology of DR 39

1.4.3. Current treatments 41

1.5. Human induced pluripotent stem cell (hiPSC) generation and disease modelling **42**

1.6. Microfluidic chip technology **43**

1.6.1. Blood vessel generation in 3D chips 43

1.6.2. Disease modelling of diabetes in 3D chips 44

1.7. Aim of the thesis **45**

2. Material and Methods *47*

2.1. Materials **47**

2.1.1. Biological materials 47

2.1.2. Plasticware and tools 47

2.1.3. Cell culture equipment and devices 48

2.1.4. Cell culture media 49

2.1.5. Coatings 50

2.1.6. Other chemicals 50

2.1.7. Primary antibodies 52

2.1.8. Secondary antibodies 53

2.1.9. Coupled antibodies 54

2.1.10. Kits and assays 55

2.1.11. Softwares 55

2.2. Methods **56**

2.2.1. hiPSC culture 56

2.2.2. Endothelial cells and mesodermal pericyte differentiation 57

2.2.3. Neural crest stem cell differentiation 59
2.2.4. Neural crest stem cell-derived (ectodermal) pericyte differentiation 60
2.2.5. Astrocyte differentiation 61
2.2.6. Müller glia isolation from retinal organoids 62
2.2.7. 3D cell culture chip loading 63
2.2.8. Immunocytochemistry assay 64
2.2.9. Microscopy 65
2.2.10. Tube formation assay 65
2.2.11. Flow cytometry 65
2.2.12. Western blot 66
2.2.13. Permeability assay with dextran 66
2.2.14. TUNEL staining of endothelial cells 67
2.2.16. Blood vessel diameter calculations 67
2.2.17. Fluorescence activated cell sorting (FACS) protocol 68
2.2.18. Statistical analysis 68

3. Results 69

3.1. Generation of retinal blood vessel components from hiPSCs 69
3.1.1. Generation of endothelial cells (ECs) and mesoderm-derived pericytes (mPCs) 69
3.1.2. Characterization of endothelial cells and mesodermal pericytes 74
3.1.3. Functionality of endothelial cells 77
3.1.4. Generation of neural crest stem cell-derived pericytes 79

3.2. Blood vessel formation in 3D microfluidic chip using hiPSC-derived endothelial cells and pericytes 82
3.2.1. Role of NC-derived pericytes in the microvascular network 83
3.2.2. Formation of a microvascular network 87

3.3. Induction of diabetes in 3D microfluidic chip on blood vessels 91
3.3.1. Reactive oxygen species (ROS) production in hyperglycemic conditions 91
3.3.2. MGO toxicity test via TUNEL assay 93

3.4. Assessment of blood vessels on chip 95
3.4.1. Quantification of blood vessel diameter and shape 95
3.4.2. Effect of TGF-β pathway on blood vessel and shape 97

3.5. Development of the disease model 99
3.5.1. Müller glia extraction and addition to the blood vessel chip 99
3.5.2. Generation of iPSC-derived astrocytes 102
3.5.3. FACS of chips for RNA sequencing plan 105

4. Discussion 108

4.1. Recapitulation of iBRB using hiPSC-derived endothelial cells and pericytes 108
4.1.1. hiPSC-derived endothelial cells 108
4.1.2. Neural-crest stem cell-derived pericytes 111
4.1.3. Müller glia and astrocytes – additional components of iBRB 112

4.2. Self-assembly of blood vessels in 3D chip shows retinal capillary-like properties 114
4.2.1. Microvascular network formation in chip resembles physiological blood vessel formation 115
4.2.2. Pericytes are crucial for vessel coverage and maturing endothelial cells 116

4.3. Induction of diabetes in iBRB *in vitro* 118
4.3.1. Hyperglycemia and MGO treatment on blood vessels 118
4.3.2. ROS production and toxicity assays 119

4.4. Effect of diabetes on blood vessel diameter and shape in diabetic vs. control blood vessels 120
4.4.1. Increased blood vessel diameter in diabetic blood vessels 120
4.4.2. Pivotal role of TGF-β pathway in blood vessels 120

4.5. Future developments of the disease model 121
4.5.1. Comparative gene analysis of diabetic vs. control blood vessels 121
4.5.2. 3D chip culture improvements & drug testing 122
5. References 123
Statement of contributions 143

Abbreviations

%: per cent
2D: 2-dimensional
3D: 3-dimensional
AGE: advanced glycation end products
ALK1: Activin A receptor type II-like 1
ALK5: Transforming growth factor-beta type 1 receptor
Ang1: angiopoietin-1
Ang2: angiopoietin-2
BBB: blood-brain barrier
BDNF: brain-derived neurotrophic factor
bFGF: basic fibroblast growth factor, FGF-2
BM: basement membrane
BMP-4: bone morphogenic protein 4
c-Myc: Myc Proto-Oncogene Protein
Ca^{++}: calcium
cAMP: cyclic adenosine monophosphate
CNS: central nervous system
Col. IV: collagen IV
CRALBP: Cellular retinaldehyde–binding protein
CXCR4: C-X-C Motif Chemokine Receptor 4
DAPI: 4',6-diamidino-2-phenylindole
DCFDA: 2',7'-dichlorofluorescin diacetate
DCP: deep capillary plexus
dLGN: dorsal lateral geniculate nucleus
DMEM: Dulbecco's Modified Eagle Medium
DMSO: dimetylsulfoxide
DPBS: Dulbecco's Phosphate Buffered Saline
DR: diabetic retinopathy
E1: Human episomal iPSC line
EB: embryoid body
EC(s): endothelial cell(s)
ECM: extracellular matrix
EGF: epidermal growth factor
eNOS: endothelial nitric oxide synthase
Erg: ETS related gene
ESC(s): embryonic stem cells
FACS: Fluorescence-activated cell sorting
FAZ: foveal avascular zone
FBS: fetal bovine serum

FITC: fluorescein isothiocyanate
FOXO1: Forkhead box protein O1
Fzd-4: Frizzled-4
GABA: gamma-aminobutyric acid
GCL: ganglion cell layer
GDNF: glial cell line-derived neurotrophic factor
GFAP: glial fibrillary acidic protein
GLAST: Sodium-dependent glutamate/aspartate transporter 1
HBSS: Hanks' Balanced Salt Solution
HIF-1: hypoxia-inducible factor-1
hiPSC(s): human induced-pluripotent stem cell(s)
hPSC(s): human pluripotent stem cells
HUVEC(s): human umbilical vein endothelial cell(s)
iBRB: inner blood-retinal barrier
ICAM-1: Intercellular Adhesion Molecule 1
ICP: intermediate capillary plexus
IgG: immunoglobulin G
IL-1β: interleukin 1β
IL-6: interleukin 6
IMDM: Iscove's Modified Dulbecco's Medium
immunocytochemistry: ICC
INL=inner nuclear layer
IPL=inner plexiform layer
iPSC: induced-pluripotent stem cells
K^+: potasium
K3: Human keratinocyte-derived iPSC line 3
K5: Human keratinocyte-derived iPSC line 5
kDa: kilodalton
Kir4.1: ATP-Sensitive Inward Rectifier Potassium Channel 10
Kir6.1: ATP-Sensitive Inward Rectifier Potassium Channel 8
Klf4: Kruppel like factor 4
Lhx2: LIM Homeobox 2
LIF: leukemia inhibitory factor
MACS: magnetic-activated cell sorting
MAPK: mitogen-activated protein kinase
MGO: methylgloxal
MMP(s): matrix metalloprotease(s)
mPCs: mesoderm-derived pericytes
Msfd2a: Major Facilitator Superfamily Domain Containing 2A
mSin3a: mammalian Histone Deacetylase Complex Subunit Sin3a
MVEC(s): microvascular endothelial cell(s)

NC: neural crest
NCSC(s): Neural crest stem cell(s)
NDS: normal donkey serum
NFL=nerve fiber layer
NG2: neural/glial antigen 2
NGF: nerve growth factor
NHS: National Health Service
nm: nanometre
NOS: nitric oxide synthase
NPDR: non-proliferative diabetic retinopathy
NSAID(s): Non-steroidal anti-inflammatory drugs
NT-3: neurotrophin-3
NT-4: neurotrophin-4
NVU: neurovascular unit
oBRB: outer blood-retinal barrier
Oct3/4: Octamer-Binding Protein 4
OCTA: optical coherence tomography angiography
OLM: outer limiting membrane
ONL=outer nuclear layer
OPL: outer plexiform layer
Pax2: Paired Box 2
Pax6: Paired Box 6
PC(s): pericyte(s)
PDGFR-β: platelet-derived growth factor-β
PDGFR-α: platelet-derived growth factor-α
PDMS: Polydimethylsiloxane
PDR: proliferative diabetic retinopathy
PFA: paraformaldehyde
PI3K: phosphatidylinositol kinase 3
PLVAP: Plasmalemma vesicle protein 1
PRC(s): photoreceptor cell(s)
PTM(s): post-translational modification(s)
RAGE: receptor for advanced glycation end products
Rax: Retina and Anterior Neural Fold Homeobox
RO(s): retinal organoid(s)
ROCK: rho-associated protein kinase
ROI(s): region of interest(s)
ROP: retinopathy of prematurity
ROS: reactive oxygen species
RPC(s): retinal progenitor cell(s)
RPCP: radial peripapillary capillary plexus

RPE: retinal pigment epithelium
RT: room temperature
S100β: S100 calcium binding protein β
SD: standard deviation
Shh: Sonic Hedgehog
Six3: Sine Oculis Homeobox Homolog 3
Six6: SIX Homeobox 6
Slc16a1: Solute carrier family 16 member 1
SMA: smooth muscle actin
Sox10: SRY-Box Transcription Factor 10
Sox2: SRY-Box Transcription Factor 2
Sox9: SRY-Box Transcription Factor 9
SVP: superficial vascular plexus
Tbx3: T-Box Transcription Factor 3
TF(s): transcription factor(s)
TGF-β: Transforming Growth Factor-β
Tie2: angiopoietin-1 receptor
TII: Nuclear Receptor TLX
TJs: tight junctions
TNF-α: tumor necrosis factor-α
TUBB3: β-tubulin class III
VE-cadherin: vascular endothelial cadherin
VEFG-A: vascular endothelial growth factor a
VEGF: vascular endothelial growth factor
VEGFR2: vascular endothelial growth factor receptor 2
VSMC(s): vascular smooth muscle cell(s)
Vsx2: Visual System Homeobox 2
WG: gestational week
x g: times gravity
ZO-1: Zonula occludens protein 1
ZO-2: Zonula occludens protein 2
ZO-3: Zonula occludens protein 3
ZO: zonula occludens
μm: micrometre

List of Figures

FIGURE 1: DEVELOPMENT OF VERTEBRATE EYES. 22
FIGURE 2: NEURONAL LAYERS IN HUMAN RETINA. 24
FIGURE 3: FORMATION OF HUMAN RETINAL VASCULATURE. 27
FIGURE 4: ARTERIES OF THE HUMAN EYE. 28
FIGURE 5: VASCULAR PLEXUSES IN HUMAN RETINA. 29
FIGURE 6: BLOOD-RETINAL BARRIERS: INNER BLOOD-RETINAL BARRIER (IBRB) OF RETINAL CAPILLARIES AND OUTER BLOOD-RETINAL BARRIER (OBRB) BETWEEN RPE CELLS. 31
FIGURE 7: MICROVASCULAR CHANGES IN DIABETIC RETINOPATHY. 39

FIGURE 8: GENERATION OF ENDOTHELIAL CELLS FROM HIPSC - PROTOCOL OUTLINE. 71
FIGURE 9: SIMULTANEOUS DIFFERENTIATION OF ENDOTHELIAL CELL AND PERICYTES. 72
FIGURE 10: EFFICIENCY OF ENDOTHELIAL CELL DIFFERENTIATION AND VIABILITY. 73
FIGURE 11: CELL SURFACE MARKERS OF IPSC-DERIVED ENDOTHELIAL CELLS. 75
FIGURE 12: FLOW CYTOMETRY ANALYSIS OF MACS-SORTED ENDOTHELIAL CELLS. 75
FIGURE 13: MAINTENANCE OF ENDOTHELIAL CELL MORPHOLOGY AND MARKER CD31 DURING PASSAGING. 76
FIGURE 14: CHARACTERIZATION OF IPSC-DERIVED MESODERMAL PERICYTES. 77
FIGURE 15: TUBE FORMATION ASSAY OF ENDOTHELIAL CELLS. 78
FIGURE 16: INCREASED ICAM-1 EXPRESSION IN RESPONSE TO TUMOUR NECROSIS FACTOR ALPHA (TNF-A TREATMENTS). 78
FIGURE 17: NEURAL CREST STEM CELL-DERIVED PERICYTE DIFFERENTIATION SCHEME. 80
FIGURE 18: CHARACTERIZATION OF NEURAL CREST STEM CELL-DERIVED PERICYTES. 81
FIGURE 19: FLOW CYTOMETRY ANALYSIS OF NEURAL CREST STEM CELL-DERIVED PERICYTES ON D23.. 82
FIGURE 20: EFFECT OF PERICYTES IN BLOOD VESSEL FORMATION. 84
FIGURE 21: ENDOTHELIAL CELL:PERICYTE RATIO TEST IN 3D CELL CULTURE CHIP. 86
FIGURE 22: FORMATION OF MICROVASCULAR NETWORK IN THE CHIP FROM D1-D7.. 87
FIGURE 23: LUMEN FORMATION IN THE BLOOD VESSELS. 88
FIGURE 24: PERFUSION OF BLOOD VESSELS WITH 40 KDA DEXTRAN. 90
FIGURE 25: INDUCTION OF HYPERGLYCEMIA IN ECS AND PCS AND ROS DETECTION IN HYPERGLYCEMIC ECS, PCS, AND MÜLLER GLIA. 92
FIGURE 26: APOPTOSIS INDUCTION UPON A RANGE OF MGO CONCENTRATIONS.. 94
FIGURE 27: SCHEMATIC OF QUANTIFICATION ON BLOOD VESSELS. 95

FIGURE 28: DIAMETERS AND SHAPE IN DIABETIC VS. CONTROL BLOOD VESSELS. 97
FIGURE 29: EFFECT OF TGF-β PATHWAY INDUCTION AND INHIBITION ON BLOOD VESSELS. 98
FIGURE 30: GENERATION OF MÜLLER GLIA FROM HIPSCS. ROS WERE GENERATED FROM HIPSCS. 100
FIGURE 31: MÜLLER GLIA CHARACTERIZATION BY IMMUNOCYTOCHEMISTRY. 101
FIGURE 32: MÜLLER GLIA INCORPORATION INTO THE MICROVASCULATURE SHOWS INTERACTION WITH THE BLOOD VESSELS. 102
FIGURE 33: ASTROCYTE DIFFERENTIATION FROM HIPSC. 103
FIGURE 34: HIPSC-DERIVED ASTROCYTE CHARACTERIZATION MY IMMUNOFLUORESCENCE. 105
FIGURE 35: RNA SEQUENCING PLAN OF ENDOTHELIAL CELLS AND PERICYTES..... 107

List of Tables

TABLE 1: LIST OF BIOLOGICAL MATERIALS 47
TABLE 2: LIST OF PLASTICWARE AND TOOLS 47
TABLE 3: LIST OF CELL CULTURE EQUIPMENT AND DEVICES 48
TABLE 4: LIST OF CELL CULTURE MEDIA 49
TABLE 5: LIST OF COATINGS 50
TABLE 6: LIST OF OTHER CHEMICALS 50
TABLE 7: LIST OF PRIMARY ANTIBODIES 52
TABLE 8: LIST OF SECONDARY ANTIBODIES 53
TABLE 9: LIST OF COUPLED ANTIBODIES 54
TABLE 10: LIST OF KITS 55
TABLE 11: LIST OF SOFTWARES 55
TABLE 12: COMPOSITION OF HIPSC MEDIA 56
TABLE 13: COMPOSITION OF ENDOTHELIAL CELLS AND PERICYTE DIFFERENTIATION MEDIA 58
TABLE 14: COMPOSITION OF NCSCS AND ECTODERMAL PERICYTE MEDIA 60
TABLE 15: COMPOSITION OF ASTROCYTE MEDIUM 62
TABLE 16: COMPOSITION OF MÜLLER GLIA MEDIUM 63
TABLE 17: CELL DEATH OF NCSCS AND NCSC-DERIVED PERICYTES AFTER CRYOPRESERVATION. CELLS WERE COUNTED WITH TRYPAN BLUE AFTER BEING THAWED. 81

Summary

Diabetic retinopathy (DR) is one of the most common diabetes mellitus complications that affects several hundred million people worldwide. DR disrupts the inner blood-retinal-barrier (iBRB), which protects the retina, causing visual impairment, therefore significantly decreases the quality of life. The development of new therapies, especially at the early stages of the disease is very important, since they could prevent retinal complications and vision loss. Current treatments are limited to therapies which alleviate the symptoms of the disease. Also, these therapies (e.g. intraocular anti-VEGF antibody injections) are targeting the later stages of the disease, when it is often late to prevent the pathological pathways in retinal blood vessels. Early stages of DR are associated with pathology of main vascular cells: the number of perivascular pericytes is gradually decreasing, endothelial cells undergo apoptosis and the basement membrane between pericytes and endothelial cells is becoming thicker. TGF-β pathway is a critical regulator of endothelial cell-pericyte crosstalk during development and DR, and TGF-β levels are elevated in diabetes.

Although the iBRB plays a critical role in retinal homeostasis, the iBRB function under physiological and pathological conditions is mostly unknown, due to the lack of suitable *in vitro* human iBRB models. To tackle this problem, we aimed to generate an *in vitro* human disease model for DR by using human induced pluripotent stem cell (hiPSC)-derived endothelial cells (ECs) and pericytes (PCs).

Initially, to recapitulate the iBRB, blood vessel components were generated from hiPSC-derived cells. Endothelial cells and pericytes, as the main components of iBRB were generated from the same hiPSC source. We have developed a novel protocol for endothelial cell generation which included the combination of a 3D suspension and 2D monolayer culture and used it for our model. Pericytes, the second crucial part of iBRB were generated from neural crest stem cells considering their embryonic resemblance to the retinal pericytes. Generated ECs and PCs were characterized based on morphology, and cell markers by immunocytochemistry and flow cytometry, and were proven to be functional. Co-cultured ECs and PCs in a physiological iBRB ratio (EC:PC ; 1:1) in the chip formed 3D blood vessel network within 24 hours and were viable for 7 days. Blood vessels were perfusable, allowing testing of blood vessel functionality. In order to mimic diabetes on blood vessels,

hyperglycemic culture media (75 mM glucose) and advanced glycation end product (AGE)-precursor methylgloxal (MGO) treatment were applied in the chip. Diabetic vs. control blood vessels were quantitatively compared in terms of blood vessel diameter and shape. Interestingly, hyperglycemia treatment caused a slight decrease in blood vessel diameter, whereas MGO caused an enlargement in blood vessels. Blood vessel shape was not affected by diabetic conditions. I also investigated the effect of TGF-β pathway on blood vessels, since TGF-β levels are elevated in DR and its signalling is crucial for EC-PC crosstalk and vessel maturation. TGF-β and its inhibitor (SB431542) both caused a significant decrease in vessel diameter, and SB431542 treatment resulted in the roundest vessel shape compared to control. Additionally, macroglial components of iBRB, Müller glia and astrocytes have been generated and characterized from hiPSCs.

Therefore, the main accomplishments of this thesis are:

1. The development of the first microvasculature on the 3D cell culture chip, using exclusively human iPSC-derived cells
2. Recapitulation of inner blood-retinal-barrier using hiPSC-derived functional endothelial cells and pericytes *in vitro*
3. Generation of a disease model for diabetic retinopathy by two different approaches (hyperglycemia and MGO) in blood vessels
4. Investigating the effect of TGF-β treatment and its inhibition in the disease model
5. Quantitative analysis, which displayed an enlargement of blood vessel diameter in MGO-treated blood vessels.
6. Generation of glial components (Müller glia and astrocytes) of inner blood-retinal-barrier for further developments of the disease model

The DR disease model described here is a promising tool for studying the disease etiology of diabetic retinopathy *in vitro*. Co-culture of multiple human cell types in 3D to recapitulate a tissue or an organ allows disease etiologies to be studied in detail. Additionally, defining metabolites or altered gene expression patterns would allow for early diagnostic markers for DR to be discovered. Furthermore, additional co-cultures of blood vessels with generated and characterized hiPSC-derived glial cells can improve the recapitulation of iBRB. When upscaled,

3D cell culture and the use of hiPSC-derived cells are suitable for high-throughput analysis of blood vessel properties and potential drug candidates.

Zusammenfassung

Die diabetische Retinopathie (DR) ist eine der häufigsten Komplikationen des Diabetes mellitus, von der weltweit mehrere hundert Millionen Menschen betroffen sind. DR stört die innere Blut-Retina-Schranke (iBRB), die die Netzhaut schützt, was zu Sehstörungen führt und somit die Lebensqualität erheblich beeinträchtigt. Die Entwicklung neuer Therapien, insbesondere in den frühen Stadien der Krankheit, ist sehr wichtig, da sie Netzhautkomplikationen und Sehverlust verhindern könnten. Gegenwärtige Behandlungen sind auf Therapien beschränkt, die die Symptome der Krankheit lindern. Außerdem zielen diese Therapien (z. B. intraokulare Injektionen von Anti-VEGF-Antikörpern) auf die späteren Stadien der Krankheit ab, wenn es oft spät ist, die pathologischen Bahnen in retinalen Blutgefäßen zu verhindern. Frühe Stadien der DR sind mit einer Pathologie der Hauptgefäßzellen verbunden: Die Anzahl der perivaskulären Perizyten nimmt allmählich ab, Endothelzellen unterliegen einer Apoptose und die Basalmembran zwischen Perizyten und Endothelzellen wird dicker. Der TGF-β-Weg ist ein kritischer Regulator des Endothelzell-Perizyten-Crosstalks während der Entwicklung und der DR, und die TGF-β-Spiegel sind bei Diabetes erhöht.

Obwohl das iBRB eine entscheidende Rolle bei der retinalen Homöostase spielt, ist die iBRB-Funktion unter physiologischen und pathologischen Bedingungen aufgrund des Fehlens geeigneter humaner iBRB-in-vitro-Modelle weitgehend unbekannt. Um dieses Problem anzugehen, wollten wir ein menschliches *in vitro* Krankheitsmodell für DR generieren, indem wir Endothelzellen (ECs) und Perizyten (PCs) aus humanen induzierten pluripotenten Stammzellen (hiPSC) verwenden.

Um das iBRB zu rekapitulieren, wurden zunächst Blutgefäßkomponenten aus hiPSC-abgeleiteten Zellen generiert. Endothelzellen und Perizyten als Hauptkomponenten von iBRB wurden aus derselben hiPSC-Quelle generiert. Wir haben ein neuartiges Protokoll für die Generierung von Endothelzellen entwickelt, das die Kombination einer 3D-Suspension und einer 2D-Monolayer-Kultur beinhaltet und für unser Modell verwendet. Perizyten, der zweite entscheidende Teil von iBRB, wurden aufgrund ihrer embryonalen Ähnlichkeit mit den retinalen Perizyten aus Neuralleisten-Stammzellen generiert. Generierte ECs und PCs wurden basierend auf Morphologie und Zellmarkern durch Immunzytochemie und

Durchflusszytometrie charakterisiert und erwiesen sich als funktionsfähig. Kokultivierte ECs und PCs in einem physiologischen iBRB-Verhältnis (EC:PC ; 1:1) im Chip bildeten innerhalb von 24 Stunden ein 3D-Blutgefäßnetzwerk und waren 7 Tage lebensfähig. Die Blutgefäße waren perfundierbar, wodurch die Funktionalität der Blutgefäße getestet werden konnte. Um Diabetes auf Blutgefäßen nachzuahmen, wurden hyperglykämische Kulturmedien (75 mM Glukose) und eine Behandlung mit fortgeschrittenem Glykationsendprodukt (AGE)-Vorläufer Methylgloxal (MGO) im Chip angewendet. Blutgefäße von Diabetikern und Kontrollen wurden quantitativ im Hinblick auf Durchmesser und Form der Blutgefäße verglichen. Interessanterweise verursachte die Behandlung mit Hyperglykämie eine leichte Verringerung des Durchmessers der Blutgefäße, während MGO eine Vergrößerung der Blutgefäße verursachte. Die Form der Blutgefäße wurde durch diabetische Zustände nicht beeinflusst. Ich habe auch die Wirkung des TGF-β-Signalwegs auf Blutgefäße untersucht, da die TGF-β-Spiegel bei DR erhöht sind und seine Signalgebung für das EC-PC-Crosstalk und die Gefäßreifung entscheidend ist. TGF-β und sein Inhibitor (SB431542) verursachten beide eine signifikante Verringerung des Gefäßdurchmessers, und die Behandlung mit SB431542 führte im Vergleich zur Kontrolle zu der rundesten Gefäßform. Darüber hinaus wurden Makroglia-Komponenten von iBRB, Müller-Glia und Astrozyten aus hiPSCs generiert und charakterisiert. Die wichtigsten Errungenschaften dieser Arbeit sind daher:

1. Die Entwicklung der ersten Mikrovaskulatur auf dem 3D-Zellkulturchip unter ausschließlicher Verwendung von humanen iPSC-abgeleiteten Zellen
2. Rekapitulation der inneren Blut-Retina-Schranke unter Verwendung von hiPSC-abgeleiteten funktionellen Endothelzellen und Perizyten in vitro
3. Generierung eines Krankheitsmodells für diabetische Retinopathie durch zwei unterschiedliche Ansätze (Hyperglykämie und MGO) in Blutgefäßen
4. Untersuchung der Wirkung der TGF-β-Behandlung und ihrer Hemmung im Krankheitsmodell
5. Quantitative Analyse, die eine Vergrößerung des Blutgefäßdurchmessers in MGO-behandelten Blutgefäßen zeigte.
6. Generierung von Gliakomponenten (Müller-Glia und Astrozyten) der inneren Blut-Retina-Schranke zur Weiterentwicklung des Krankheitsmodells

Das hier beschriebene DR-Krankheitsmodell ist ein vielversprechendes Werkzeug zur Untersuchung der Krankheitsätiologie der diabetischen Retinopathie *in vitro*. Die Co-Kultur mehrerer menschlicher Zelltypen in 3D zur Rekapitulation eines Gewebes oder eines Organs ermöglicht die detaillierte Untersuchung von Krankheitsursachen. Darüber hinaus würde die Definition von Metaboliten oder veränderten Genexpressionsmustern die Entdeckung früher diagnostischer Marker für DR ermöglichen. Darüber hinaus können zusätzliche Co-Kulturen von Blutgefäßen mit generierten und charakterisierten hiPSC-abgeleiteten Gliazellen die Rekapitulation von iBRB verbessern. Bei Hochskalierung eignen sich 3D-Zellkulturen und die Verwendung von hiPSC-abgeleiteten Zellen für die Hochdurchsatzanalyse von Blutgefäßeigenschaften und potenziellen Arzneimittelkandidaten.

1. Introduction

1.1. Neural Retina – development and function

Vertebrate eye consists of several ocular tissues: cornea, lens, ciliary body, iris, neural retina, retinal pigment epithelium (RPE), choroid, sclera. Different compartments of the eye are structurally and spatially specialized to conduct visual function (Fig. 1I). During development, spatiotemporal expression of various transcription factors (TFs) shapes these eye-specific tissues (Jean, Evan, and Gruss, 1998). Anterior part of the eye is derived from surface ectoderm, whereas neural retina and RPE is solely derived from neural tube (Fig. 1A-C) (Stone, 1988).

In vertebrates, following gastrulation and neural tube formation, neural ectoderm evaginations by eye-specific transcription factors result in eye field formation (Fig. 1D). The single eye field later is separated into bilateral optic sulci via sonic hedgehog (Shh) and Sine Oculis Homeobox Homolog 3 (Six3) signaling (Gallardo et al., 2018; Giger and Houart, 2018). Migration of optic sulci into non-neural ectoderm initiates optic vesicle formation (Fig. 1E). Transcription factors such as Retina and Anterior Neural Fold Homeobox (*Rax/Rx*), Paired Box 6 (*Pax6*), LIM Homeobox 2 (*Lhx2*), *Six3*, Nuclear Receptor TLX (*Tll*), T-Box Transcription Factor 3 (*Tbx3*) and SIX Homeobox 6 (*Six6*) are responsible for proper eye field and subsequent optic vesicle formation (Fuhrmann, 2010; Sinn and Wittbrodt, 2013; Miesfeld and Brown, 2019). Invaginations of optic vesicles later form optic cups (Fig. 1G), from which neural retina and retinal pigment epithelium (RPE) cells develop (Fig. 1H) (Dash et al., 2016). Posterior-most part of the retinal tissue is called optic stalk and consists of retinal ganglion cell axons.

Cornea, as the outer-most layer of the eye serves a protective role and has a refractive surface for light focus. It consists of three parts: corneal epithelium (surface ectoderm-derived), stroma, and epithelium (peri-ocular mesenchyme-derived).
Lens is found posterior to the cornea and has three structural units: lens capsule, epithelium, and fibers. It focuses refracted light of objects in different distances via a phenomenon called accommodation, by changing its curvature via ciliary muscles.
The ciliary body and iris are both derived from non-neural progenitors and peri-ocular mesenchyme following optic cup formation. Ciliary body secretes aqueous humor to the

anterior eye and aids lens accommodation. Iris helps to arrange the amount of light delivered the retina as well as focusing light and regulating intraocular pressure (Davis-Silberman and Ashery-Padan, 2008).

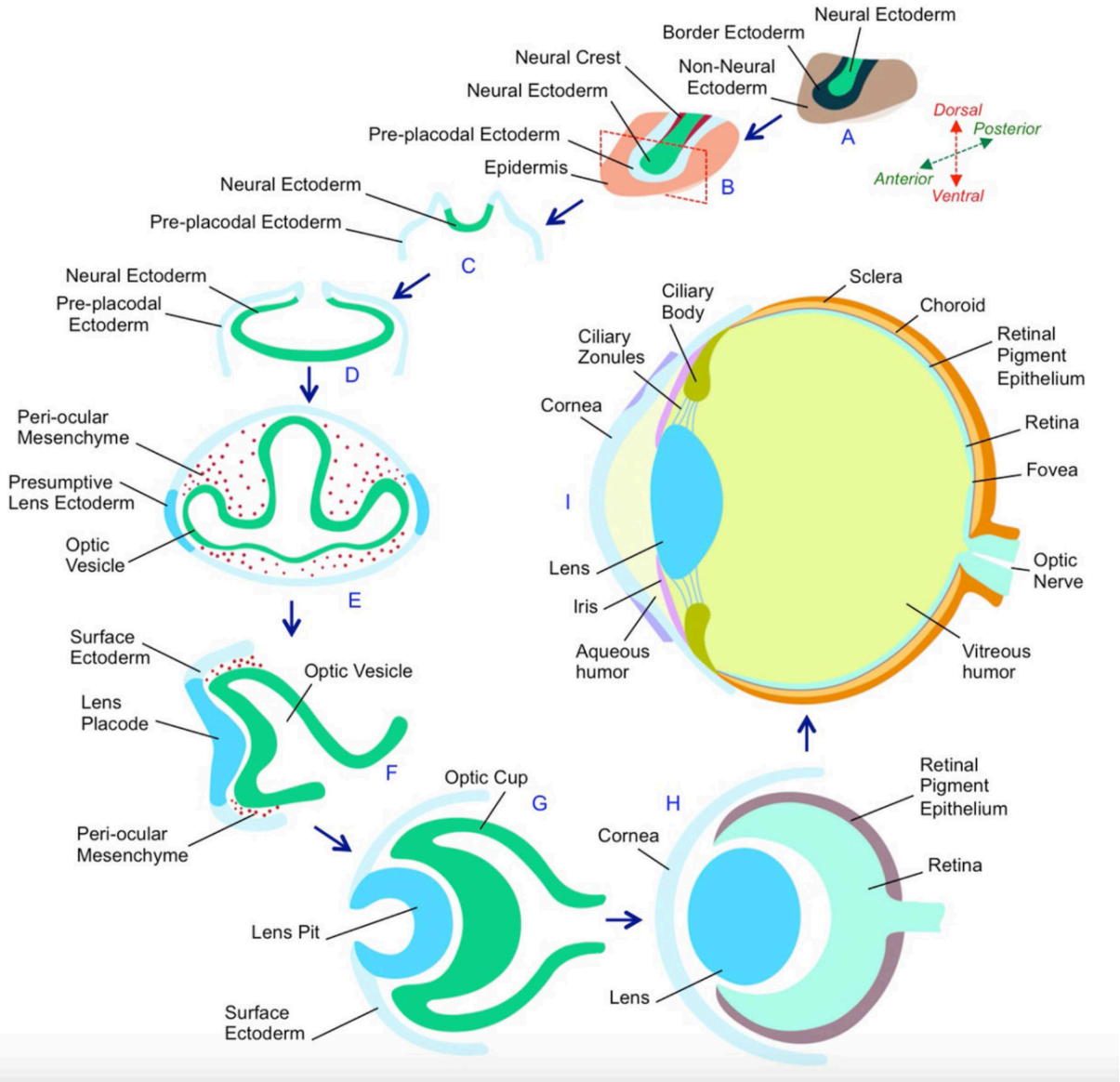


Figure 1: Development of vertebrate eyes. Neural ectoderm, border ectoderm and non-neural ectoderm are parts of ectodermal tissue following gastrulation (A). Border ectoderm later gives rise to pre-placodal ectoderm and neural crest (B). Neural ectoderm invaginations form the neural tube (C). Eye-field specific TFs result in optic vesicle formation, which is formed as a single vesicle and later bifurcates into bilateral vesicles (D, E). Migration of anterior optic vesicles into surface ectoderm shapes the optic cup as lens placode forms from pre-placodal ectoderm (F). Further invaginations of optic cup midline to the posterior continues to shape the optic cup, whereas the lens placode forms

the lens pit (G). Next, lens pit pinches off from the surface ectoderm and forms the lens, as retina and RPE forms at the posterior eye (H). The functional vertebrate eye consists of anterior structures cornea, lens, iris, ciliary body and zonules, filled with aqueous humor. At the posterior eye, retina and retinal pigment epithelium derived from neural ectoderm, in addition to sclera, choroid, and optic nerve that is connected to central nervous system (I). *Adapted from Dash et al., 2016.*

Retina is the light conducting part of the visual system, 100 – 200 µm thick in humans, and consists of continuous neural layers that are processing visual information gradually. Human eye development begins as early as gestational week (WG) 3 and continues to develop until 8th month of gestation (O'Rahilly, 1975; Graw, 2010). Key developmental stages of eye in vertebrate species are highly conserved (Lamb, Collin, and Pugh, 2007). However, in human retinae, fovea fating is determined earlier than other parts, and retinal development takes place from central to peripheral direction (Hoshino et al., 2017). Neural retina in vertebrates consist of five neuronal layers: photoreceptor cells, horizontal cells, bipolar cells, amacrine cells, and ganglion cells (Fig. 2). These neuronal layers are supported by three types of glial cells: Müller glia, astrocytes, and microglia. Retinal neurons as well as Müller glia are generated from retinal progenitor cells (RPCs), that require complex expression patterns of TFs such as *Rax*, Visual System Homeobox 2 (*Vsx2*), *Pax6*, *Lhx2*, *Six3*, Six6, and SRY-Box Transctiption Factor 2 (*Sox2*) *(*Pandit et al., 2015; Chen et al., 2017*)*.

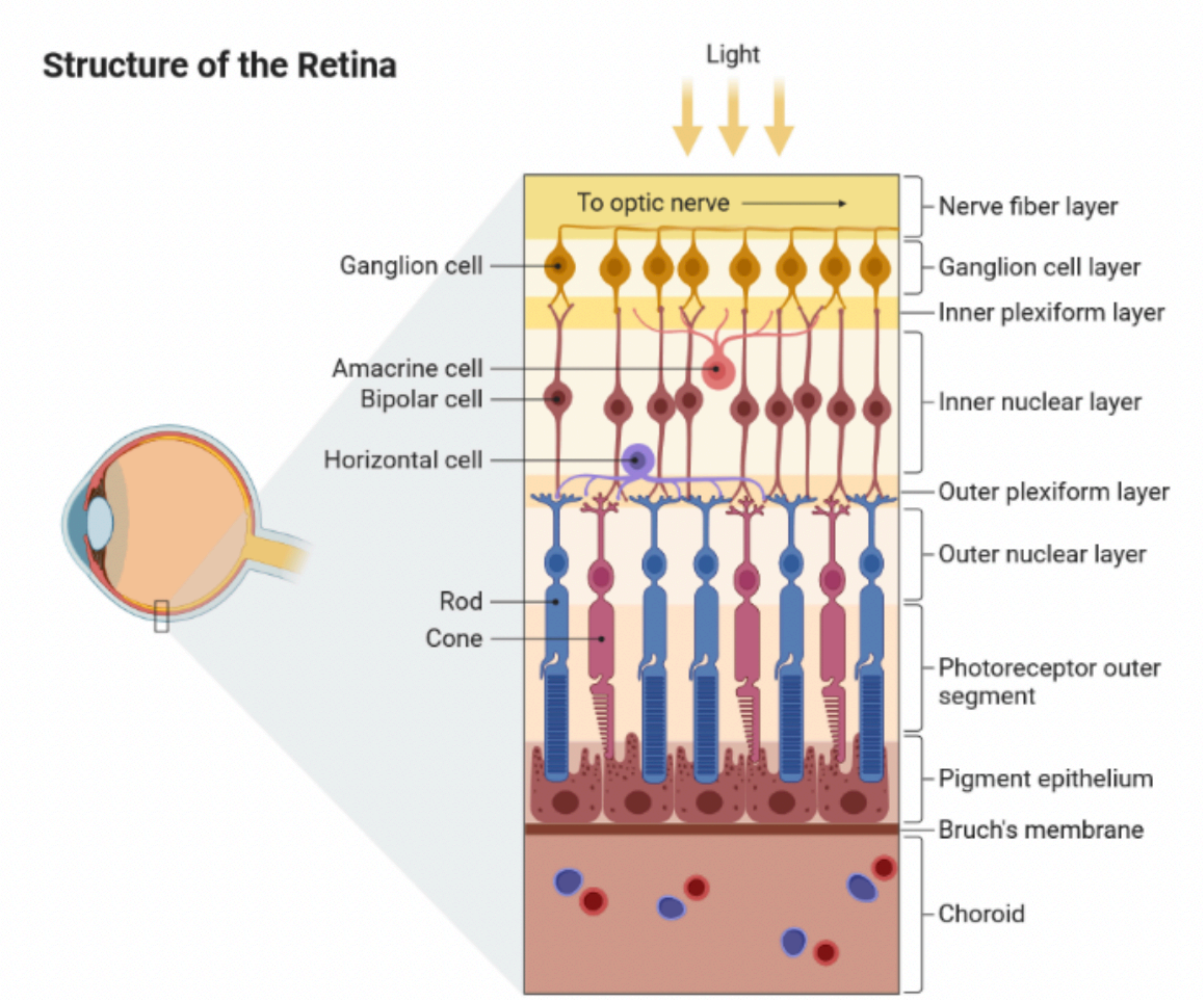


Figure 2: Neuronal layers in human retina. Neural retina consists of five types of cells: rod and cone photoreceptor cells, horizontal cells, bipolar cells, amacrine cells, and ganglion cells. Retinal pigment epithelium (RPE) cells are in direct contact with PRCs at the posterior retina. Choroid layer has choricapillaris and provide oxygen and nutrients to the posterior retina. Bruch's membrane is found between choroid and RPE cell layer. Created with BioRender.

Photoreceptor cells (PRCs) receive direct light and convert it into visual information through their photosensitive proteins in their cell membranes. In humans, due to highly specialized function of retinal neurons, visual stimuli that is received in PRCs must be processed into a compressed form. This task is fulfilled by interneurons; horizontal cells and amacrine cells. Overall, there is a flow of information from PRCs into ganglion cells. The structure that forms axons of ganglion cells is called optic nerve fiber and is connected to the dorsal lateral geniculate nucleus (dLGN) in thalamus. Next, axons of the neurons in LGN send visual

information to visual cortex so that the information can be interpreted (Sefton, Dreher, and Harvey, 2004).

Photoreceptor cells are glutamatergic neurons that consist of rods and cones. There is only one type of rod cell, whereas there are three types of cones (S-cones, M-cones, L-cones) in primates. Cone cells are named after the wavelengths of light that they can detect: short-wavelength (437 nm, S-cones), medium-wavelength (533 nm, M-cones), and long-wavelength (564 nm, L-cones). Rods have rhodopsin protein, which is highly sensitive to light. Therefore, in dim-light condition, rod PRCs are active.

Horizontal cells are the interneurons located anterior to PRCs. They are classified depending on the presence of axons (a-type: axon lacking, b-type: axon-bearing). They help in PRC adaption of integration time, and generation of receptive fields (Thoreson and Mangel, 2012).

Bipolar cells are synapsing PRCs and relaying PRC signals into ganglion cells. There are various types of BPCs such as ON-OFF (ON: depolarizing, OFF: hyperpolarizing) type, rod contacting or cone contacting type (Hoon et al. 2014). Dendrites of horizontal and bipolar cells form the outer plexiform layer (OPL).

Amacrine cells are located in the inner retina, and they have dendritic processing, which means they receive inputs and send out signals through their dendrites.

Ganglion cells are the neurons that receive the processed visual information convert it into spike trains. Ganglion cell axons are connecting the retina to the visual cortex. There are 20 - 25 types of ganglion cells, which are classified based on the feature of visual information that is received such as edges, motion, direction, and orientation (Sernagor, Eglen, and Wong, 2001).

At the posterior of neural retina, an epithelial cell monolayer called retinal pigment epithelium (RPE) is located. RPE cells have direct contact with PRCs and help in visual cycle, shedding of photoreceptor outer segments, and maintaining a barrier at the posterior retina. They secrete vascular endothelial growth factor (VEGF), which maintains the health of endothelial cells in choriocapillaris (Saint-Geniez et al., 2009; Klettner et al., 2015).

High neuronal activity in retina, especially in PRCs and RPE requires a vast amount of energy. This energy requirement is fulfilled by retinal blood vessels, that mainly carry oxygen and nutrients, and maintains retinal homeostasis.

1.2. Retinal blood vessels

Human brain uses 20% of the total energy in an organism, which retina is a part of (Herculano-Houzel, 2011). Oxygen consumption in the resting retina can be as high as 10% in some fly species due to photoreceptor activity (Howard, Blakeslee, and Laughlin, 1987). This brings about an advanced vascular system for the nourishment of the retinal tissue, which must be finely controlled.

Vascular system in the human eye consists of three structures: hyaloid vessels, choriocapillaris, and retinal vessels. Hyaloid vessels are the transient vasculature that exists from 6 WG- 13 WG, before retina fully forms (Selvam, Kumar, and Fruttiger, 2018). Choriocapillaris are fenestrated lobular blood vessels that are forming the choroid. They are located near RPE cells, that express VEGF and are nourishing the outer retina. Retinal vasculature is formed lastly by vascular progenitors that co-express C-X-C Motif Chemokine Receptor 4 (CXCR4) and $CD39^{+}$ and are found within the optic nerve fiber layer around 12 WG (Fig. 3A). These spindle-shaped cells start to form cords around 18 WG and migrate to the peripheral retina. By about 20 WG, erythrocytes are found in vascular cords formed by endothelial cells (Hughes et al. 2000). Until 21 WG, the vascular progenitors form blood vessels and form a superficial retinal vasculature by vasculogenesis (Fig. 3B) (McLeod et al. 2006). Once the main retinal vasculature is formed, around 25 – 26 WG, deep capillary retinal vasculature formation follows by angiogenesis (Fig. 3C) (Lutty and McLeod, 2018).

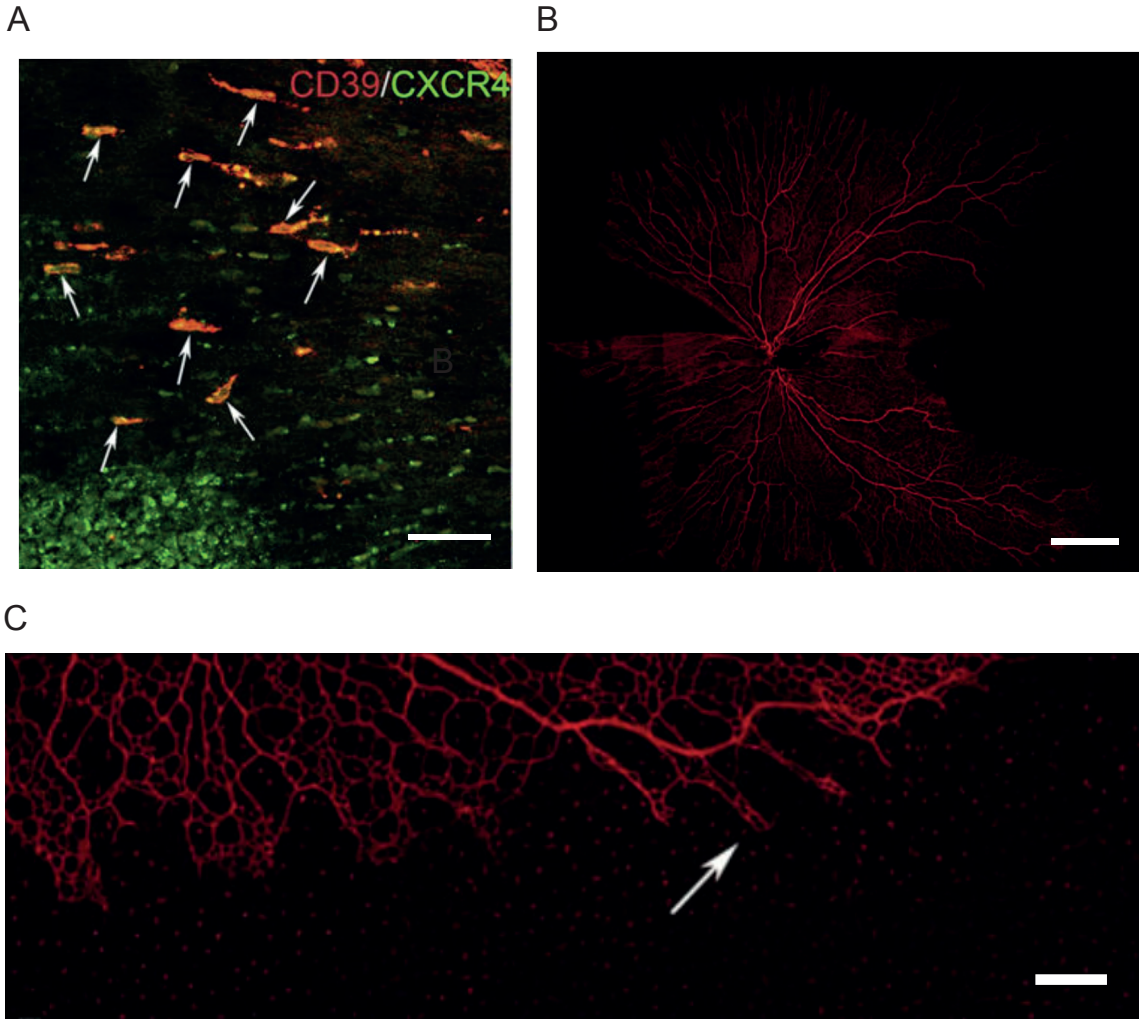


Figure 3: Formation of human retinal vasculature. CD39^{+}/CXCR4^{+} cells within the optic nerve (A) populate the retinal quadrants (B) in human fetal samples. Once a scaffold of primary vessels is formed, it expands and populates the entire retina (C). *Adapted from Lutty and McLeod, 2018.*

Retinal blood supply is provided through ophthalmic artery, which branches off from internal carotid artery (Fig. 4). One of the main branches from the ophthalmic artery is the central retinal artery, which is found within the optic nerve at the posterior of the eye. Central retinal artery is branching off into several arterioles and is the main source of retinal blood vessels. Choroid blood supply is provided by posterior ciliary arteries that derive from ophthalmic arteries, whereas lacrimal artery is nourishing the anterior eye (Burns, Elsner, and Gast, 2021).

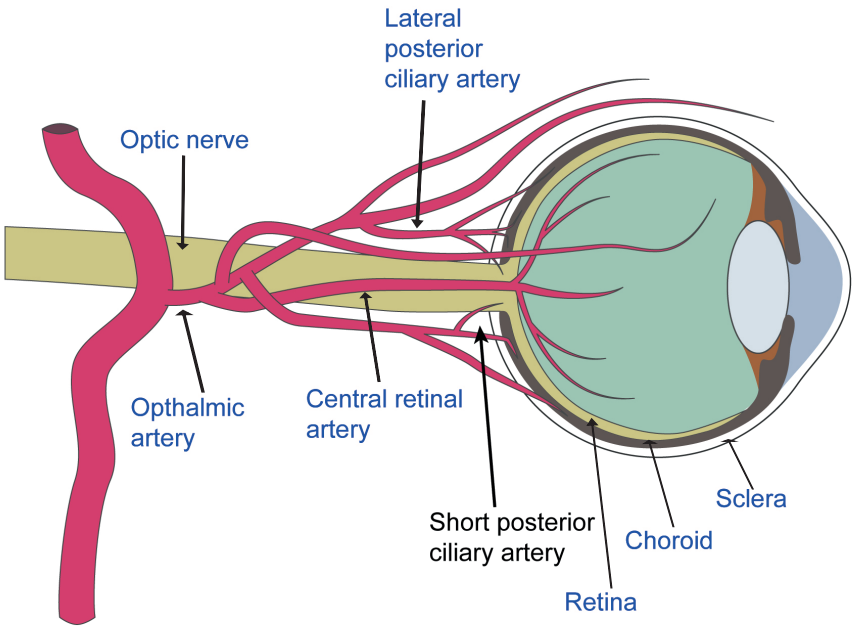


Figure 4: Arteries of the human eye. Internal carotid artery branches off to ophthalmic artery and one of the branches is forming central retinal artery, from which arterioles and capillaries derive from. Ciliary arteries nourish choroid layer of the eye, whereas lacrimal arteries nourish the anterior retina. *Drawn with Abode Illustrator.*

In adult human retina, four plexuses provide oxygen and nutrients to retinal tissues regionally (Fig. 5A). Ganglion cell axons (optic nerve fiber layer) are supplied by radial peripapillary capillary plexus (RPCP), ganglion cell layer (GCL) is supplied by superficial vascular plexus (SVP). Deep and intermediate capillary plexuses (DCP and ICP, respectively) supply the inner retina (Campbell et al, 2017). Fig 5B depicts the optical coherence tomography angiography (OCTA) images of SVP, ICP, and DCP in humans. In primates, fovea has an avascular zone to ensure visual acuity, which is not vascularized in normal conditions.

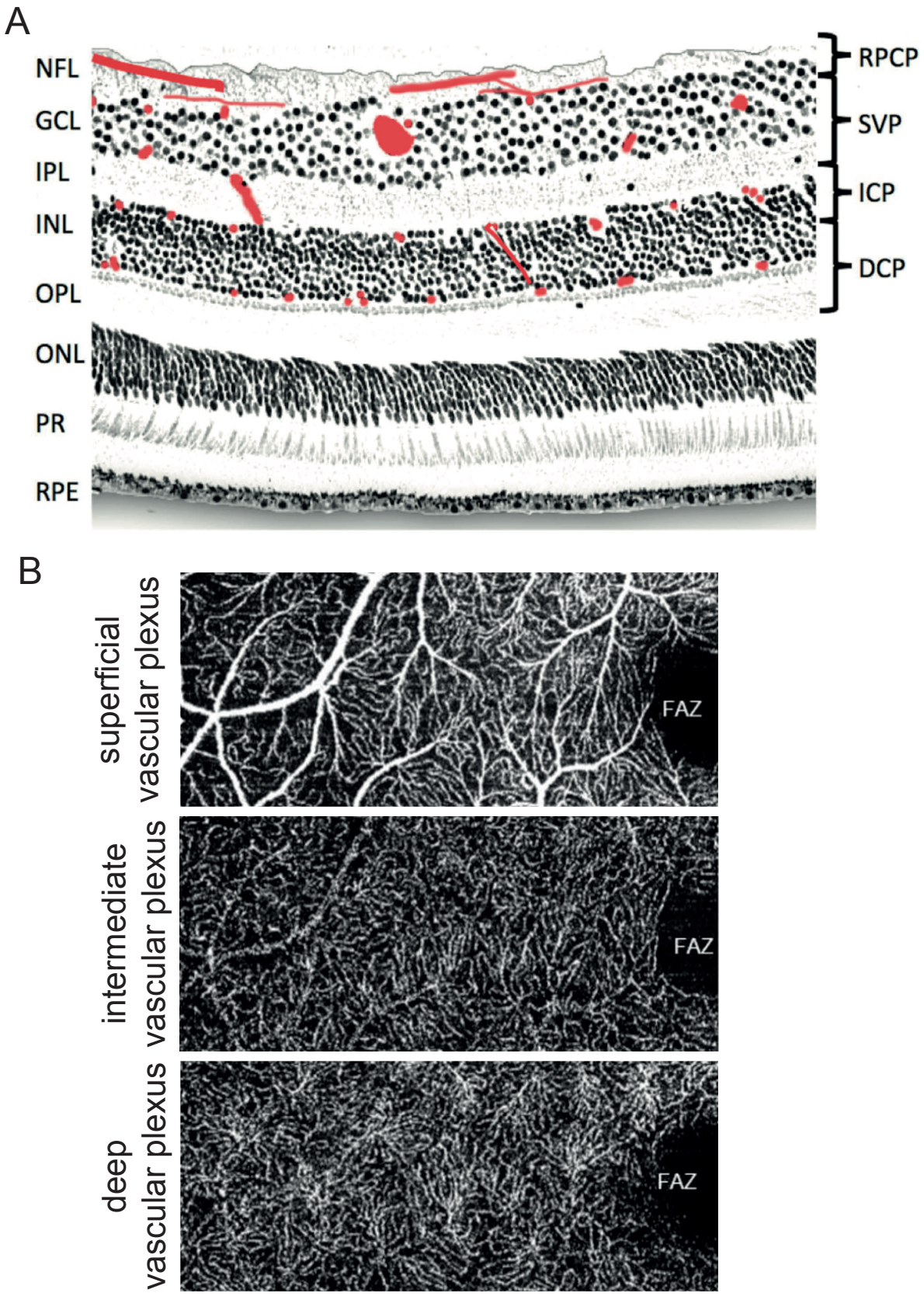


Figure 5: Vascular plexuses in human retina. NFL=nerve fiber layer, GCL=ganglion cell layer, IPL=inner plexiform layer, INL=inner nuclear layer, OPL=outer plexiform layer, ONL=outer nuclear layer, PR=photoreceptor cells, RPE=retinal pigment epithelium, RPCP=radial peripapillary capillary plexus,

SVP=superficial vascular plexus, ICP=intermediate capillary plexus, DCP=deep capillary plexus. *Adapted from Campbell et al. 2017* (A). OCTA images of three plexuses in the global human retina (superficial plexus, intermediate plexus, deep vascular plexus). FAZ= foveal avascular zone. *Adapted from Burns, Elsner, and Gast, 2021* (B).

1.3. Retinal barriers

Retinal tissue has two barriers that provide a controlled gateway from the peripheral blood to retina: inner blood-retinal barrier (iBRB) and outer blood-retinal barrier (oBRB). Intercellular tight junctions (TJs) of endothelial cells in retinal capillaries, supported by pericytes and glial cells (Müller glia and astrocytes) form the iBRB. Outer BRB is formed by retinal pigment epithelium (RPE) cell tight junctions, which are in close contact with photoreceptor cells. Inner retina is protected by iBRB, whereas outer retina is protected by oBRB.

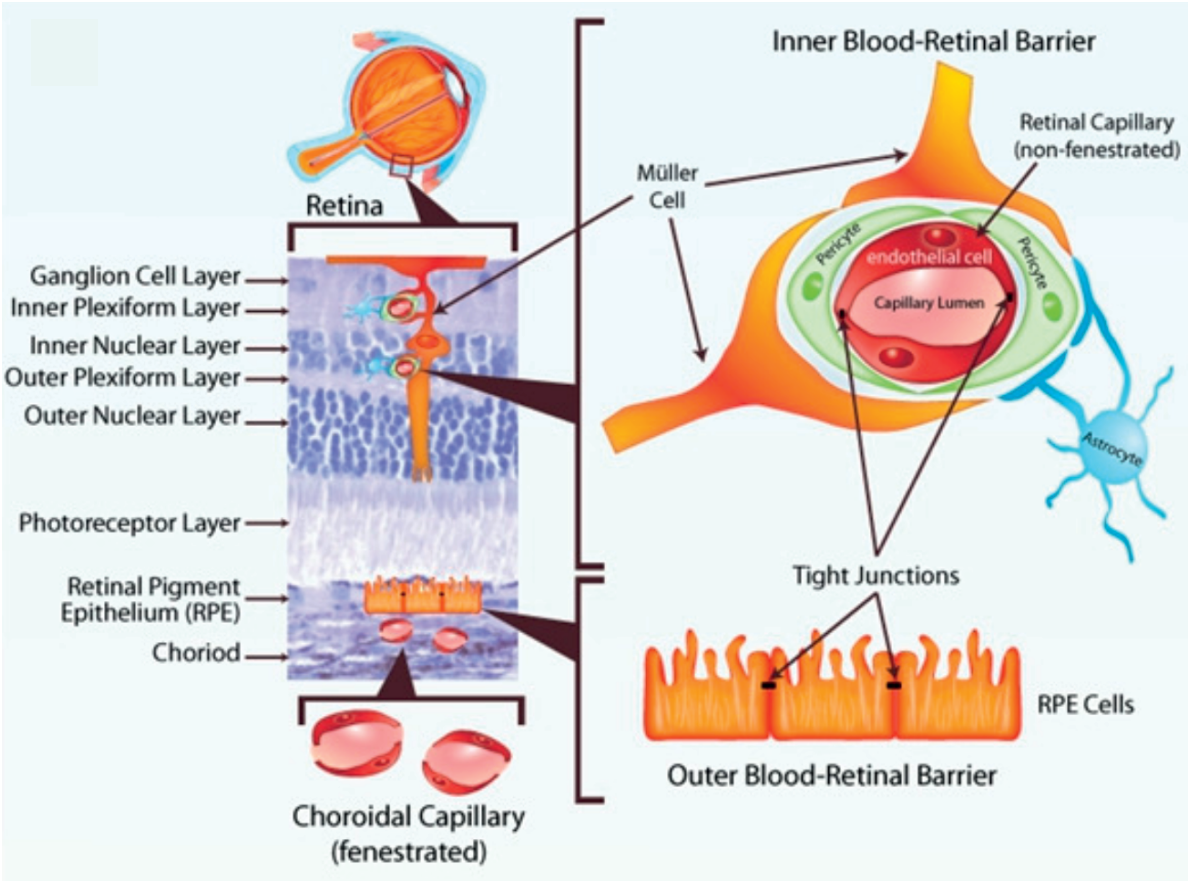


Figure 6: Blood-retinal barriers: inner blood-retinal barrier (iBRB) of retinal capillaries and outer blood-retinal barrier (oBRB) between RPE cells. In retinal capillaries, iBRB is formed with endothelial cells that are tightly connected with tight junctions, and surrounding pericytes. In addition to that, Müller glia and astrocytes surround the endothelium with their end-feet. Outer blood-retinal barrier is formed between the tight junctions of adjacent RPE cells at the posterior retina. *Adapted from Yang and Huang, 2012.*

1.3.1. Outer blood-retinal barrier (oBRB)

Outer BRB is composed of tight junctions of RPE cells. Outer retina is nourished by choriocapillaris, which is a lobular and dense vascular system in the posterior retina. Due to the fenestrations of choriocapillaris, endothelial cells cannot provide a barrier for the outer retina. However, RPE cell monolayer have intercellular adherens and tight junctions in apical region and maintain an epithelial barrier between the choriocapillaris and the retina. Another important part of oBRB is the Bruch's membrane, which is composed of extracellular matrix proteins and lays between the RPE layer and choriocapillaris (Field et al., 2020). Tight

junctions between RPE cells are formed with occludins, claudins, and Zonula Occludens protein 1 (ZO-1), similar to endothelial cell TJs in iBRB. However, the predominant claudin isoform is Claudin-19 in RPE cells (Naylor et al., 2020). In general, transcellular transport in RPE cells is highly controlled via ions pumps, protein channels, and tight junctions according to the need of retinal tissue (Fields et al., 2020).

1.3.2. Inner blood-retinal barrier (iBRB)

The inner blood-barrier (iBRB) is a physical barrier that limits the diffusion and transport of ions and biomolecules in retina. This limitation is vital for the proper functioning of retina, since many blood-borne toxins may affect neuronal signaling needed for vision (Yang et al., 2020). Also, pro-angiogenic factors in systemic blood would affect retinal capillaries, which threatens vision due to neovascularization or edema.

Inner BRB is formed by adherens and tight junctions of endothelial cells in retinal capillaries. Retinal capillaries are formed by a single layer of EC tubes that have a basement membrane, where mural cells (pericytes) and glia ensheath with their processes (Klaassen, van Noorden, and Schlingemann, 2013). This forms the neurovascular unit (NVU), which is composed of ECs, pericytes, Müller glia, and astrocytes in retina.

The structure and function of iBRB are highly similar to blood-brain-barrier (BBB) of central nervous system (CNS). Both barriers need to strictly regulate their microenvironment such as ion concentrations due to high neuronal activity (Abbott et al., 2019). This regulation is mainly ensured with the tight junctions between the ECs, which have reduced permeability mediated via selective transport mechanisms. In the absence of tight junction complexes, endothelial cells can be permeable to various proteins, lipids, and cytokines, which may negatively affect neuronal function in retina. ECs of both iBRB and BBB also lack fenestrae via suppression of Plasmalemma vesicle protein 1 (PLVAP), which ensures the low permeability of barriers (Yemanyi et al., 2021).

Each component of iBRB is crucial in maintaining retinal homeostasis. The degeneration of iBRB and changes in blood vessel permeability therefore causes detrimental retinal diseases such as diabetic retinopathy, macular edema, retinopathy of prematurity (ROP), retinal vein occlusion (Cunha-Vaz. 2009; Vinores, 2010).

1.3.2.1. Endothelial cells

Endothelial cells in retinal capillaries play a fundamental role in inner blood-retinal barrier formation. Retinal ECs regulate the cellular transport from the luminal site to the abluminal site in order to maintain the retinal homeostasis. For that purpose, high amount of efflux pump proteins is expressed on the cell membrane of retinal ECs. Dependent on Wnt/β-catenin pathway, transcytosis and paracellular transport is kept at a minimal level to maintain the ion and solute concentrations in balance (Wang et al., 2020). When transcytosis is needed, transport vesicles are used for the passage of solutes.

In addition to the transporters and efflux pump proteins, tight junction (TJ) complexes play a major role in establishing a barrier. Tight junction complexes are formed by several proteins in or around cellular membrane that are interconnected. Zonula occludens (ZO) proteins are scaffold proteins that connect transmembrane proteins and actin cytoskeleton. Among three isotypes (ZO-1, ZO-2, ZO-3), ZO-1 is the isotype in retinal ECs that is regulating capillary permeability (Russ et al., 1998). Occludin, a tetraspan transmembrane protein binds all three isotypes of ZOs and act as a regulator of barrier rather than having a structural role (Furuse et al., 1993; Matter and Balda, 1999). It can go under various post-translational modifications (PTMs) that regulate cell signaling and protein trafficking. Claudins are transmembrane proteins that have 27 isoforms in mammals, from which claudin-5 is highly expressed in retinal and brain ECs. They connect actin cytoskeleton (Díaz-Coránguez, Ramos, Antonetti, 2017). Expression of claudin-5 in ECs is related to barrier integrity, as it ensures low transcytosis levels, along with suppression of PLVAP, which is found in fenestrated ECs (Yemanyi et al., 2021). Frizzled-4 (Fzd-4), a downstream Wnt pathway affector is required for the integrity of iBRB, as well as BBB, which causes an upregulation of PVLAP and downregulation of claudin-5 when absent (Daneman and Prat, 2015). Tight junctions between the ECs act as a physical barrier that limits the paracellular transport from circulating blood to the retinal tissue. In mice, the timing of reduced transcytosis and blood-retinal barrier formation is highly correlated, and leakiness of blood vessels is attributed to transcytosis (Chow and Gu, 2017).

Adherens junctions also play a supportive role in barrier integrity. Among adherens junction proteins in retinal endothelium, vascular endothelial cadherin (VE-cadherin) is highly important. As a cadherin family protein, VE-cadherin is specifically expressed in vascular

endothelial cells and its cytoplasmic domain to actin filaments via β-catenin and plakagobin (Dejana, Orsenigo, and Lampugnani, 2008). VE-cadherin also limits the sprouting of endothelial cells, therefore aids in vessel maturation (Szymborska and Gerhardt, 2018). Additionally, N-cadherin is also expressed in retinal ECs, although not specifically, and possibly responsible for adherens junctions between pericytes and ECs (Gerhardt et al., 1999; Zheng et al., 2016).

1.3.2.2. Pericytes

Pericytes are a type of mural cells, along with vascular smooth muscle cells. They are found in blood vessels of various organs and their main role is to ensheath capillaries and protect them. In retinal capillaries, pericytes directly contact endothelial cells and their main role is to regulate angiogenesis and blood vessel maturation. In larger vessels, they may also have contractile properties (Bandopadhyay et al., 2001). For the integrity of iBRB, pericytes are highly important as retinal blood vessels have the highest ratio of pericytes per endothelial cell in human body (Frank, Turczyn, and Das, 1990). In the retinal capillaries of rats, endothelial cell to pericyte ratio was found to be 1.8, which has a higher endothelial cell coverage than brain microvasculature with a ratio of 2.7 (Li et al., 2018).

Developmental origin of retinal pericytes is controversial, as there is evidence of both ectodermal and mesodermal origin for their ontogeny. Generally, during brain development, forebrain pericytes are originated from neural crest, whereas midbrain and hindbrain regions have mesoderm-derived pericytes. It was shown that in quail, forebrain pericytes originate from neural crest, which derives from ectoderm (Etchevers et al., 2001). Another avian study also displayed that brain PCs could be differentiated from neuroectodermal tissue, which mesodermal tissue failed to replicate (Korn, Christ, and Kurz, 2002). Supporting the neuroectodermal origin of brain PCs, retinal capillary and choroidal PCs were shown to originate from neural crest, using Sox10 as a marker for fate mapping in mice (Trost et al., 2013). Alternatively, mesodermal and bone marrow origin of retinal PCs has also been suggested. However, this origin was mainly associated with pathological angiogenesis and tumors, which may not reflect the healthy origin of pericytes (Pfister et al., 2013: Trost et al., 2016). Also, when primary retinal PCs were used in culture, their transdifferentiation capacity to mesodermal lineages (osteogenic and adipose tissue) were minimal compared to mesodermal PCs or vascular smooth muscle cells (VSMCs) (Herrmann et al., 2016). This result

may demonstrate the non-mesodermal origin of retinal pericytes, which differentiates them from PCs of other organs. Neural-crest derived pericytes that populate the forebrain may have a specialized role since they contribute to BBB and BRB integrity, and regulate the blood flow (Girolamo et al., 2021).

Characterization of pericytes is controversial since they do not possess cell-specific markers. However, it is known that retinal pericytes mainly express platelet-derived growth factor-β (PDGFRβ) and neural/glial antigen 2 (NG2), as well as CD13, ATP-Sensitive Inward Rectifier Potassium Channel 8 (Kir6.1), Sodium-dependent glutamate/aspartate transporter 1 (GLAST, desmin, nestin, and CD248 (Kumar et al., 2017; Santos et al., 2018). They are usually characterized by their morphology and functionality (blood vessel coverage) in addition to expression of cell markers (Symth et al., 2018).

Retinal pericytes resemble pericytes of brain capillaries, as they also regulate blood vessel maturation and the size of capillaries. In the absence of brain pericytes, vessel diameter and the vessel density increase in mice (Armulik et al., 2010). Peg-and-socket interactions between ECs and PCs in BBB are highly similar in iBRB, which is mediated by N-cadherin and connexin proteins (Liebner et al., 2018). This direct connection between ECs and PCs allows the transport and signaling of biomolecules. Among those, PDGFR-BB - PDGFRβ signaling is very crucial, as EC-derived PDGFR-BB regulates the recruitment and proliferation of pericytes (Zhao et al., 2015). In the absence of PDGFRβ in PCs in mice, upregulation of angiogenesis markers in retinal ECs, as well as a reduced expression of transporters such as Major Facilitator Superfamily Domain Containing 2A (*Mfsd2a*) and Solute carrier family 16 member 1 (*Slc16a1*) are observed (Mäe et al., 2021). In retina, pericytes regulate the expression of several genes that protect endothelial cells such as Forkhead Pox protein O1 (FOXO1), angiopoietin-2 (Ang2), and Vascular Endothelial Growth Factor Receptor 2 (VEGFR2) (Park et al., 2017). Additionally, CD146 expression in retinal and brain ECs are downregulated upon the attachment of pericytes to the blood vessels. Pericytes also have a regulatory role in endothelial cell survival, proliferation, and permeability via Ang/Tie2 pathway (Szymborska and Gerhardt, 2018). Angiopoietin-1 (Ang-1) is mainly expressed in pericytes. Upon its binding to angiopoietin-1 receptor (Tie2), which is expressed in endothelial cells, phosphorylation of

this receptor results in the activation of several downstream signaling pathways such as phosphatidylinositol kinase 3 (PI3K), mitogen-activated protein kinase (MAPK), and endothelial nitric oxide synthase (eNOS) (Fagiani and Christofori, 2013). Angiopoietin-2 (Ang2), which also binds to Tie2 and may act as an agonist or an antagonist on Ang/Tie pathway. Ang1/Ang2 levels should be kept balanced since they can compete for the Tie2 receptor binding, and overexpression of Ang2 is associated with reduced permeability in retinal ECs. In physiological conditions, Ang-1 expression in pericytes stabilize the newly formed blood vessels, and prevents pathological angiogenesis (Joussen et al., 2021). Therefore, further proliferation of endothelial cells is prevented, which is highly important in blood vessels of iBRB.

1.3.2.3. Astrocytes

Astrocytes are found in ganglion cell layer and within the optic nerve in the retina. They enter the neural retina from the optic nerve head and migrating through the retinal ganglion cell layer by platelet-derived growth factor-α (PDGFR-α) signaling (Tao and Zhang, 2014). Immature astrocytes express Paired Box 2 (Pax2), vimentin, and glial fibrillary acidic protein (GFAP), and when mature, they retain GFAP expression in addition to S100 calcium binding protein β (S100β).

In blood-brain-barrier of CNS, astrocytes are a part of the neurovascular unit. They ensheath the blood vessels and contact endothelial cells through the basement membrane of the brain endothelium. It is known that astrocytes help for VSMCs or pericytes to contract so that the blood flow can be regulated (Daneman and Prat, 2015). BBB permeability is affected by cytokines and inflammatory factors released by astrocytes such as transforming growth factor-β (TGF-β), glial cell line-derived neurotrophic factor (GDNF), basic fibroblast growth factor (bFGF), interleukin-1β (IL-1β), interleukin 6 (IL-6), and tumor necrosis factor-α (TNF-α) (Abbott, 2002). In *in vitro* co-culture studies, it is also observed that the barrier properties are increased through the upregulation of tight junction proteins and transporters in brain ECs (Heithoff et al., 2021). Another important function of astrocytes in BBB is the ion and water regulation. Due to high neuronal activity of CNS, excess water and ions need to be redistributed or eliminated. Astrocytes perform these functions by the water channel

aquaporin-4 and ATP-Sensitive Inward Rectifier Potassium Channel 10 (Kir4.1) located in their end-feet (Abbott, Rönnbäck, and Hansson, 2006).

The role of astrocytes in retina and iBRB, especially in humans, is unclear. Their major role in rodent retinae is the guidance of endothelial cells in retinal angiogenesis, apart from providing support to retinal neurons. It is speculated that, instead of astrocytes, Müller glia or ganglion cell axons can be responsible for the vessel guidance in humans (Lutty and McLeod, 2018). Also, astrocyte differentiation is triggered by soluble factors such as leukemia inhibitory factor (LIF) from retinal endothelial cells. Since the retinal astrocytes are present as early as the appearance of endothelial cells, when the iBRB is not fully functional, it is suggested that astrocytes are not directly responsible for the formation of iBRB (Langen, Ayloo, and Gu, 2019).

1.3.2.4. Müller glia

Müller glia is the largest cell type in retina, and one of the macroglial cell types along with astrocytes. They encompass the entire retina along the anterior-posterior axis. Their cell processes expand throughout the retina, which also provides a backbone structure for the retinal neurons. Müller glia closely contact photoreceptor cells and bipolar cells and are involved in metabolism of glutamate and gamma-aminobutyric acid (GABA) neurotransmitters.

The main function of Müller glia is to protect the neural retina physically, as well as release neurotrophic factors such as brain-derived neurotrophic factor (BDNF), nerve growth factor (NGF), GDNF, neurotrophin-3 (NT-3), neurotrophin-4 (NT-4) and regulate the water and ion metabolism (Eastlake, Luis, and Limb, 2020). Similar to brain astrocytes, Müller glia also possess aquaporin-4 water channel and Kir4.1 K^+ channel. Therefore, excess water and ions in extracellular space is buffered into blood vessels or vitreous humor (de Hoz et al., 2016). Regulation of water metabolism upon metabolic function is very crucial, since edema takes place if excess water cannot be removed from the retina (Reichenbach and Bringmann, 2020). They also protect the neurons against oxidative stress due to the high concentration of antioxidants they have. Besides that, their end-feet encompass the retinal vessels and form part of the neurovascular unit in the iBRB. Their role in iBRB formation and maintenance can

be observed by the induction of tight junctions between the ECs (Tout et al., 1993). Also, the expression of growth factors such as VEGF and bFGF or inflammatory cytokines is regulating angiogenesis of retinal blood vessels in injury or in pathological conditions (Bringmann and Wiedemann, 2012; Vecino et al., 2016; Graça, Hippert, and Pearson, 2018). Using Ca^{++} waves, Müller glia also help the retinal capillaries to dilate (Benfey, Foubert, and Ruthazer, 2022).

Considering their role in neuronal support, regulation of ion and water metabolism, and the maintenance of iBRB and BBB, Müller glia share numerous similarities with brain astrocytes (Vecino et al., 2016). Upon injury and chronic inflammation, Müller glia undergo gliosis, which is also observed in astrocytes in the brain (Yoo, Shanmugalingam, and Smith, 2021). Since Müller glia is encompassing the entire retina and therefore capillaries, whereas retinal astrocytes are only confined to retinal ganglion cell and optic nerve area, Müller glia may fulfill metabolic functions of astrocytes in BBB.

1.4. Diabetic retinopathy (DR)

1.4.1. Disease etiology and clinical manifestations

Diabetic retinopathy (DR) is a complication of diabetes, and the leading cause of blindness in developed countries. Disease onset can be seen as early as in prediabetic stage with a prevalence of 7.1 % (Kirthi et al. 2022). Although glycemic control and routine screening programs reduce the consequences, it still is a threatening condition for vision.

Clinically, retinal capillaries, arterioles, and venules are affected and are causing occlusions or leakages from the vessels, depending on the stage of the disease. Red spots of various sizes (< 125 µm: microaneurysm, > 125 µm: haemorrhage) is observed in DR patients. In addition to that, soft and hard exudates, and vascular abnormalities in retinal arterioles, venules, and capillaries are observed. The initial stage of the disease is referred as non-proliferative DR, where microaneursyms and cotton wool spots (retinal arteriol occlusions) are observed. In pre-proliferative DR, new retinal capillaries start to emerge. In the latest stage, namely proliferative DR (PDR), angiogenesis in retinal vessels takes place, which threatens vision if

left untreated (Scanlon, 2014). Often, macular edema follows DR, as avascular zone in macula widens and threats vision later in disease.

1.4.2. Pathophysiology of DR

Chronic hyperglycemia induces various changes in retinal vessels, especially in capillaries. Pericyte loss, basement membrane thickness, and endothelial cell apoptosis are some of the earliest effects of DR and are followed by retinal ischemia and neovascularization in later stages (Fig. 7).

As one of the earliest symptoms in DR, microaneurysms are associated with loss of pericytes in retinal capillaries (Bergers and Song, 2005). In the absence of pericytes, endothelial walls become vulnerable and lose their integrity over time. It was also shown in mice that pericyte loss has accelerated the progression of DR (Park et al., 2017).

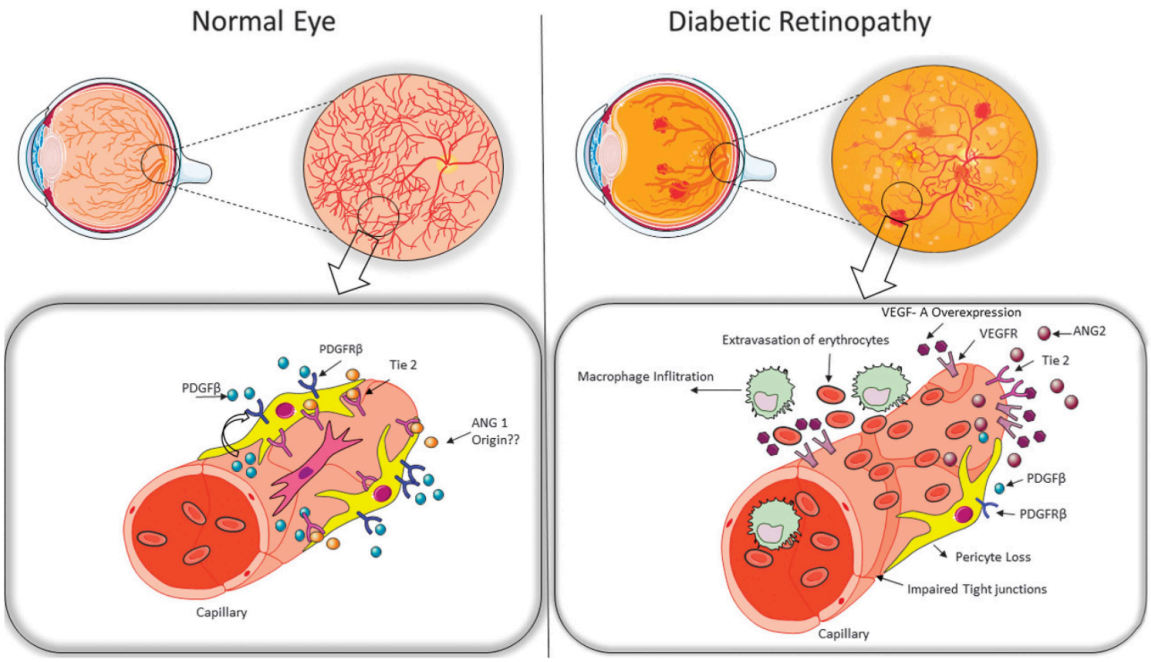


Figure 7: Microvascular changes in diabetic retinopathy. Retinal capillaries undergo several changes in DR, such as loss of pericytes, hyperpermeability, erythrocyte infiltration, VEGF increase and Ang2/Tie2 activation. *Santos et al., 2018.*

There are also various metabolic changes associated with hyperglycemia. Chronic exposure to systemic high glucose concentrations causes proteins and lipids to be glycosylated

abnormally. This class of molecules are called advanced glycation end products (AGEs) and are accumulated in retinal capillaries of DR patients over time (Koga et al., 2002). The expression of AGE receptors, namely RAGEs, are also upregulated in DR and cause an increase in oxidative stress in retinal ECs. AGEs alter the metabolic function of retinal endothelial cells, and eventually cause endothelial cell dysfunction. AGE-precursor methylgloxal (MGO) has been associated with retinal pericyte loss and increased expression of RAGEs (Matafome, Sena, and Seiça, 2013). In type 2 diabetes patients, serum levels of MGO are elevated compared to healthy individuals (Fosmark et al., 2006). Glycation of proteins such as fibrinogen and collagen, as well as immunoglobulin G (IgG) have been found to be associated with elevated MGO (Singh et al., 2014). Vascular function is affected by MGO-derived glycation of hypoxia-inducible factor-1 (HIF-1) and Müller glia-derived mammalian Histone Deacetylase Complex Subunit Sin3a (mSin3a), which in turn increases Ang2 expression in retina (Milne and Brownstein, 2014). MGO also caused retinal angiogenesis in zebrafish, as an increased retinal capillary density was detected upon treatment (Li et al., 2019). The induction of MGO-derived angiogenesis is induced through VEGF signalling. DR manifestations such as vasoregression, acellular capillaries, immune activation in addition to pericyte loss have also been observed in rats that were subject to MGO treatment without DR (Schlotterer, 2019). In cultured ECs, MGO also showed cytotoxicity and vascular dysfunction (Tóth et al., 2014; Lee et al., 2020).

Inflammatory cytokines, adhesion molecules, and growth factors such as TNF-α, IL-1β, IL-6, VEGF, Intercellular Adhesion Molecule 1 (ICAM-1) are also released in response to AGEs accumulation, which initiates the disruption of iBRB via several pathways (Gui et al., 2020).

Ang/Tie2 pathway also contributes to the regulation of DR pathology in iBRB. Binding of angiopoietins (Ang1 and Ang2) to their receptors Tie2 regulate retinal capillary permeability, and cell survival. Ang1/Tie2 interaction regulates the retinal capillary permeability and inhibits angiogenesis, whereas Ang2 has the opposite effect to Ang1. Ang2 causes increased permeability of retinal capillaries and is associated with elevated VEGF levels and a decrease in VE-cadherin in retinal ECs (Whitehead et al., 2019).

Müller glia also contribute to DR pathology and progression via a state called reactive gliosis. In healthy conditions, Müller glia respond to neural injury by extending its processes to cushion the retina or releasing pro-angiogenic factors upon hypoxia to prevent neuronal

death. However, the fine-tuning of gliosis is highly critical, since the extended effects may cause neuronal death and neovascularization (Graça, Hippert, and Pearson, 2018). DR triggers reactive gliosis via oxidative stress and metabolic changes in Müller glia, which affect the integrity of iBRB. For instance, increased VEGF release by Müller glia initiates retinal angiogenesis. Additionally, expression of matrix metalloproteases (MMPs) in extracellular matrix (ECM) degrades the tight junction proteins such as occludin and claudin in retinal endothelial cells (Coorey et al., 2012). The maintenance of tight junction proteins between retinal ECs are crucial for the integrity and impermeability of iBRB. Diabetic retinopathy also causes increased expression of GFAP and nitric oxide synthase (NOS) in Müller glia, which causes neuronal damage (Bringmann et al., 2006).

1.4.3. Current treatments

Early diagnosis with the help of national screening programs aids to control the progression of the disease. For instance, due to the National Health Service (NHS) Diabetic Eye Screening Programme, DR was no longer the major cause of blindness in working age individuals (Scanlon, 2017). Glycemic control, as well as managing blood pressure and blood lipids can also be listed as preventative measures for DR.

Current treatments for later stages of DR, laser photocoagulation, vitrectomy, and/or pharmacotherapy are routinely conducted. Laser photocoagulation uses laser beam to burn the leaky vessels to control retinal ischemia or neovascularization.

Vitrectomy is used to replace the vitreous humor with injections in eyes with DR, in order to improve visual acuity. Pharmacotherapy includes the administration of drugs such as anti-VEGF antibodies, corticosteroids and non-steroidal anti-inflammatory drugs (NSAIDs). Among those listed, anti-VEGF antibodies are the most common treatment for PDR. Ocular injections of anti-VEGF antibodies aim to stop neovascularization in patients and require continuous administrations.

Laser photocoagulation, vitrectomy, and anti-VEGF therapies mostly are administered to patients with PDR. It is shown that the benefits of these treatments are not significantly improving visual acuity in non-proliferative DR (NPDR) (Mansour et al. 2020).

1.5. Human induced pluripotent stem cell (hiPSC) generation and disease modelling

Induced pluripotent stem cells (iPSCs) are resembling embryonic stem cells, which have the potential to differentiate into cells from three germ layers (endoderm, mesoderm, ectoderm) and divide indefinitely. First discovered in 2006 by Yamanaka and colleagues, terminally differentiated murine fibroblasts were able to gain stemness with a cocktail of four transcription factors: Octamer-Binding Protein 4 (Oct3/4), Sox2, Kruppel like factor 4 (Klf4), Myc Proto-Oncogene Protein (c-Myc) (Takahashi and Yamanaka, 2006). A year later, human cells were differentiated with the same method (Takahashi et al. 2007).

During the last decade, number of protocols have been published to differentiate hiPSCs from various types of somatic cells such as keratinocytes, exfoliated renal epithelial cells, blood cells (hematopoietic stem cells, T-lymphocytes, peripheral blood mononuclear cells), mesenchymal stem cells (Swistowski et al. 2010; Brown et al. 2010; Kambal et al. 2011; Ray et al. 2021).

HiPSCs are useful in generating human cells in large quantities, which are hard to receive such as neurons and cardiomyocytes. Moreover, since the use of embryonic stem cells (ESCs) raises ethical concerns, hiPSCs serve as a great alternative due to its resemblance to ESCs and the use of easily accessible adult cells. The use of human cells instead of commonly used model organisms can also help in understanding complex diseases that do not represent common pathways.

To this day, hiPSCs are used in several fields such as drug screening, toxicity studies, disease modelling, developmental biology, and personalized medicine.

Disease modelling using hiPSCs is useful since several cell types can be generated from the genetically same cell source. Generated cells can also be obtained in large quantities due to the unlimited proliferation capacity of hiPSCs. Therefore, complex tissue or organ systems can be recapitulated, and disease onset and progression can be studied closely. A validated disease model can also be used for large amounts of candidate drugs in patient-specific human cells or tissues. Disease models involving several tissues, especially neural and cardiac, using hiPSCs are being generated in order to recapitulate diseases that are not reflected best in murine models (Chang et al. 2020).

1.6. Microfluidic chip technology

Microfluidic chips are miniaturized cell culture chips where fluidics can be applied to mimic the natural environment of a certain tissue or an organ. The design of the chips can be tailored for the scientific question associated with the studied cell or organ type. Such designs would include the geometry of the chips, incorporation of perfusion, and the production material such as polydimethylsiloxane (PDMS). Chips also offer a controlled microenvironment, where cells can be grown in desired hydrogels which mimic the *in vivo* extracellular matrix. Growth factors and drugs can also be easily applied in the culture medium, as well as mechanical cues along with perfusion. Another advantage of microfluidic chips is that it allows co-culture of various cell types in order to mimic tissue models. That is highly helpful in terms of disease modelling because one can mimic the cell interactions and manipulate them to observe the effects of these changes.

1.6.1. Blood vessel generation in 3D chips

Blood vessels can be generated in microfluidic chips using various endothelial cell sources such as human umbilical vein endothelial cells (HUVECs), microvascular endothelial cells (MVECs), or hiPSC-derived ECs. Since blood vessels are hollow tube structures, studying of endothelium requires a 3D environment. By using microfluidic chips, one can mimic the blood vessel formation *in vitro* using various hydrogels such as fibrin or laminin. Also, to mimic the blood flow within the endothelial tubes, certain chips can be perfused with a controlled shear stress, which is a mechanical cue that ECs highly respond to.

ECs can form tubes by surrounding a scaffold and forming a hollow tube or self-assemble when embedded on hydrogels of certain thickness and composition. ECs can form vessels by themselves in 3D chips, however, they can also be co-cultured with pericytes, vascular smooth muscle cells, or leukocytes. One can observe the vessel morphology and apply immunofluorescence staining to validate blood vessel parameters such as vessel diameter, branching, and apply functional tests such as dextran perfusion assay (Haase and Kamm, 2017).

Blood vessel generation on chips is used for studying vasculogenesis, physiological or pathological angiogenesis. Additionally, vascularization of complex tissue models or organoids are also highly desirable for organ-on-a-chip models.

1.6.2. Disease modelling of diabetes in 3D chips

DR is a complex complication of a systemic disease, which requires the crosstalk of many organs and cell types, as well as the blood circulation. Therefore, many parameters must be considered while modeling such a disease. Few of these parameters include 1) the way that diabetes is induced and 2) the crosstalk between ECs/PCs/and glia and neurons in the retina. DR is studied in both *in vivo* and *in vitro* disease models. Rodents and large animals are widely used in in vivo models, where either pancreatic ß-cells are damaged (by streptozotocin treatment or pancreatectomy), or by high glucose diet to induce hyperglycemia. Disease progression in animal models is time consuming and laborious, in addition to ethical concerns with their use. Additionally, the use of animal models will result in species differences in crucial pathophysiological pathways of DR and cannot be easily upscaled for drug screening (Mi et al., 2014).

Alternatively, ex vivo retinal explants can be used from both mice and human, which is useful for manipulation.

Another advanced method to model DR is 3D cell culture chips, as they can be generated to mimic a desired microenvironment and various cell types can be co-cultured to observe the cell crosstalks (Maurissen et al., 2022).

Several groups have worked on modelling DR in 3D chips with the combination of endothelial cells, pericytes, vascular smooth muscle cells, and astrocytes. However, frequently, primary, or immortalized ECs and PCs have been used to form blood vessels in the chips (Campisi et al., 2018; Ragelle et al., 2020). Primary and immortalized endothelial cells are known to lose their characteristics upon *in vitro* culturing and possess variance between lots.

Alternatively, hiPSC-derived endothelial cells and mural cells (pericytes and vascular smooth muscle cells) can be exploited for this purpose. There is a variety of endothelial cell generation protocols, depending on adherent or embryoid body (EB)-based differentiation method, small molecules used for mesoderm induction, and the type of purification method and markers used for resulting ECs (Orlova et al., 2014; Patsch et al., 2015; Jang et al., 2019). Pericyte differentiation protocols also vary depending on the derivation from mesodermal or ectodermal germ layer, as well as the marker combination used for purification or enrichment (Orlova et al., 2014; Stebbins et al., 2019; Gastfriend et al., 2021). The great advantage of hiPSC-derived cell differentiation protocols is that the cells can be generated in large

quantities, batch-to-batch variation is minimized, and personalized disease models can be generated with patient-derived hiPSC.
The use of iPSC-derived cells of NVU can pave the way for DR modelling, since using the same source of cell types would reduce the variance in cell cross-talks, as well as their potential in upscaling.

1.7. Aim of the thesis

The aim of this thesis was to generate a disease model for diabetic retinopathy using hiPSC-derived blood vessels in 3D microfluidic chip. In the initial phase of the project, hiPSC-derived endothelial cells and pericytes have been generated from the same hiPSC line. ECs and PCs proved to express cell specific markers with immunocytochemistry and flow cytometry. EC functionality have been assessed with ICAM-1 overexpression upon TNF-α exposure. In the next step, ECs and PCs have been co-cultured in a commercial 3D chip in order to mimic retinal blood vessels. ECs have formed an endothelium covered with pericytes as mural cells in fibrin gel. During that phase, a second source of pericytes (neural crest-derived PCs) have been generated as an improvement to the model. Permeability of blood vessels were analyzed using 40kDa fluorescein isothiocyanate (FITC)-dextran.

To introduce diabetes, blood vessels were exposed to hyperglycemic conditions and AGE-precursor MGO in the 3D chip. Once diabetic retinal vessels have been generated, blood vessel diameter and roundness have been measured using immunofluorescence staining and quantified.
Lastly, as an addition to the project, additional components of iBRB, hiPSC-derived Müller glia and astrocytes have been generated and characterized. Glial cells were also generated from the same hiPSC line as endothelial cells and pericytes.

In summary, during this project I developed a novel human *in vitro* iBRB model, by merging the hiPSC and microfluidic chip technology. The use of hiPSCs allowed to receive all main iBRB components (ECs, PCs, and Müller glia) from the same source, enabling the personalized approach in the future studies. Moreover, the developed model allows to study the main iBRB barrier function, since microvasculature on the chip can be perfused and the tightness of the

network can be studied, using molecules with different sizes or chemical properties. The developed iBRB chip was used to model the early stages of DR. Quantified blood vessel properties have shown that hyperglycemia did not affect vessel diameter, whereas MGO treatment significantly enlarged blood vessels compared to control vessels.

2. Material and Methods

2.1. Materials

2.1.1. Biological materials

Table 1: List of biological materials

Material Name	**Company**
Human Episomal iPSC line	Thermo Fisher Scientific, Waltham, MA, USA
Human keratinocyte-derived iPSC line (K5)	obtained from a healthy donor
Human keratinocyte-derived iPSC line (K3)	obtained from a healthy donor

2.1.2. Plasticware and tools

Table 2: List of plasticware and tools

Plasticware/Tool Name	**Company**
6-, 12-, 24-, 48-well plates (tissue-treated, non tissue-treated)	Corning, New York, NY, USA
96-well culture plate (flat bottom)	Sarstedt, Nürnbrecht, Germany
96-well culture plate (V-bottom)	Sarstedt, Nürnbrecht, Germany
Cap inserts for cyrovials 1.2 - 5 ml	Carl Roth, Karlsruhe, Germany
Cell Scraper	Thermo Fisher Scientific, Waltham, MA, USA
Cell strainer (30µm), MACS® SmartStrainer	Miltenyi Biotec, Bergisch Gladbach, Germany
CELLSTAR® cell culture flask (25 cm^2, 75 cm^2)	Greiner Bio-One, Frickhausen, Germany
Combitip® advanced (5ml, 10ml)	Eppendorf, Hamburg, Germany
Cryogenic vials (1.2 ml)	Corning, New York, NY, USA
EASY Strainer™ 40µm	Greiner Bio-One, Frickhausen, Germany
Falcon 5 ml Round Bottom Polystyrene Test Tube	Corning, New York, NY, USA
Gloves Peha-Soft® nitrile	Hartmann, Heidenheim, Germany
idenTx 3 chip	AIM Biotech, Nucleos, Singapore
LS Column	Miltenyi Biotec, Bergisch Gladbach, Germany

MACS™ MultiStand	Miltenyi Biotec, Bergisch Gladbach, Germany
Microtiter Plate Holder with Cover	AIM Biotech, Nucleos, Singapore
MidiMACS™ Separator	Miltenyi Biotec, Bergisch Gladbach, Germany
Petri dishes (6 cm, 10 cm)	Greiner Bio-One, Frickhausen, Germany
Pipette tips (10 µl, 100µl, 200 µl, 1 ml, 5 ml)	Eppendorf, Hamburg, Germany
Reaction tubes (0.5 ml, 1.5 ml, 2.0 ml)	Sarstedt, Nürnbrecht, Germany
Reaction tubes (15 ml, 50 ml)	Sarstedt, Nürnbrecht, Germany
Serological pipette (5 ml, 10 ml, 25 ml, 50 ml)	Sarstedt, Nürnbrecht, Germany
Sterile filter (0.22 µm)	Merck Millipore, Darmstadt, Germany
Ultra-Fine-Clipper-Scissors-II	Fine Science Tools, Heidelberg, Germany

2.1.3. Cell culture equipment and devices

Table 3: List of cell culture equipment and devices

Equipment/Device Name	**Company**
Centrifuge, Heraeus™ MegaFuge™ 16	Thermo Fisher Scientific, Waltham, MA, USA
Confocal LSM510 Meta	Zeiss, Oberkochen, Germany
FACS Aria II cell sorter	BD Biosciences, Franklin Lakes, NJ, USA
EVOS® FL Cell Imaging System	Thermo Fisher Scientific, Waltham, MA, USA
Galaxy 5D Digital Microcentrifuge	VWR, Radnor, PA, USA
Heraus 6000 Incubator	Thermo Fisher Scientific, Waltham, MA, USA
Incubator 37°C Heracell™ 240i	Thermo Fisher Scientific, Waltham, MA, USA
Lab Line Water Bath	Thermo Fisher Scientific, Waltham, MA, USA
BD LSRFortessa™ Cell Analyzer	BD Biosciences, Franklin Lakes, NJ, USA
Microscope Axio Imager M2	Zeiss, Oberkochen, Germany
Microscope Axio Observer Z1	Zeiss, Oberkochen, Germany
Mr. Frosty™ Freezing Container	Thermo Fisher Scientific, Waltham, MA, USA
MSC-Avdan	
Multipipette® E3x	Eppendorf, Hamburg, Germany
Pipetus®	Hirschmann Laborgeräte, Eberstadt, Germany
Primovert Compact Inverted Microscope	Zeiss, Oberkochen, Germany
Vacuum pump Integra Vacusafe	Integra Biosciences, Biebertal, Germany

Vortex Mixer, 7-2020	Neolab, Heidelberg, Germany

2.1.4. Cell culture media

Table 4: List of cell culture media

Medium Name	**Company**
DMEM, high glucose, pyruvate	Thermo Fisher Scientific, Waltham, MA, USA
DMEM/F-12 (1:1) (1X)	Thermo Fisher Scientific, Waltham, MA, USA
DMEM/F-12 (1:1) (1X) + 15mM HEPES	Thermo Fisher Scientific, Waltham, MA, USA
DMEM/F-12 (1:1) (1X) + GlutaMAX™-I	Thermo Fisher Scientific, Waltham, MA, USA
Endothelial Cell Growth Medium MV (Ready-to-use)	PromoCell, Heidelberg, Germany
Essential 8™ Medium	Thermo Fisher Scientific, Waltham, MA, USA
Human Endothelial SFM	Thermo Fisher Scientific, Waltham, MA, USA
IMDM, no phenol red	Thermo Fisher Scientific, Waltham, MA, USA
Neurobasal® Medium (1X)	Thermo Fisher Scientific, Waltham, MA, USA
NutriFreez™ D10 cryopreservation medium, ACF, Protein-free	Biological Industries, Kibbutz Beit Haemek, Israel
PeproGrow™ hESC (embryonic stem cell) medium	PeproTech, Hamburg, Germany
Pericyte Medium (PM)	ScienCell, Carlsbad, CA, USA
StemFlex™ medium	Thermo Fisher Scientific, Waltham, MA, USA
StemPro®-34 SFM (1X)	Thermo Fisher Scientific, Waltham, MA, USA
Synth-A-Freeze® cryopreservation medium	Thermo Fisher Scientific, Waltham, MA, USA

2.1.5. Coatings

Table 5: List of coatings

Coating Name	**Company**
Gelatin from porcine skin	Sigma-Aldrich, St. Louis, MO, USA
Geltrex®, hESC-qualified	Thermo Fisher Scientific, Waltham, MA, USA
Human Plasma Fibronectin Purified Protein	Merck Millipore, Darmstadt, Germany
Matrigel®, growth factor reduced	Corning, New York, NY, USA
Matrigel®, hESC-qualified	Corning, New York, NY, USA
Vitronectin (VTN-N)	Thermo Fisher Scientific, Waltham, MA, USA

2.1.6. Other chemicals

Table 6: List of other chemicals

Chemical Name	**Company**
(-)-Blebbistatin	Sigma-Aldrich, St. Louis, MO, USA
β-Mercaptoethanol	Thermo Fisher Scientific, Waltham, MA, USA
AccuMAX™ solution	Sigma-Aldrich, St. Louis, MO, USA
Activin A	Cell Guidance Systems LLC, St. Louis, MO, USA
Ampuwa®	Fresenius Kabi, Bad Homburg vor der Höhe, Germany
Antibiotic-Antimycotic	Thermo Fisher Scientific, Waltham, MA, USA
Ascorbic acid	Carl Roth, Karlsruhe, Germany
B-27™ without Vitamin A	Thermo Fisher Scientific, Waltham, MA, USA
BD™ CompBeads Anti-mouse Ig, κ	BD Biosciences, Franklin Lakes, NJ, USA
BD™ CompBeads Negative Control	BD Biosciences, Franklin Lakes, NJ, USA
Bio-Pure Human Serum Albumin	Biological Industries, Kibbutz Beit Haemek, Israel
BMP-4	PeproTech, Rocky Hill, NJ, USA
Bovine Serum Albumin	Sigma-Aldrich, St. Louis, MO, USA
Calcein, AM, cell-permeant dye	Thermo Fisher Scientific, Waltham, MA, USA
Chemically defined lipid concentrate	Thermo Fisher Scientific, Waltham, MA, USA

CHIR99021	Selleckchem, Munich, Germany
D-Mannitol	Sigma-Aldrich, St. Louis, MO, USA
D(+)-Glucose	Thermo Fisher Scientific, Waltham, MA, USA
DAPI	Sigma-Aldrich, St. Louis, MO, USA
Dispase	Thermo Fisher Scientific, Waltham, MA, USA
DMSO	Corning, New York, NY, USA
Dorsomorphine dihydrochloride	Tocris Bio-techne, Wiesbaden-Nordenstadt, Germany
EDTA BioChemica	AppliChem, Darmstadt, Germany
EGF	Cell Guidance Systems LLC, St. Louis, MO, USA
Ethanol 99%	SAV Liquid Production, Flintsbach am Inn, Germany
Fetal bovine serum (FBS)	Thermo Fisher Scientific, Waltham, MA, USA
Fibrinogen from bovine plasma	Corning, New York, NY, USA
Forskolin	Sigma-Aldrich, St. Louis, MO, USA
GlutaMAX™ Supplement	Thermo Fisher Scientific, Waltham, MA, USA
Hanks' Balanced Salt Solution (HBSS) (1X)	Thermo Fisher Scientific, Waltham, MA, USA
Heparin sodium salt from porcine intestinal mucosa	Sigma-Aldrich, St. Louis, MO, USA
Holotransferrin	Sigma-Aldrich, St. Louis, MO, USA
Holotransferrin	Sigma-Aldrich, St. Louis, MO, USA
Human recombinant insulin	Sigma-Aldrich, St. Louis, MO, USA
Ins/Trans/SodSel (ITS)	BD Biosciences, Franklin Lakes, NJ, USA
Isopropanol 100%	SAV Liquid Production, Flintsbach am Inn, Germany
KnockOut™ Serum Replacement	Thermo Fisher Scientific, Waltham, MA, USA
Methanol	Merck Millipore, Burlington, MA, USA
Methylgloxal solution	Sigma-Aldrich, St. Louis, MO, USA
N2 Supplement	Thermo Fisher Scientific, Waltham, MA, USA
Non Essential Amino Acids (NEAA)	Thermo Fisher Scientific, Waltham, MA, USA
Normal donkey serum	Sigma-Aldrich, St. Louis, MO, USA
Paraformaldehyde	Carl Roth, Karlsruhe, Germany
Phosphate-buffered saline (PBS) w/o Mg^{++} and Ca^{++}	Thermo Fisher Scientific, Waltham, MA, USA
Platelet-poor Plasma derived Serum (PPDS)	Alfa Aesar, Heysham, UK
ProLong™ Gold Antifade Mountant	Thermo Fisher Scientific, Waltham, MA, USA

Progesterone 2mM	Sigma-Aldrich, St. Louis, MO, USA
Putrescin (1,4 Diaminobutane dihydrochloride)	Sigma-Aldrich, St. Louis, MO, USA
Recombinant human FGF-2	PeproTech, Rocky Hill, NJ, USA
Recombinant human TGFβ	Cell Guidance Systems LLC, St. Louis, MO, USA
RevitaCell™ Supplement (100X)	Thermo Fisher Scientific, Waltham, MA, USA
ROCK inhibitor (Y-27632)	Stem Cell Technologies, Vancouver, BC, Canada
SB431542	Selleckchem, Munich, Germany
Sodium bicarbonate 7.5% solution	Thermo Fisher Scientific, Waltham, MA, USA
Sodium Pyruvate 100 mM (100X)	Thermo Fisher Scientific, Waltham, MA, USA
Sodium selenite 3 mM	Sigma-Aldrich, St. Louis, MO, USA
StemPro Accutase	Thermo Fisher Scientific, Waltham, MA, USA
Sucrose	Carl Roth, Karlsruhe, Germany
Taurine	Sigma-Aldrich, St. Louis, MO, USA
Thrombin	Sigma-Aldrich, St. Louis, MO, USA
Triton™ X-100	Sigma-Aldrich, St. Louis, MO, USA
Trypan Blue Solution	Sigma-Aldrich, St. Louis, MO, USA
TrypLE™ Express	Thermo Fisher Scientific, Waltham, MA, USA
VEGF-A	PeproTech, Rocky Hill, NJ, USA
Versene 1:5000 (1X)	Thermo Fisher Scientific, Waltham, MA, USA
Water, demineralized	Carl Roth, Karlsruhe, Germany
Mini-PROTEAN TGX Precast Gels	Bio-Rad, Hercules, CA, USA

2.1.7. Primary antibodies

Table 7: List of primary antibodies

Antibody Name	**Host Species**	**Catalog Nr.**	**Company**	**Dilution**
CD146	mouse	361001	BioLegend, San Diego, USA	1:100
CD31	mouse	ab9498	Abcam, Cambridge, UK	1:100
CD31	rabbit	ab28364	Abcam, Cambridge, UK	1:100
Claudin-5	mouse	35-2500	Invitrogen, Waltham, MA, USA	1:100

Collagen IV	goat	AB769	Chemicon, Limburg, Germany	1:50
CRALBP (B2)	mouse	ab15051	Abcam, Cambridge, UK	1:250
Erg-1/2/3	mouse	sc-376293	Santa Cruz Biotechnology, USA	1:100
GFAP	mouse	MAB360	Chemicon, Limburg, Germany	1:100
Glutamine synthase	mouse	MAB302	Merck Millipore, Darmstadt, Germany	1:500
Hoechst	N/A	33342	Thermo Fisher Scientific, Waltham, MA, USA	1:1000 (1mg/ml)
ICAM-1	mouse	MA5-13021	Thermo Fisher Scientific, Waltham, MA, USA	1:50
ICAM-1	rabbit	AB53013	Abcam, Cambridge, UK	1:100
NG2	rabbit	AB5320	Chemicon, Limburg, Germany	1:100
Pax6	rabbit	901301	BioLegend, San Diego, USA	1:100
PDGFRβ	rabbit	3169T	Cell Signalling Technology, Cambridge, UK	1:100
S100β	rabbit	ab52642	Abcam, Cambridge, UK	1:150
Sox9	rabbit	ab5535	Merck Millipore, Darmstadt, Germany	1:100
Tubulin β3	mouse	801202	BioLegend, San Diego, USA	1:250
VE-cadherin	rabbit	#2158	Cell Signalling Technology, Cambridge, UK	1:100
Vimentin	chicken	ab73159	Abcam, Cambridge, UK	1:150
ZO-1	mouse	33-9100	Invitrogen, Waltham, MA, USA	1:50

2.1.8. Secondary antibodies

Table 8: List of secondary antibodies

Antibody Name	**Host Species**	**Catalog Nr.**	**Company**	**Dilution**
Anti-chicken IgY H&L (AlexaFluor® 647)	goat	ab150171	Abcam, Cambridge, UK	1:300

Anti-goat IgG H&L (AlexaFluor® 647)	donkey	ab150131	Abcam, Cambridge, UK	1:300
Anti-mouse IgG H&L (AlexaFluor® 488)	donkey	ab150105	Abcam, Cambridge, UK	1:300
Anti-mouse IgG H&L (AlexaFluor® 488)	donkey	Ab175472	Abcam, Cambridge, UK	1:300
Anti-mouse IgG H&L (AlexaFluor® 647)	donkey	ab150107	Abcam, Cambridge, UK	1:300
Anti-rabbit IgG H&L (AlexaFluor® 488)	donkey	ab150073	Abcam, Cambridge, UK	1:300
Anti-rabbit IgG (H+L) Highly Cross-Adsorbed (AlexaFluor® Plus 488)	donkey	A32790	Invitrogen, Waltham, MA, USA	1:500
Anti-rabbit IgG H&L (AlexaFluor® 568)	donkey	ab175470	Abcam, Cambridge, UK	1:300
Anti-rabbit IgG H&L (AlexaFluor® 647)	donkey	ab150075	Abcam, Cambridge, UK	1:300

2.1.9. Coupled antibodies

Table 9: List of coupled antibodies

Antibody Name	**Host Species**	**Catalog Nr.**	**Company**	**Dilution**
CD31-488	mouse	ab215911	Abcam, Cambridge, UK	1:100

CD44-FITC	mouse	ab9498	BioLegend, San Diego, USA	1:50
Phalloidin-647		ab28364	Invitrogen, Waltham, MA, USA	1:500

2.1.10. Kits and assays

Table 10: List of kits

Kit or Assay Name	**Company**
CD31 MicroBead Kit, human	Miltenyi Biotec, Bergisch Gladbach, Germany
Click-iT TUNEL Alexa Fluor™ 488 Imaging Assay	Thermo Fisher Scientific, Waltham, MA, USA
Neural Crest Stem Cell MicroBeads	Miltenyi Biotec, Bergisch Gladbach, Germany
Neurosphere Dissociation Kit	Miltenyi Biotec, Bergisch Gladbach, Germany

2.1.11. Softwares

Table 11: List of softwares

Software Name	**Company**
Adobe Illustrator	https://www.adobe.com/au/
BioRender	biorender.com
Flowing software	https://bioscience.fi/services/cell-imaging/flowing-software/
GraphPad Prism	GraphPad Software
ImageJ (Fiji)	https://imagej.net/Fiji/Downloads
Zen 3.0 (blue edition)	Zeiss, Oberkochen, Germany
Image Studio™ Acquisition Software	LI-COR, Lincoln, NE, USA

2.2. Methods

2.2.1. hiPSC culture

In this project, three hiPSC lines were used: two of them were keratinocyte derived (K3 and K5, add ref.) and the other one was an episomal commercial line. For most of the experiments, hiPSCs were cultured in Essential 8™ medium and on Geltrex® (hESC-qualified) coating. RO and astrocyte differentiation required hiPSCs to be grown in FTDA medium (adapted from Frank et al. 2012) on Matrigel® (hESC-qualified) coating. Cells on Essential 8™ medium were passaged with Versene solution every 4-5 days with a ratio of 1:8-1:12, when they reached 85% confluency. Differentiated cells were manually scratched to retain stemness. When required, hiPSCs were cryopreserved in Nutrifreeze medium in Mr. Frosty™ Freezing Container as colonies and thawed with 1:100 RevitaCell supplement. When singularization was required, cells were detached with TrypLE, counted and plated according to the required cell density. All hiPSCs were incubated in humidified incubators in 37°C with 5% O_2 and 5% CO_2.

Table 12: Composition of hiPSC media

Medium Name	Medium Recipe
Essential™ 8 medium	Essential™ 8 Basal medium
	1% Essential™ 8 Supplement
	1X Antibiotic-Antimycotic (100 U/ml penicillin, 100 µg/ml streptomycin, 250 ng/ml Gibco amphotericin B)
FTDA Medium	DMEM:F12 + Glutamax™ medium
	0.1% Human Serum Albumin
	1:100 Chemically Defined Lipid Concentrate
	5 ng/ml Activin A
	10 ng/ml FGF2
	0.5 ng/ml TGFβ
	50 nM Dorsomorphin
	1X Antibiotic-Antimycotic (100 U/ml penicillin, 100 µg/ml streptomycin, 250 ng/ml Gibco amphotericin B)

For endothelial cell differentiation, unless otherwise indicated, mCherry-infected hiPSCs were used for visualization of blood vessels during chip cultures.

2.2.2. Endothelial cells and mesodermal pericyte differentiation

Endothelial cell and mesodermal pericyte differentiation were carried out followed from a published protocol with minor modifications (Pars et al. 2021). Cells from K3 and K5 hiPSC lines were produced without the minor modifications stated here. Same differentiation protocol was carried out for both cell types up to MACS separation.

Differentiations were started with healthy, about 85% confluent hiPSCs grown in E8 medium. On D-1, hiPSCs were singularized with TrypLE and $0.5x10^6$ -$0.7x10^6$ cells were plated on non tissue-treated 6-well-plates in 3 ml of aggregation medium with 10µM ROCK-inhibitor Y-27632. The next day (D0), aggregate diameters were checked with EVOS microscope to ensure their size for an efficient differentiation. Since small aggregates will not grow fast enough and big aggregates will start developing necrotic cores, diameter between 50µm-100µm were considered ideal. Aggregates were then collected in a Falcon tube for media exchange in 37°C for about 35 minutes. Once the aggregates settled, aggregation medium was exchanged with N2B27 medium with 12µM CHIR99021 and 60 ng/ml BMP-4 for mesoderm induction. Cells were kept in N2B27 medium until D3 and were resuspended by pipetting up and down to stop clumping of aggregates. On D3, aggregates were collected in a Falcon tube and in 5-10 minutes after, they were settled, and medium was exchanged to N2B27 medium with 2 µM forskolin and 100 ng/ml VEGF-A for vascular specification. Until D5, no medium change was required, and aggregated were resuspended only. Cells were starting to attach on the wells on D5, and that usually was a sign of an efficient differentiation. On D5, 6-well-plates were coated with 0.2% gelatin for at least 1 hour in 37°C (2 gelatin-coated wells for 1 well of differentiation was needed). After the aggregates were collected, medium was replaced to 1,5 ml StemPro-34 + 100 ng/ml VEGF-A, 100 ng/ml FGF-2 and 10µM SB451342 and aggregates were seeded on gelatin-coated plates. In this step, it was important to distribute the aggregates equally in the plate, since cells needed adequate space to grow and differentiate in the next 4-5 days.

After the embedding on D5, 3D aggregates were switched to adherent culture from suspension culture and endothelial cell and pericyte morphologies were detectable.

StemPro-34 medium with 100 ng/ml VEGF-A, 100 ng/ml FGF-2 and 10µM SB451342 was replaced on D7 and D9. When cells were confluent on D9 or D10, MACS separation with CD31 MicroBead kit was carried out according to manufacturer's instructions. With this joint protocol for endothelial cells and pericytes, after MACS separation, $CD31^+$ cells were cultured as endothelial cells and $CD31^-$ population as mesodermal pericytes.

Following MACS separation, endothelial cells were cultured with a density of 30.000 cells/cm^2 on 0.2% gelatin-coated plates in MV medium with 30 ng/ml VEGF-A and 20ng/ml FGF-2, and 10µM Y-27632 to increase cell survival. The next day, medium was replaced with MV medium + 30 ng/ml VEGF-A and 20ng/ml FGF-2 and thereafter changed every other day. ECs could be cultured up to passage 4.

Pericytes were cultured on 0.2% gelatin-coated plates in Pericyte Medium with 10µM Y-27632 with a density of 15.000 cells/cm^2. Medium was changed to Pericyte Medium only the next day and thereafter every other day. Passaging of pericytes were possible until passage 6.

Both ECs and mesodermal PCs could be cryopreserved immediately after MACS or during cell culture, whenever they reached 95-100% confluency. Cryopreservation medium consisted of 50% FBS, 40% culture medium, and 10% DMSO. When thawed, 10µM ROCK-inhibitor Y-27632 was added to the respective culture medium for 1 day.

All cell types except for hiPSCs were incubated in humidified incubators in 37°C and 5% CO_2, in normoxia.

Table 13: Composition of endothelial cells and pericyte differentiation media

Medium Name	Medium Recipe
Aggregation Medium	DMEM:F12 + GlutaMAX™ medium
	20% KnockOut™ Serum Replacement
	2mM GlutaMAX™ Supplement (L-alanyl-L-glutamine)
	1X Non-Essential Amino Acids
	1X Antibiotic-Antimycotic (100 U/ml penicillin, 100 µg/ml streptomycin, 250 ng/ml Gibco amphotericin B)
	0.5 mM β-mercaptoethanol
N2B27 Medium	1:2 DMEM:F12 + Glutamax™ medium
	1:2 Neurobasal medium

	2mM GlutaMAX™ Supplement (L-alanyl-L-glutamine)
	1% B27 supplement
	1% N2 supplement
	1X Antibiotic-Antimycotic (100 U/ml penicillin, 100 µg/ml streptomycin, 250 ng/ml Gibco amphotericin B)
	0.5 mM β-mercaptoethanol
StemPro-34 Medium	StemPro™-34 SFM Basal Medium
	1% StemPro™-34 Nutrient Supplement
	2mM GlutaMAX™ Supplement (L-alanyl-L-glutamine)
	1X Antibiotic-Antimycotic (100 U/ml penicillin, 100 µg/ml streptomycin, 250 ng/ml Gibco amphotericin B)
	15% Fetal Bovine Serum
MV Medium	Endothelial Cell Growth Medium MV
	SupplementMix - Endothelial Cell Growth Medium MV
	1X Antibiotic-Antimycotic (100 U/ml penicillin, 100 µg/ml streptomycin, 250 ng/ml Gibco amphotericin B)
Pericyte Medium	Pericyte Medium (PM)
	1% Pericyte Growth Supplement
	2% Fetal Bovine Serum
	1X Antibiotic-Antimycotic (100 U/ml penicillin, 100 µg/ml streptomycin, 250 ng/ml Gibco amphotericin B)

2.2.3. Neural crest stem cell differentiation

Neural crest stem cell differentiation was carried out according to the protocol Gastfriend et al. 2021, with minor modifications.

On D0, plates were coated with Matrigel® (growth factor reduced) for at least 1 hour in 37°C. Healthy and confluent hiPSCs were singularized using TrypLE, and $0.875x10^6$ cells / 6-well-plate were plated in Matrigel-coated wells in Essential 8™ medium with 10µM Y-27632 and cells were switched to normoxic incubator.

Medium was replaced to E6-CSFD medium on D1. Cells were split with StemPro Accutase with 1:6 ratio until D15, whenever they reached 90% confluency. This usually corresponded to every 3-4 days. Medium was refreshed daily. On D15, MACS was performed with Neural Crest

Stem Cells MicroBeads according to manufacturer's instructions. Separated cells were plated on Matrigel-coated plates in E6-CSFD medium and medium was changed every day. Alternatively, neural crest stem cells could be cryopreserved on D15 following MACS separation. Cryopreservation medium consisted of 60% FBS, 30% E6-CSFD medium, and 10% DMSO. Cell culture lasted until passage 3.

Table 14: Composition of NCSCs and ectodermal pericyte media

Medium Name	Medium Recipe
E6 Medium	DMEM:F12 + HEPES medium
	1% ITS
	64 mg/l ascorbic acid
	543 mg/l sodium bicarbonate ($NaHCO_3$)
	1X Antibiotic-Antimycotic (100 U/ml penicillin, 100 µg/ml streptomycin, 250 ng/ml Gibco amphotericin B)
E6-CSFD Medium	E6 Medium
	22.5 µg/ml Heparin sodium salt
	10 ng/ml FGF-2
	10 µM SB431542
	1 µM dorsomorphin
	1 µM CHIR99021

2.2.4. Neural crest stem cell-derived (ectodermal) pericyte differentiation

Ectodermal pericyte differentiation from neural crest stem cells was carried out according to Gastfriend et al. 2021, with minor modifications.

Neural crest stem cells (NCSCs) were detached with StemPro Accutase and cultured on uncoated cell culture plates in a density of 20.000 cells/cm^2 in E6-CSFD medium with 10µM Y-27632. The following day, dead cells were washed with Dulbecco's Phosphate Buffered Saline (DPBS) and medium was replaced with E6 medium + 10% FBS and thereafter changed daily. Cells were split 3-4 days after the differentiation with StemPro Accutase in 1:2 ratio. NCSCs were differentiated into ectodermal pericytes in 7-9 days (or D22-D24 from the beginning of NCSC differentiation), with 85-95% confluency.

Since passaging was not recommended, ectodermal pericytes were cryopreserved on 3rd or 4th days of differentiation (or D18-D19) in 60% FBS, 30% E6 medium, and 10% DMSO. When needed, they were thawed, and the differentiation continued until D22-D24 as usual.

2.2.5. Astrocyte differentiation

Astrocyte differentiation was based on the protocol published by Krencik and Zhang, 2011 with major modifications.

Initially, hiPSCs grown in FTDA medium were singularized with TrypLE and plated in 96-well-plates as 20.000 cells/well in PeproGrow™ medium with 10µM Y-27632. Medium was replaced with N2 medium on D1, and on D4 or D5. On D7, embryoid body formation was achieved and EBs were transferred to Matrigel® (growth factor reduced) coated plates for neural rosette formation. In order to do that, 6-well-plates were coated with Matrigel® for at least 1 hour in 37°C. Once the coating was ready, EBs were seeded in 6-well-plates (32 EBs per well) in N2 medium. It was critical to distribute the EBs equally in the culture plates to allow adequate neural rosette formation. From D7 on, N2 medium was refreshed every second day and on D15, neural rosettes could be distinguished and were picked with a 1000 µl pipette tips by manual force. About 48 neural rosettes were transferred into 100 mm petri dishes and cultured in N2 medium as suspension culture. Medium was changed every second day until D21. On D21, N2 medium was supplemented with 10 ng/ml EGF and 10 ng/ml FGF-2 and replaced every second day until D90. During this time, spheres were partially dissociated every 7 days by up-and-down movements of pipette tips (1000 µl and 100 µl pipette tips were stacked on top of each other to help dissociation). Partial dissociation was required to favor astroglial progenitor growth instead of neuroepithelial clusters. Between D90-D120, astrospheres were ready to be dissociated and grown in adherent cultures. For that purpose, culture plates were coated with 7,5 µg/ml fibronectin dissolved in Hanks' Balanced Salt Solution (HBSS). Plates had to be dried under the hood for 40 minutes to ensure adequate fibronectin-coating. During the course of coating, astrospheres were collected in Falcon tube. After the spheres have settled, medium was discarded, and spheres were washed with 2 ml DPBS. After that, all DPBS was removed and 1 ml of prewarmed AccuMAX™ solution was added to the Falcon tube and the spheres were incubated in 37°C for 5 minutes. After 5 minutes, spheres were resuspended 10-15 times to help the dissociation and

incubated for additional 10-15 minutes. After the second incubation period, spheres were dissociated with stacked 1000 µl and 100 µl pipette tips and slowly disintegrated by up-and-down movements of the tips. Disintegration followed until no clumps were seen in the Falcon tube. If clumps could not be dissociated, cells would be incubated for an additional 5 minutes in 37°C. When all the cells were singularized, 3 ml of Dulbecco's Modified Eagle Medium (DMEM) was added to the Falcon to stop the reaction and cells were centrifuged in 300 x g for 5 minutes. Since dissociation would bring about cell death, live cell were counted with Trypan Blue solution and 30.000-35.000 cells/cm^2 were plated on fibronectin-coated plates in N2 medium with 10 ng/ml EGF, 10 ng/ml FGF-2, and 10µM Y-27632 to increase cell survival. The next day, dead cells were washed with DPBS and medium was replaced, and astrocytes would reach confluency approximately in 7 days. When confluent, astrocytes could be cryopreserved (in 90% FBS and 10% DMSO medium) or passaged up to passage 4.

Table 15: Composition of astrocyte medium

Medium Name	Medium Recipe
N2 Medium	DMEM:F12 + GlutaMAX™ medium
	88 µM putrescin
	16 nM progesterone
	20 µg/ml insulin
	80 µg/ml holotransferrin
	24 nM sodium selenite
	1X Non-Essential Amino Acids
	1X Antibiotic-Antimycotic (100 U/ml penicillin, 100 µg/ml streptomycin, 250 ng/ml Gibco amphotericin B)

2.2.6. Müller glia isolation from retinal organoids

Retinal organoids were grown according to the protocol published by Zhong et al. 2014 with minor modifications (Achberger, K 2018).

Since Müller glia markers in retinal organoids (ROs) were detected as early as D125, retinal organoids of D125 age or older were used for isolation. Between 15-20 healthy retinal organoids were picked and dissociated with Neurosphere Dissociation Kit according to manufacturer's instructions. This kit made sure that tightly connected cells in retinal

organoids were singularized smoothly. Once dissociation was completed, cells were centrifuged in 300 x g for 5 minutes and resuspended in Müller glia medium with 40 ng/ml FGF-2 and 40 ng/ml EGF. Culture plates were coated with 10 µg/ml fibronectin dissolved in HBSS before the isolation and let dry under the hood for 40 minutes. Live/dead counting was performed with Trypan Blue Solution and cells were plated with a density of 10 ROs per one well of 48-well-plate. On the day of isolation, 10µM of Y-27632 was added to the Müller glia medium, and after that medium was refreshed every second day. Initially, neurons within ROs have attached on Müller glia in culture plates and were washed off 2-3 days after plating and only Müller glia survived and proliferated. Müller glia could be cryopreserved with Synth-A-Freeze® cryopreservation medium and expanded in culture for 4 passages.

Table 16: Composition of Müller glia medium

Medium Name	Medium Recipe
Müller Glia Medium	DMEM:F12 + GlutaMAX™ medium
	10% Fetal Bovine Serum
	2mM GlutaMAX™ Supplement (L-alanyl-L-glutamine)
	1X Non-Essential Amino Acids
	1X Antibiotic-Antimycotic (100 U/ml penicillin, 100 µg/ml streptomycin, 250 ng/ml Gibco amphotericin B)

2.2.7. 3D cell culture chip loading

Blood vessel formation was performed in a commercial 3D cell culture chip (idenTx 3, AIM Biotech). One chip consisted of 3 channels, which independently possessed one 3D gel channel, where cells can be loaded and two media channels, where the cells were nourished. For blood vessel formation, endothelial cells and pericytes loaded in the 3D gel channel. For that purpose, initially, 3D gel components fibrinogen and thrombin were prepared. Fibrinogen was diluted in DPBS in a concentration of 6 mg/ml and placed in water bath at 37°C for solubilization for at least 1 hour. After it was dissolved, it was sterilized using a 0.22 µm low-protein binding filter and kept in 4°C. Thrombin was solubilized in sterile H_2O in 100 U/ml and was kept in -20°C.

Once the gel components were prepared, endothelial cells and pericytes in 6-well-plates were washed with DPBS once and incubated with 0,5 ml of AccuMAX™ solution at 37°C. ECs were detached in 5-7 minutes, whereas pericytes were detached in ~3 minutes. When all the cells were detached, they were resuspended to ensure singularization. Reaction was then stopped with 2 ml of MV medium for both cell types. Ectodermal pericytes were occasionally clumped, and if that was observed, cells were strained with 70 µm and 40 µm strainers, respectively. Cells were centrifuged at 300 x g for 5 minutes and kept on ice after that point. Following centrifugation, supernatant was removed, and cells were resuspended in 10µl of resuspension medium (4 U/ml thrombin dissolved in MV medium). At that point, each cell suspension was diluted around 1:60 ratio and counted. Endothelial cells and pericytes were mixed in a total concentration of $16x10^6$ cells/ml ($8x10^6$/ml of each cell type in the case of 1:1 ratio of endothelial cell : pericyte) and medium was adjusted to 5 µl/channel. Afterwards, 5 µl fibrinogen was mixed with 5µl of cell suspension, mixed briefly and loaded in the gel channel through the gel inlet. End concentration of all the cells in the chip then was $8x10^6$ cells/ml (40.000 endothelial cells + 40.000 pericytes in 1:1 ratio). Chips were placed in chip holders, humidified with sterile H_20 in holder reservoirs, and incubated at 37°C for 1 hour for gel polymerization. After 1 hour, MV medium + 30 ng/ml and 20 ng/ml were added in media channels. Medium was replaced daily, and cell were usually cultured up to D6.
Cell number and concentration was adjusted accordingly in case of different ratios of cells (endothelial cells, pericytes, or Müller glia) in the chip.

2.2.8. Immunocytochemistry assay

Immunofluorescence stainings were carried out with cryosectioned samples, cell grown in cover slips, and in 3D cell culture chips.

Prior to fixing, cells were washed with DPBS once. Then, they were fixed with 4% paraformaldehyde (PFA) for 20 minutes at room temperature (RT). After fixation, cells were washed with DPBS three times and blocked and permeabilized with staining buffer (10% normal donkey serum (NDS) + 0.2% Triton-X-100 + 1% Antibiotic-Antimycotic) for 1 hour at RT. For nuclear marker stainings, an extra permeabilization step followed with 0.5% Triton-X-100 for 5 minutes at RT. After that, cells were incubated with primary antibodies (see Table 7

and 8) diluted in staining buffer at 4°C overnight. Once primary antibody incubation was finished, cells were washed three times with DPBS and incubated with secondary antibodies (see Table 9) diluted in staining buffer for 2 hours at RT (cryosections and coverslips) or at 4°C overnight (chips). Cells were washed with DPBS three times and incubated with 4',6-diamidino-2-phenylindole (DAPI) or Hoechst for nuclei staining 10 minutes (cryosections and coverslips) or 1 hour at RT (chips). Cells were washed with DPBS three times after that, mounted with ProLong™ Gold Antifade Mountant and visualized in respective microscopes.

2.2.9. Microscopy

Blood vessel formation in the 3D cell culture chips and phase contract images of cells in culture was acquired using EVOS® FL Cell Imaging System.
Fluorescence micrographs were mostly obtained with Microscope Axio Imager M2. For full-length cell culture chip images, Microscope Axio Observer Z1 was used, and images were taken as tiles.

2.2.10. Tube formation assay

Coating was prepared in 96-well-plate with 75µl undiluted Matrigel® (growth factor reduced, phenol-red free) for 10 min at RT followed by 30 min. incubation at 37°C. For tube formation, endothelial cells were singularized using AccuMAX™ solution and 25.000 cells/cm^2 and 125µl ECs were plated onto coated 96-well-plates. ECs were incubated at 37°C for 16 hours to allow tube formation. Afterwards, they were washed with DPBS once and incubated with Calcein AM for live staining for 30 minutes at 37°C. Following an additional wash with DPBS after Calcein AM staining, tubules were ready to be observed with EVOS® FL Cell Imaging System.

2.2.11. Flow cytometry

Majority of flow cytometry experiments were performed with fixed samples that were stored in -20°C to reduce the workload on the same day. For that purpose, endothelial cells or pericytes were washed with DPBS once, detached with AccuMAX™ solution. To prevent clumping, cells were strainer through 30 µm cell strainer and centrifuged at 300 x g for 5 minutes. Supernatant was discarded and for fixation, pellet was resuspended with 1 ml of 1% PFA for 15 minutes at 37°C. Once fixing was finished, permeabilization followed with 9 ml ice

cold 99% methanol, that was added dropwise while vortexing the Falcon tube. Therefore, samples were kept in 90% methanol in -20°C until the day of analysis.
On the day of analysis, cells in methanol were centrifuged at 500 x g for 5 minutes, washed with staining buffer (DPBS with 0.5% bovine serum albumin, 1% Antibiotic-Antimycotic) once, and incubated with primary antibodies diluted in sorting buffer for 1 hour at room temperature. Cells were then washed with DPBS twice (centrifugation at 300 x g for 3 minutes) and incubated in secondary antibodies diluted in sorting buffer for 1 hour. Afterwards, cells were washed (centrifugation at 300 x g for 3 minutes) twice again and resuspended in sorting buffer in a concentration of $1x10^6$/ml.
In case of live flow cytometry for 2',7'-Dichlorofluorescin diacetate (DCFDA) staining, cells were directly resuspended in sorting buffer after detachment and centrifugation, incubated with DCFDA in room temperature for 20 minutes, and analyzed.

Data acquisition was performed with BD LSRFortessa™ Cell Analyzer in FACS Core Facility in University of Tübingen. Analysis of data was done using Flowing Software.

2.2.12. Western blot

Total protein was extracted from endothelial cells, and 55 mg protein was loaded in Precast Gel System for separation. Protein transfer was performed with a nitrocellulose membrane via semi-dry blotting. Afterwards, blocking of the nitrocellulose membrane was done using non-fat milk powder (5%, w/v) in TBS-T at RT for 1 hour. Primary antibody incubation has followed with ICAM-1 and CD31 antibodies at RT for 1 hour. After primary antibody incubation, membrane was washed with TBS-T 3 times for 5 minutes. Secondary antibody incubation was performed at RT for 1 hour. Before the signal detection, the membrane was washed with TBS-T 3 times with TBS-T for 5 minutes. Image Studio Software was used for image detection.

2.2.13. Permeability assay with dextran

Chips were loaded with endothelial cells and pericytes as described in section 2.2.7. Before the addition of the medium on D0 after chip loading, side channels were coated with 60 µg/ml fibronectin in 15 µl of MV culture medium in each media channel. After 1 hour of fibronectin coating inside channels, 30.000 ECs were loaded in each side channel and kept until D1. Chip

culture followed as usual after that. Side channel loading of ECs provided an optimal connection of the vessels for permeability assays.

On D6 or D7 of chip culture, chips were visualized Microscope Axio Observer Z1. Areas with optimal connectivity have been detected and the direction of perfusion was decided accordingly. Next, medium from all media channels were removed and 40 kDa FITC-dextran solution (25 μg/ml and 50 μg/ml) in DPBS were added in the media channels. Time-lapse images were taken every 60 minutes.

Analysis of perfusion was calculated with ImageJ. Visible and undisturbed vessels of each image were selected as region of interests (ROIs). Mean fluorescence intensity of FITC were measured with ROI manager inside and outside of vessel areas, as well as leakiness (outside/inside) were graphed.

2.2.14. TUNEL staining of endothelial cells

Endothelial cells were grown on coverslips in MV medium and incubated with methylgloxal (MGO) for 4 days. After that, TUNEL staining was performed with Click-iT TUNEL Alexa Fluor™ 488 Imaging Assay according to manufacturer's instructions and fluorescence images were taken with Microscope Axio Observer Z1.

2.2.16. Blood vessel diameter calculations

Diameter calculation of blood vessels was done using Fiji (ImageJj). All images used for this purpose have been stained with CD31-antibody and 4-5 Z-stack images were taken per condition. Initially, images were opened, and CD31-stained channel was selected. To see the blood vessel clearly, brightness and contrast was adjusted. Branches were selected and defined by drawing a perpendicular line. In each image, approximately, 3-6 branches would be defined. After that, reslice option (Image → Stacks → Reslice) was chosen with 1 mm of distance between the slices, with a total of 100-120 slices. This step was repeated for each branch. Reslice option enabled endothelial cells to be visualized forming vessels with lumens. On the first reslice, using the draw option, blood vessels were manually defined. Measurements (Analyze → Set Measurements) were for chosen and saved for each reslice

with Area, Perimeter, and Feret's diameter options. The measurement step was repeated for each reslice with 10 µm of distance to have an accurate representation of the blood vessels. Afterwards, approximately 10-12 measurements were obtained per branch, which was averaged for each parameter.

Overall, three experimental repeats, 4-5 technical repeats (images) were obtained per condition, and averaged to calculate blood vessel area, perimeter, and Feret's diameter.

2.2.17. Fluorescence activated cell sorting (FACS) protocol

For FACS experiments in the 3D cell culture chip, all the reagents were applied in the medium channels of the chip. Cells were initially washed with DPBS once, and all the medium was carefully removed. For detachment, cells were incubated with AccuMAX™ or TrypLE™ Express at 37°C until they were fully detached. This usually took 20-40 minutes, depending on the blood vessels and cells were frequently resuspended during the incubation time to mechanically help the detachment process. Then, cells were collected in 1,5 ml microcentrifuge tubes and reaction was stopped with FACS Buffer (IMDM with 5% FBS, 1% Antibiotic-Antimycotic). Cells were then strained through 30µm strainer and centrifuged at 600 x g for 5 minutes. Cells were incubated with coupled CD31 antibody diluted in FACS Buffer for 1 hour on ice and washed twice at 600 x g for 5 minutes. Supernatant was removed and cells were resuspended in FACS Buffer and brought to FACS Core Facility (University of Tübingen) for data acquisition. Sorting was performed with FACS Aria II cell sorter.

2.2.18. Statistical analysis

Graphs were generated and and statistical tests were applied using Prism Software. Results were displayed as mean values with standard deviation (SD). Unpaired t-test with Welch's correction was applied for blood vessel diameter calculations. P-value < 0.05 respresented non-significant difference. Statistical significance was shown as *: $p<0.5$, **: $p<0.01$, ***: $p<0.001$, ****: $p<0.0001$.

3. Results

The project aimed establishing a disease model for diabetic retinopathy *in vitro*, using hiPSC and microfluidic 3D chip technologies. For this purpose, endothelial cells (ECs) and perivascular pericytes (PCs) were differentiated from hiPSC and co-cultures in the commercial AimBiotech chip embedded in the 3D fibrin gel. Microvasculature formed on the chip were composed of EC tubes with perfusable lumens and covered with PCs. At the next stage of the project, I used microvasculature on the chip to model diabetic vasculopathy. Diabetic milieu was induced by high glucose culturing media, resembling hyperglycemic conditions in patients' blood, or by adding AGE-precursor methylgloxal (MGO). Received results demonstrated that diabetic conditions increased the diameter of microvasculature, resembling the pathological phenotype associated with diabetic retinopathies.

3.1. Generation of retinal blood vessel components from hiPSCs

In order to develop a human *in vitro* microvascular model, I aimed to differentiate ECs and PCs from the same cell source, using three independent hiPSC lines. Endothelial cells differentiation was performed by the induction of mesoderm and the further specification to vascular fate in hiPSCs (Pars et al.). The population of PCs is heterogenious in the human body: pericytes of most organs originate from mesoderm (Prazeres et al. 2017), while in the forebrain, where retina originates from, pericytes are derived from neural crest stem cells (Etchevers et al. 2001; Girolamo et al 2021). Therefore, I aimed to establish both mesodermal (Pars et al.) and ectodermal (NC-derived) (Gastfriend et al., 2021) differentiation protocols for pericytes and compare them.

3.1.1. Generation of endothelial cells (ECs) and mesoderm-derived pericytes (mPCs)

At the beginning of the project, I developed the differentiation protocol, that enabled to obtain ECs and PCs in 10 days (Pars et al. 2021).

This protocol combined two common ways to produce vascular endothelial cells: embryoid body (EB)- based and adherent culture methods. EB formation helped hiPSCs to mimic the developmental stage of germ layer formation due to its 3D nature and the presence of cell-

cell contacts that lack in adherent cultures (Keller, 1995). Figure 8 displays an overview of the endothelial cell generation protocol. Combined with bone morphogenic protein (BMP-4) and WNT activation, mesodermal lineage was induced on EBs on Day 0. During mesoderm induction (D0-D3), EBs are directed into a progenitor endothelial cell stage. On Day 3, progenitors within the EBs are supplemented with VEGF-A and cAMP activator (forskolin) in adherent culture on gelatin coating. VEGF-A supplementation started on Day 3 and is maintained in culture medium during differentiation, since it is crucial in endothelial cell survival and expansion (Marcelo, Goldie, and Hirschi, 2013). Forskolin, as a cAMP activator, helped angiogenesis in ECs through the eNOS system (Namkoong et al. 2009). On Day 5, culture medium included FGF-2 and TGF-β inhibitor (SB431542) in addition to VEGF-A, which act on a similar fashion to promote EC proliferation and survival (Jia et al. 2021). Differentiation of endothelial cells lasted until Day 9 or Day 10, and CD31-expressing endothelial cells were sorted via magnetic-activated cell sorting (MACS). Sorted cells were either immediately cultured and expanded or cryopreserved.

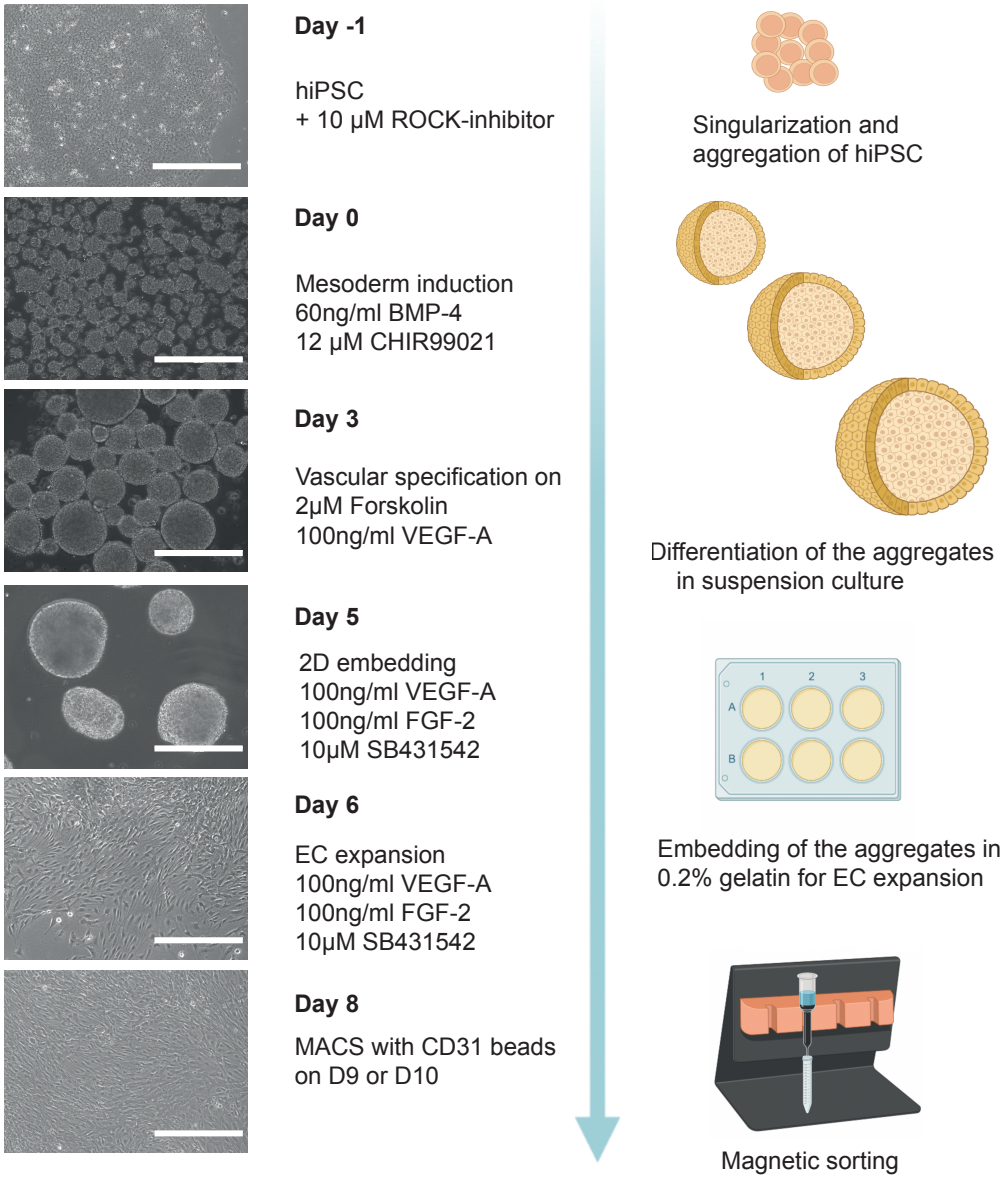


Figure 8: Generation of endothelial cells from hiPSC - protocol outline. On D-1, hiPSC colonies are singularized and grown in suspension culture for 24h with 10µM ROCK-inhibitor. On D0, hiPSC aggregates are induced to mesodermal lineage with 60ng/ml BMP-4 and 12µM CHIR99021. After 3 days, grown aggregates are specified into vascular fate with 100ng/ml VEGF-A and 2µM forskolin. On D5, they are seeded onto 0.2% gelatin-coated plates. Cells are grown in adherent culture with 100ng/ml VEGF-A, 100ng/ml FGF-2 and 10µm SB431542 and sorted via MACS D9 or D10 with CD31 beads. Created with biorender.com. Scale bars = 400µm.

On the day of magnetic sorting, EC islands as depicted in Fig. 9A could be distinguished by other cell types. EC islands usually appeared as early as Day 6 and thereafter continued to be

expanded. From the same generation protocol, mesoderm-derived pericytes could also be generated (Fig. 9B). MACS-sorted endothelial cells have thin and long morphology and grow in waves. In comparison, $CD31^-$ pericytes are larger in size and have triangular and heterogenous morphology (Fig. 9C).

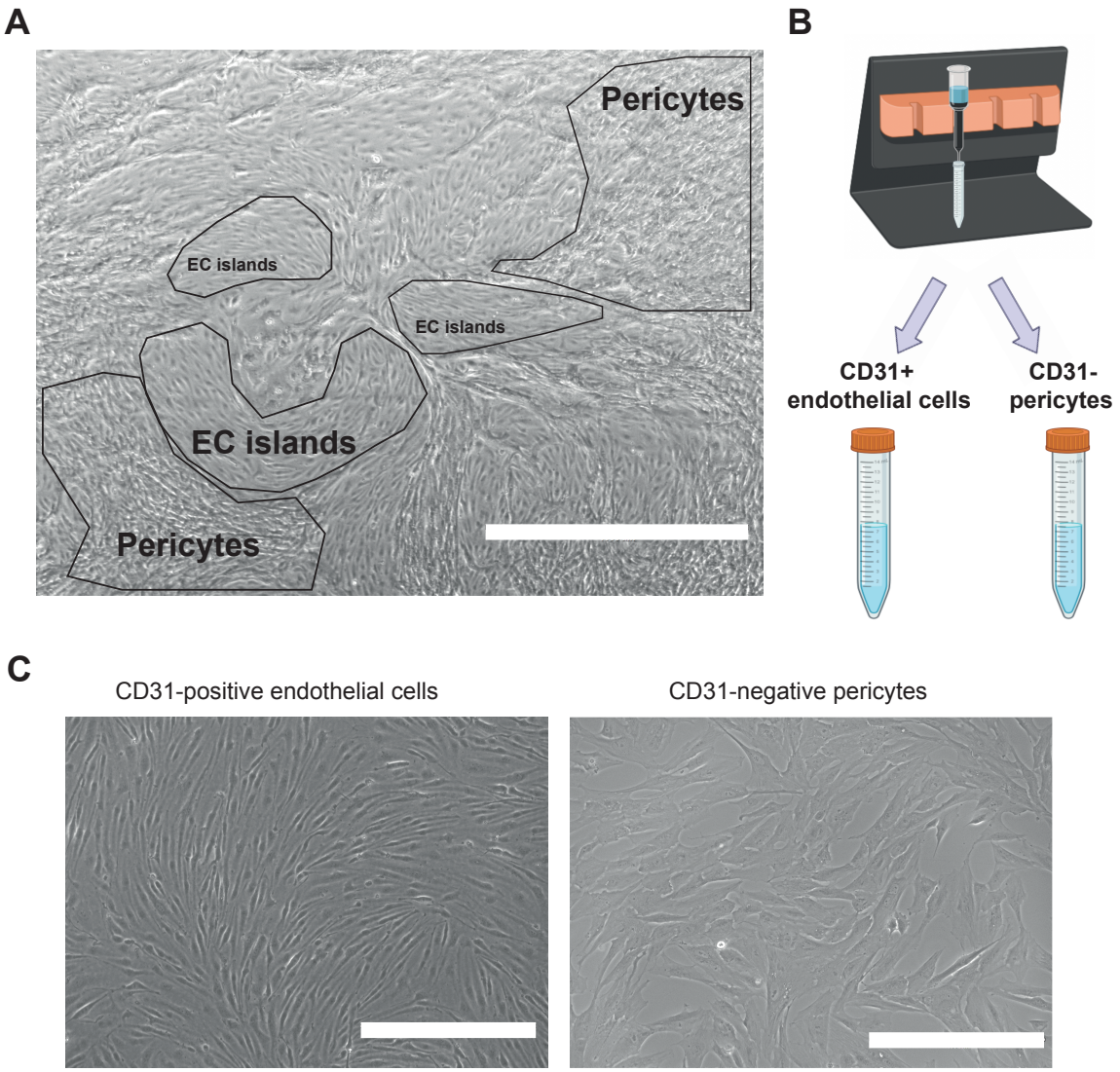
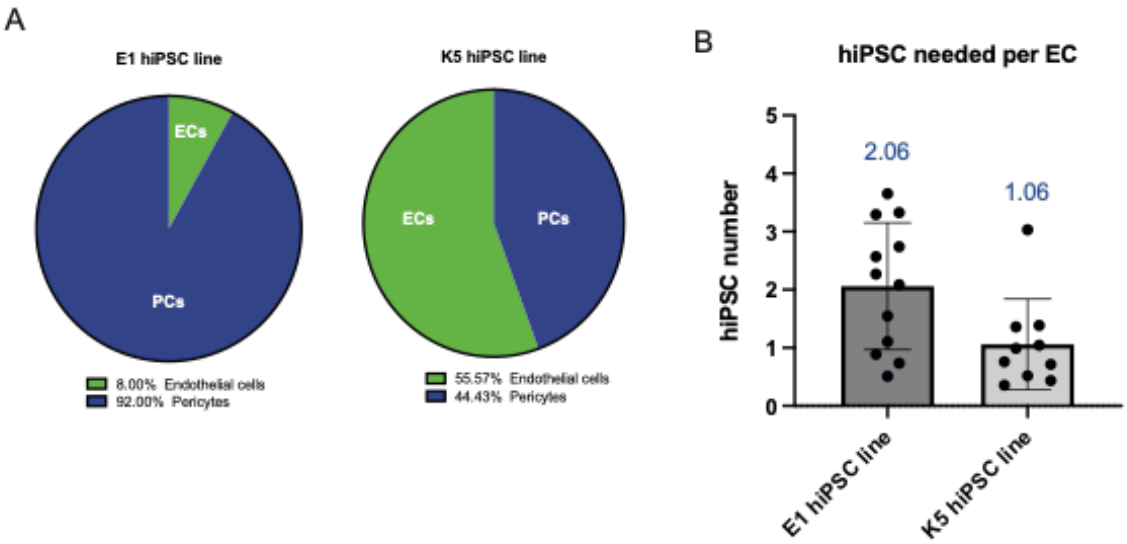


Figure 9: Simultaneous differentiation of endothelial cell and pericytes. Seeded aggregates on D5 flatten until D10 of differentiation and distinct cell types can be distinguished (A). ECs have a long and thin morphology and grow in patches, whereas pericytes grow tightly packed in a heterogenous manner on culture plate. Magnetic sorting of endothelial cells and pericytes in one differentiation. Created with biorender.com (B). Bright-field images of sorted endothelial cells and pericytes (C). Scale bars=1000µm (A), 400µm (C).



C

Endothelial cell viability after cryopreservation		
Dead cells (%)	SD	Sample Size
9,23	±6,92	n=8

Figure 10: Efficiency of endothelial cell differentiation and viability. Percentage of $CD31^+$ endothelial cells and $CD31^-$ pericytes after MACS for two (E1 and K5) hiPSC lines. SD=±2,81 for E1 and SD±18.86 for K5 hiPSC line (A). Endothelial cell yield per hiPSCs used for two (E1 and K5) hiPSC lines. SD±1,05 for E1 and SD±0.74 for K5 hiPSC line (B). Cell viability of endothelial cells after cryopreservation. Dead cells were counted with Trypan Blue solution (C).

Efficiency of endothelial cell generation was calculated by manual cell counting after MACS separation (Fig. 10A). Keratinocyte-derived hiPSC line (K5) has a significantly higher efficiency (~56%, n=12) than episomal hiPSC line E1 (8%, n=10). Additionally, endothelial cell yield per hiPSC was calculated (Fig. 10B). Per endothelial cell generated, ~2.1 hiPSCs (E1) and ~1.1 hiPSCs (K5) were needed on Day -1 of differentiation. Endothelial cells could be also cryopreserved immediately after MACS separation, or during early passages. Cell viability after thawing was not significantly affected, which resulted in ~9 % cell death (Fig. 10C).

3.1.2. Characterization of endothelial cells and mesodermal pericytes

hiPSC-derived ECs generated by the novel protocol have been characterized by cell markers (Fig. 11). All cells were positive for the widely used endothelial cell markers CD31 and VE-cadherin. Tight junction markers Claudin-5 and ZO-1 are expressed by most of the cells, as well as CD146 and CD34. As expected, endothelial cells are negative for PDGFRβ, which is a pericyte marker.

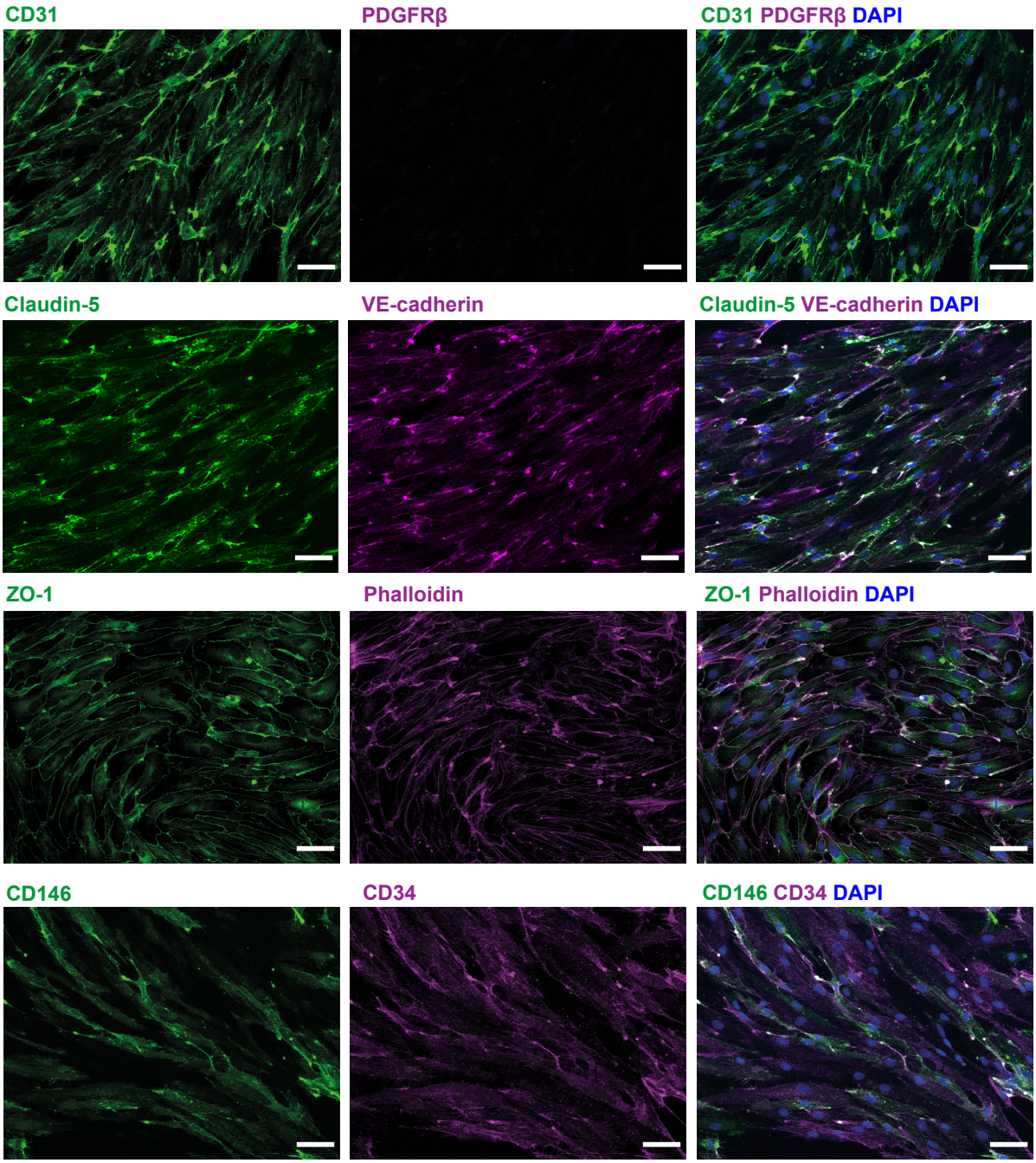


Figure 11: Cell surface markers of iPSC-derived endothelial cells. Immunostaining of ECs show cell adhesion molecule (CD31, VE-cadherin, CD146), tight junction (Claudin-5, ZO-1) and CD34 expressions. Negative expression of pericyte marker PDGFRβ supports the efficiency of MACS sorting. Scale bars = 50μm.

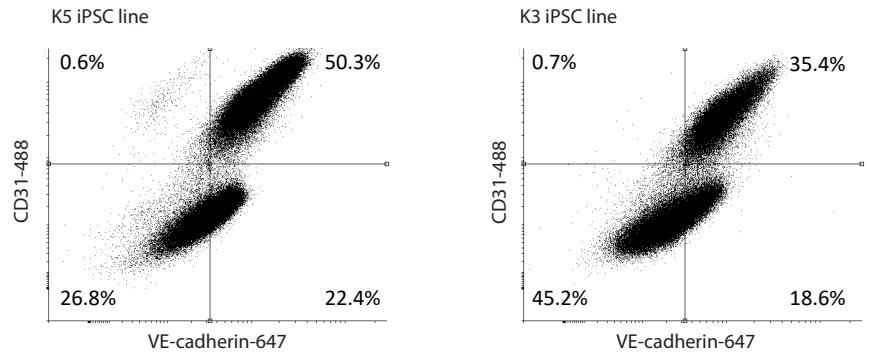
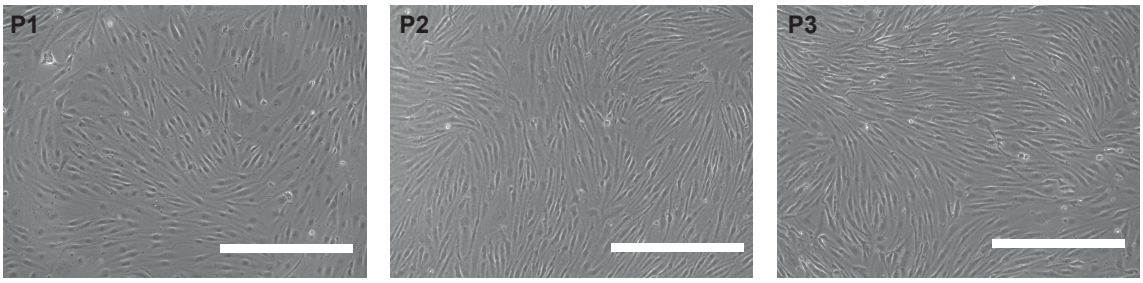


Figure 12: Flow cytometry analysis of MACS-sorted endothelial cells. $CD31^+/VE\text{-}cadherin^+$ cell populations show distinct separation from $CD31^-/VE\text{-}cadherin^-$ cells on D10 of differentiation in both hiPSC lines. (Pars et al., 2021, p. 8).

CD31 expression level of endothelial cells was also confirmed by flow cytometry. Cells from two hiPSC line (K5 and K3) were collected on Day 10 of differentiation and flow cytometry analysis was carried out for cell adhesion markers CD31 and VE-cadherin (Fig. 12). In both cell lines, distinct population of the CD31 and VE-cadherin double positive cells (50% for K5 and 35% in K3 hiPSC line) can be observed.

Endothelial cells could be subcultured until at least Passage 3 without losing their long and thin morphology (Fig. 13A), and their proliferation capacity was retained. Fig. 13B shows the unchanged CD31 marker expression of ECs from passage 0 to passage 2.

A



B

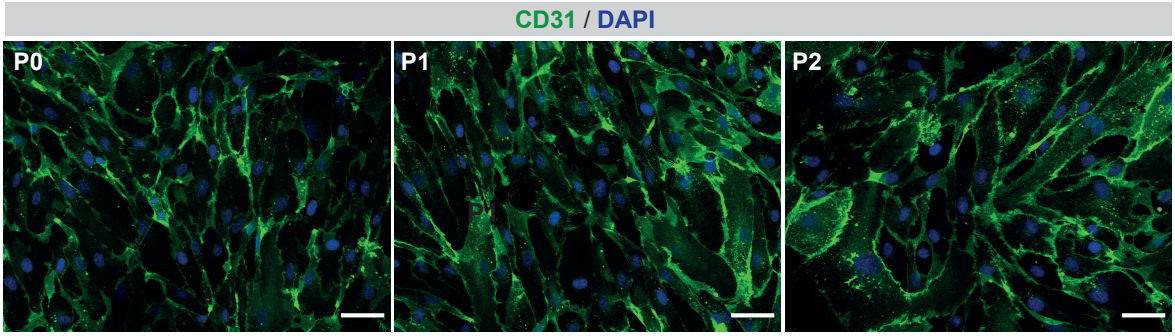


Figure 13: Maintenance of endothelial cell morphology and marker CD31 during passaging. Phase-contrast images of endothelial cells indicate typical EC morphology for Passage 1 (P1), Passage 2 (P2) and Passage 3 (P3) (A). Immunofluorescence staining of ECs with CD31 (green) from P0 – P2 (B). Scale bars = 400µm (A), 50µm (B).

Mesodermal pericytes have been generated using the EC differentiation protocol explained in Fig. 2. Immunocytochemistry showed that most cells were positive for PDGFRβ, whereas a portion of pericytes expressed NG2 and smooth muscle actin (SMA) (Fig. 14). SMA expression is associated with contractile capabilities in pericytes and lack of SMA in some pericytes were expected.

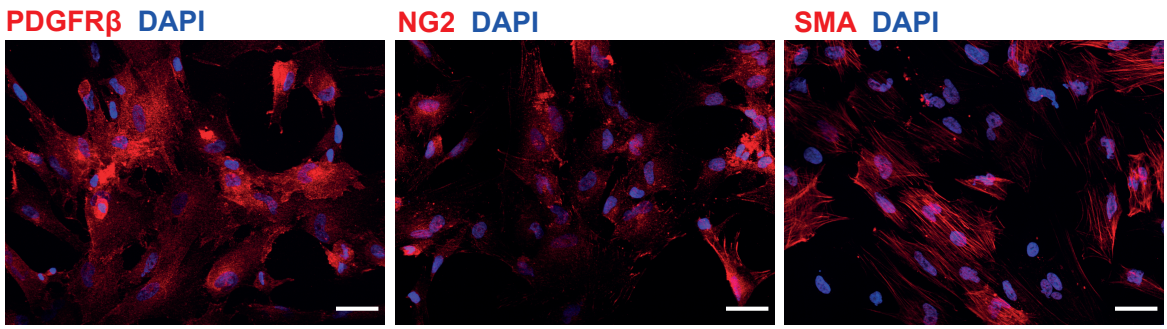


Figure 14: Characterization of iPSC-derived mesodermal pericytes. Immunofluorescence staining displays PDGFRβ, NG2 and SMA expression in mesodermal pericytes in Passage 0. Scale bar = 50 µm.

3.1.3. Functionality of endothelial cells

Generation and characterization of endothelial cells were followed by *in vitro* functionality tests. For this purpose, tube formation assay and the response of ECs to inflammatory stimuli have been analyzed.

Tube formation assay was performed to ensure the ability of endothelial cells to divide and migrate in a basement membrane matrix to form tubules (Fig. 15A). Angiogenic growth factors (VEGF-A and FGF-2) in culture medium enabled the formation of tubules resembling capillaries all through the well. Calcein staining displays the tubes that were formed within 16 hours (Fig. 15B).

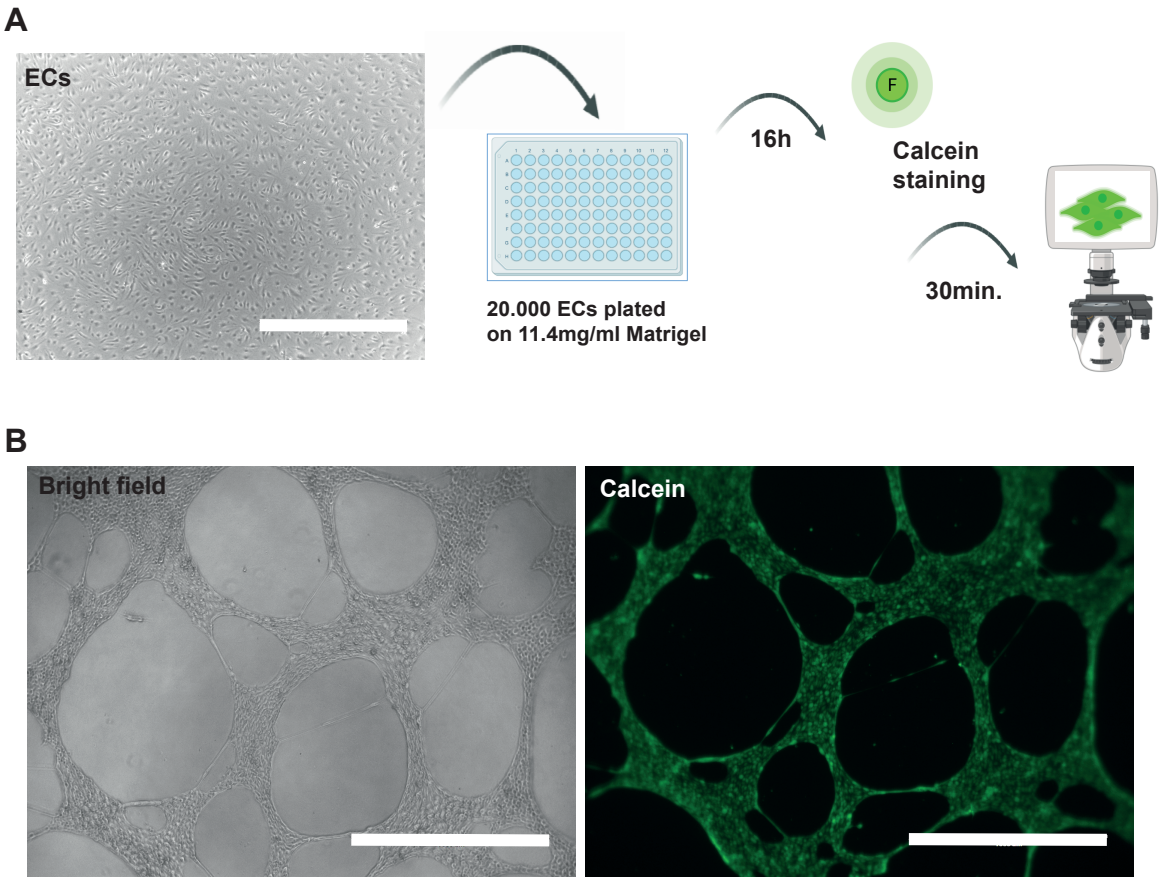


Figure 15: Tube formation assay of endothelial cells. ECs are plated on undiluted Matrigel for 16h and stained with Calcein-AM dye for 30 min. for live fluorescence imaging (A). Calcein staining shows the formation of tubules within 16h (B). Scare bars = 400µm.

An additional functionality assay was performed to assess the response of endothelial cells to inflammatory stimulus. In healthy ECs, ICAM-1 is expressed in low levels. However, upon inflammation, ICAM-1 is overexpressed in ECs for leukocyte recruitment and adhesion to the blood vessels (Bui, Wiesolek, and Sumagin, 2021). Overexpression of ICAM-1 is also associated with the breakdown of blood-retinal barrier in diabetes (Joussen et al. 2001; Kaji et al. 2007; Huang et al. 2011).

In order to assess the ICAM-1 expression upon inflammatory stimuli *in vitro*, endothelial cells were cultured with 10 ng/ml and 100 ng/ml TNF-α for 20 hours. Western blot results showed that TNF-α treatment has indeed increased the ICAM-1 expression in a dose dependent manner (28-fold with 10ng/ml TNF-α and 35-fold with 100ng/ml TNF-α) in hiPSC-derived endothelial cells (Fig. 16).

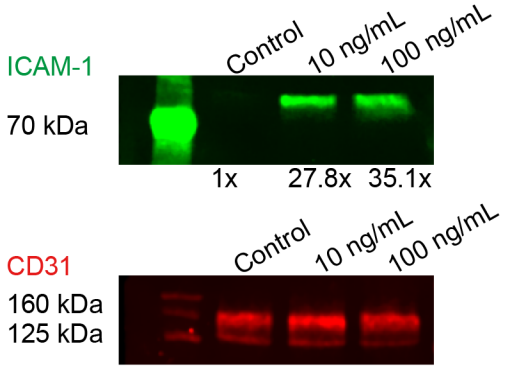


Figure 16: Increased ICAM-1 expression in response to tumour necrosis factor alpha (TNF-α treatments). Western Blot analysis shows the increased intercellular adhesion molecule 1 (ICAM-1) production in ECs after 20 h treatment with 10ng/ml or 100ng/ml TNF-α. The level of CD31 was not changed. Numbers show fold change of protein amount (measured as optical density) normalized to the CD31 expression compared to non-treated control endothelial cells, n=2. (Pars et al., 2021, Fig. S2).

3.1.4. Generation of neural crest stem cell-derived pericytes

Considering their embryonic resemblance to retinal pericytes, we have generated neural crest stem cell-derived pericytes based on a recent protocol published by Gastfriend et al. 2021 (Fig. 17A).

This protocol included two steps; differentiation of neural-crest stem cells from hiPSCs in adherent culture, followed by MACS with CD271 beads (D0-D15) and differentiation of pericytes from NCSCs (D16-D23). During the first step, hiPSC were directed into NCSCs by E6 medium supplemented with WNT signalling activator (CHIR99021), BMP-4 inhibitor (dorsomorphin), TGF-β inhibitor (SB431542) and FGF-2 for 15 days. On day 15, after MACS separation was performed, NCSCs could be frozen, cultured as NCSCs or differentiated into pericytes. Fig. 17B shows an example of the cell morphologies during NSCS-derived pericyte differentiation. NCSCs have small and triangular shapes and grew as single cells after sorting on D15. As they started to get confluent, NCSCs formed colonies similar to hiPSCs. For pericyte differentiation, NCSCs were grown for 5-7 days in E6 medium with 10% FBS. Once NSCSs were plated on uncoated plates, cell death followed and cells started to have broad and long morphology, a characteristic of pericyte shape (Fig. 17B). Towards D23, packed cell patches of pericytes were fully differentiated and ready to be used in experiments. Since passaging of pericytes were not recommend in the protocol, cells have been used between D21-D24 of differentiation, however, in the earlier stages (D18-D19), cells were cryopreserved.

After cryopreservation, 35% and 27% cell death was observed for NCSCs and NCSC-derived pericytes, respectively (Table 17).

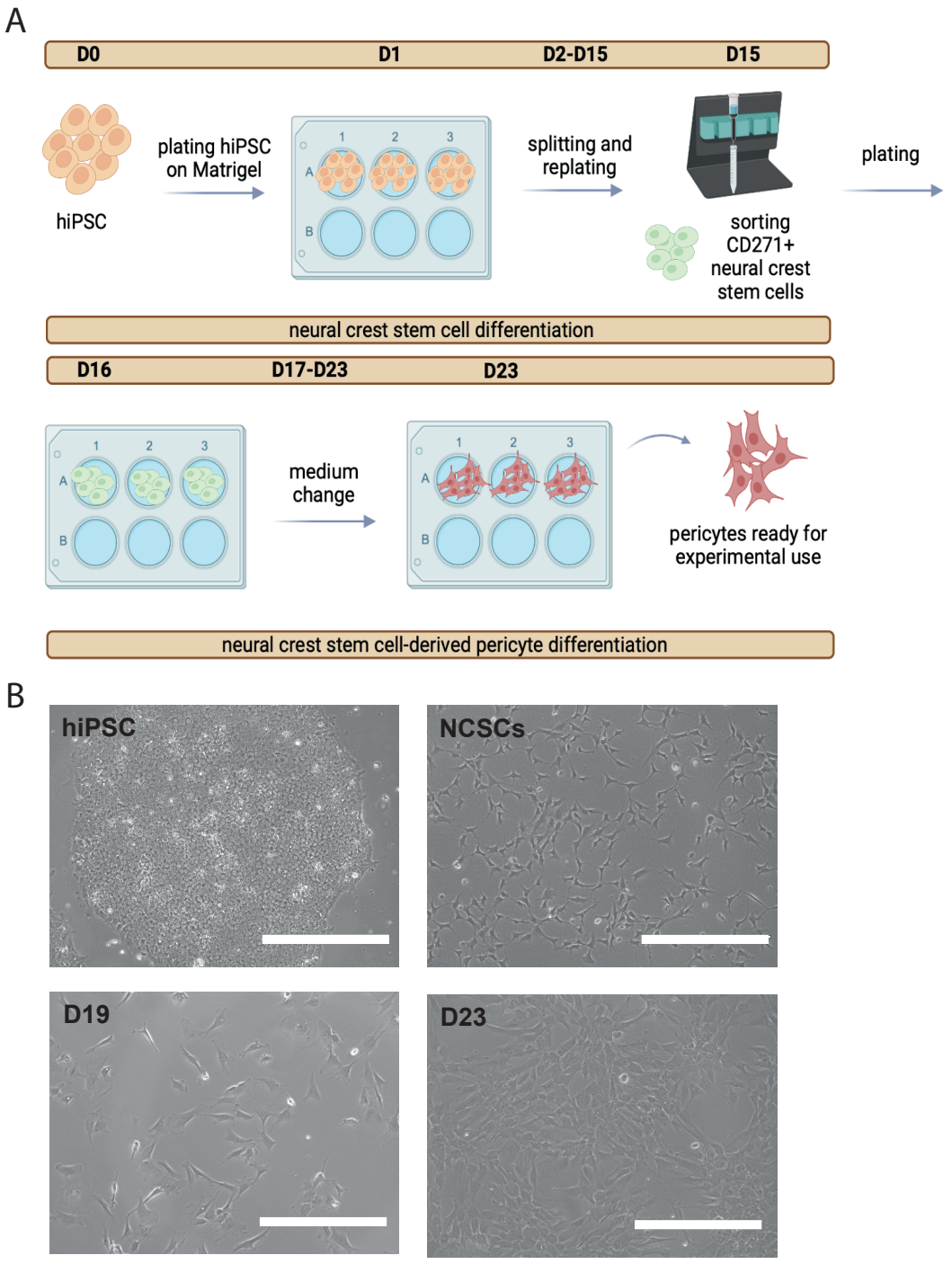


Figure 17: Neural crest stem cell-derived pericyte differentiation scheme. Initially, hiPSCs were singularized and plated on Matrigel coated plates in E8 medium for 24 hours. On D1, medium was switched to E6-CSFD to initiate NCSC differentiation. Cells were kept in E6-CSFD medium and split every 3-4 days, depending on their confluency. On D15, MACS was carried out and sorted NCSCs were plated for pericyte differentiation in E6 + 10% FBS medium. Between D21-24, pericytes were fully

differentiated (A). Cells morphologies during NSCS-derived pericyte differentiation (B). Scare bars = 400µm.

Cell viability after cryopreservation			
	Dead cells (%)	SD	Sample Size
Neural Crest Stem Cells	34,75	±21,2	n=10
Neuroectodermal Pericytes	27,00	±7,2	n=3

Table 17: Cell death of NCSCs and NCSC-derived pericytes after cryopreservation. Cells were counted with Trypan Blue after being thawed.

NCSC-derived pericytes were characterized by cell surface markers by immunofluorescence staining (Fig. 18). Most cells were positive for NG2 and CD146 and all cells were positive for PDGFRβ as well as extracellular matrix protein collagen IV.

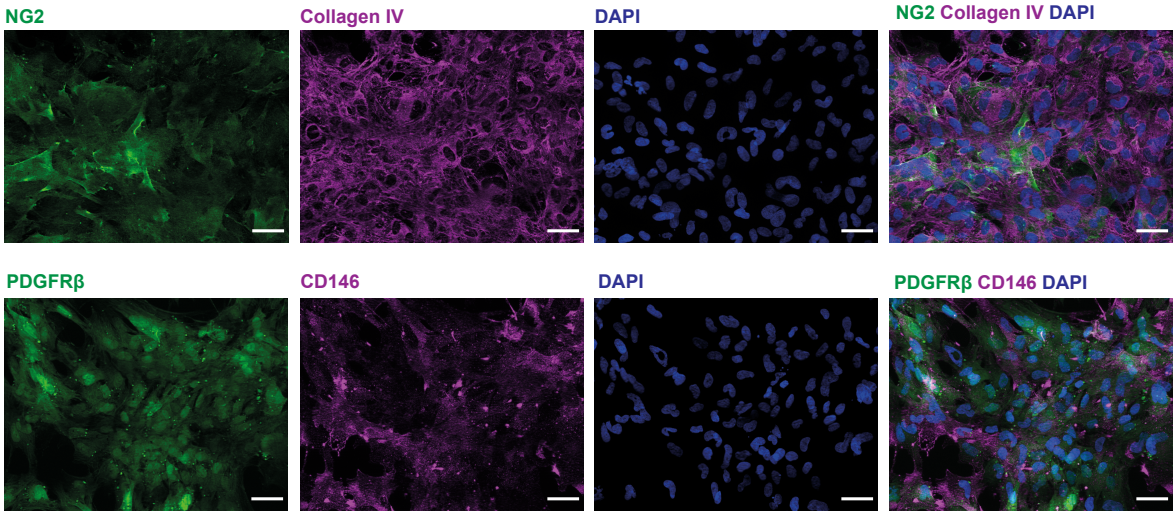


Figure 18: Characterization of neural crest stem cell-derived pericytes. Immunostaining of NCSC-derived pericytes on D24. Scale bars = 50µm.

Cell surface markers of pericytes were also confirmed by flow cytometry (Fig. 19). Cells were collected on D24 of differentiation and flow cytometry was carried out in methanol-fixed

samples. Majority of the cells expressed PDGFRβ (88%) and NG2 (86%), and co-expression of NG2 and PDGFRβ was 80% (Fig. 19C), compared to unstained controls (Fig. 19A). 81% of the pericytes were also positive for CD146 (Fig. 19B).

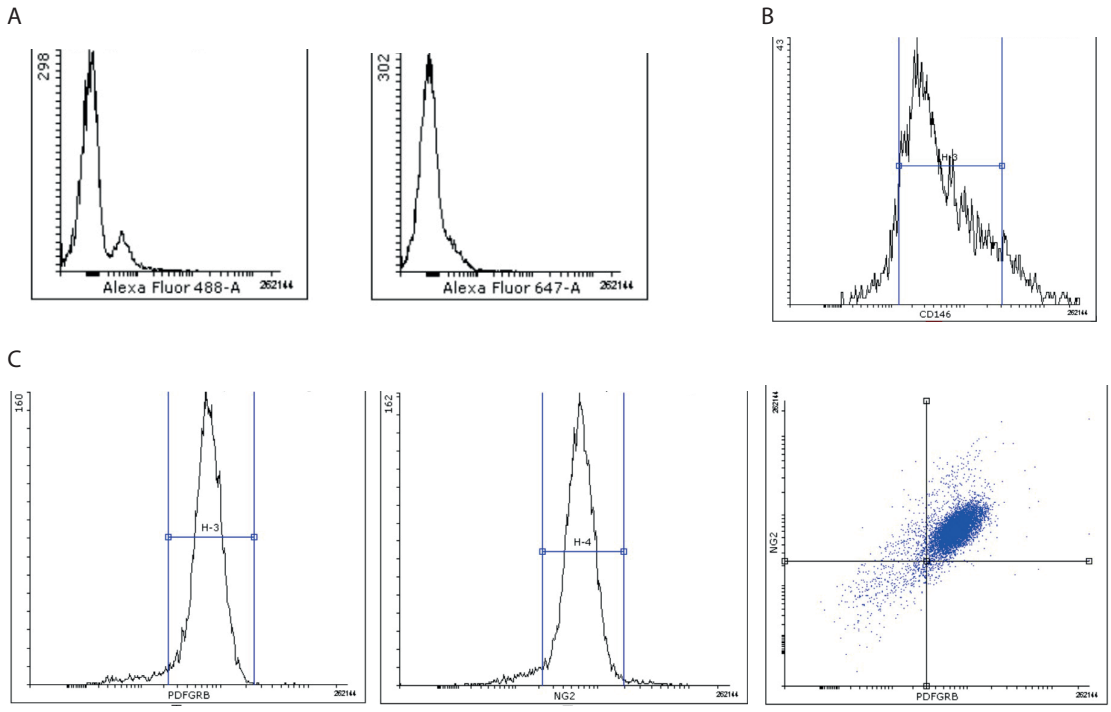


Figure 19: Flow cytometry analysis of neural crest stem cell-derived pericytes on D23. Unstained controls show lack of fluorescence (A). 81% of pericytes were positive for CD146 (B), and majority of cells were positive for PDGFRβ (88%) and NG2 (86%). In the dot plot, double positive cells for both PDGFRβ and NG2 are displayed (80%).

3.2. Blood vessel formation in 3D microfluidic chip using hiPSC-derived endothelial cells and pericytes

Once endothelial cells and pericytes have been obtained, loading a 3D cell culture chip followed, so that the functionality of the blood vessel components could be observed. Initially, a cell number test took place (data not shown), in order to optimize the concentration of the cells in the chip. During this time, 120.000 cells per chip have been used.

3.2.1. Role of NC-derived pericytes in the microvascular network

The initial step in chip experiments was to determine the effect of pericytes in blood vessel formation. In order to assess this, endothelial cells in 3D cell culture chips were compared with several conditions. In the absence of pericytes, endothelial cells (90.000 cells in the chip) sparsely formed vessels (Fig. 20A). Increased numbers of endothelial cells (120.000 cells in the chip) negatively impacted the vessel formation, as the cell number was too high for the self-assembly of the vessels. However, endothelial cells (90.000 cells) mixed with (30.000 cells) pericytes have highly improved the vessel formation. As expected, pericytes physically wrap up endothelial cells and help them mature by inhibiting their proliferation, so that a healthy vessel formation is ensured (Fig. 20B).

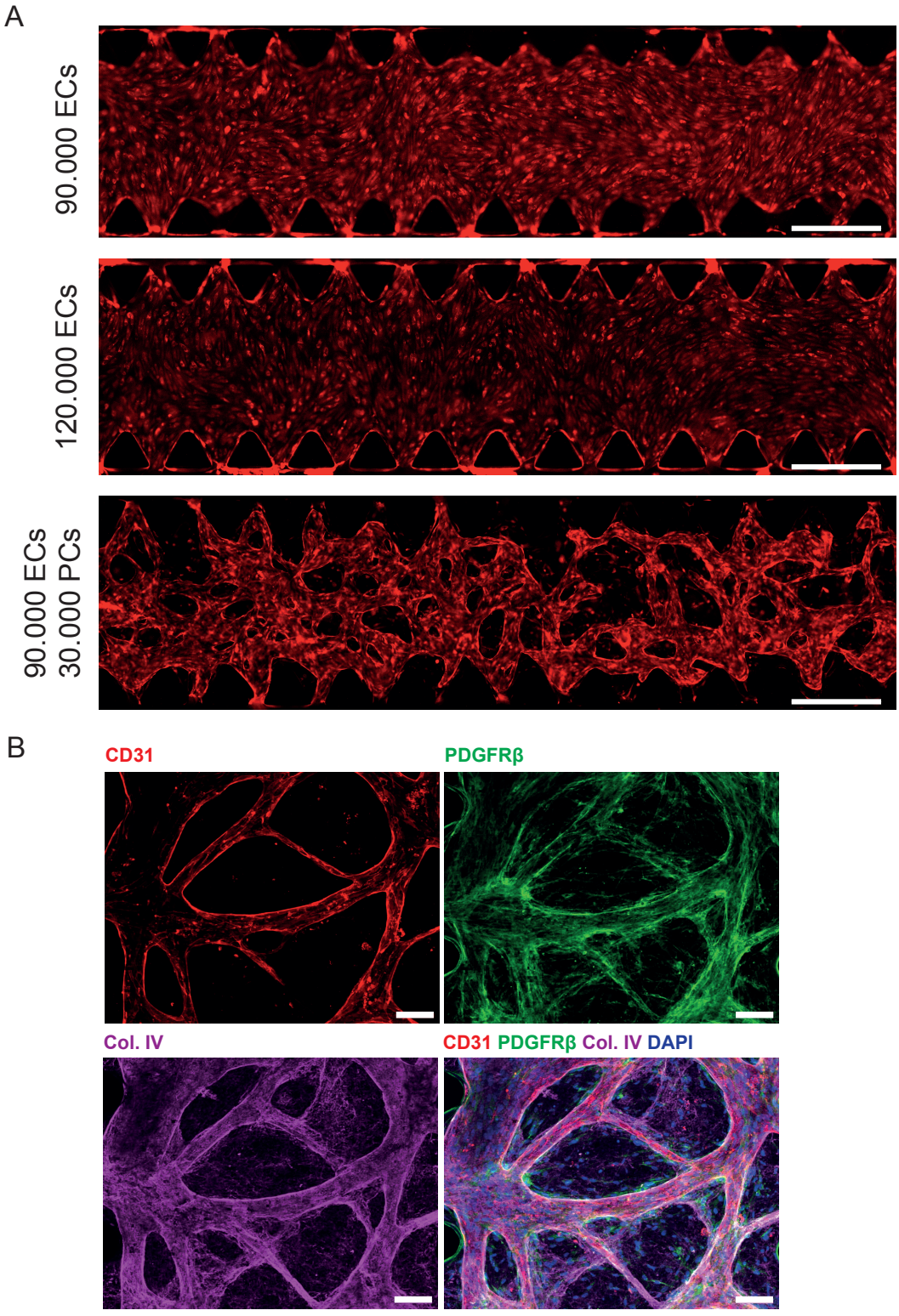


Figure 20: Effect of pericytes in blood vessel formation. ECs form single layer of vessels when plated alone in two different densities (90.000 and 120.000 cells), however, when pericytes are added (30.000 pericytes with 90.000 endothelial cells) to the chip, blood vessels start to form apparent

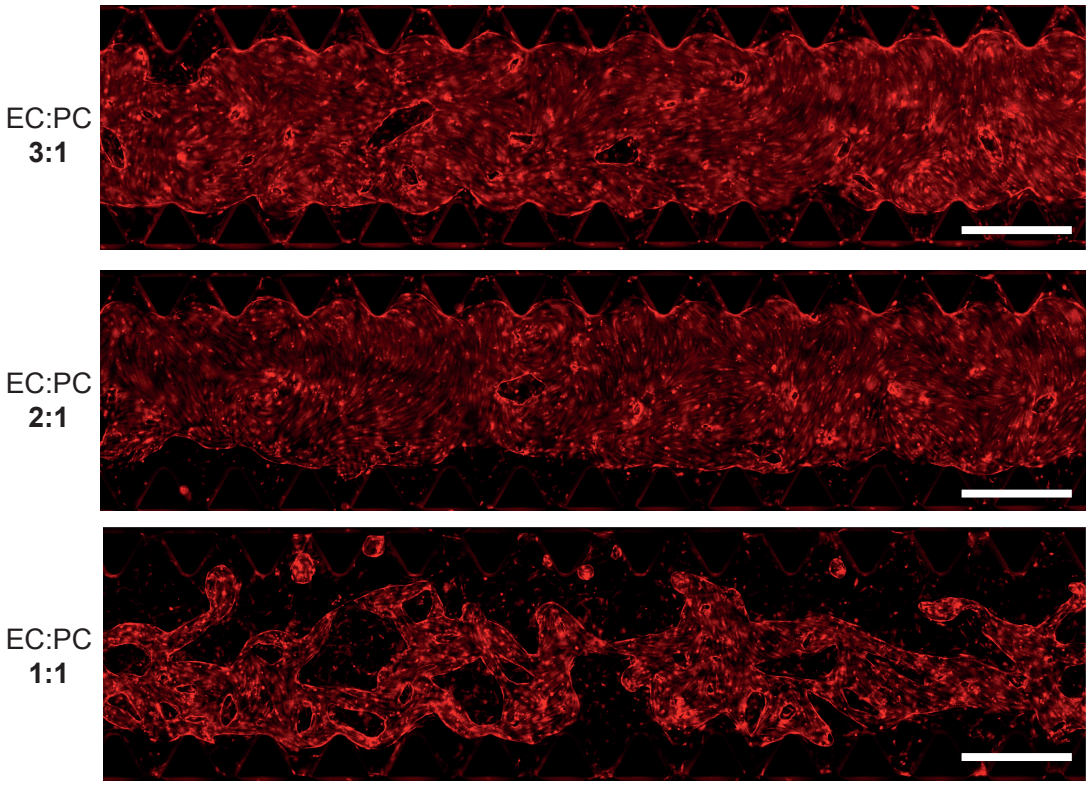
networks on D5. Endothelial cells are expressing mCherry (A). Immunofluorescence shows blood vessels (CD31 in red) and surrounding pericytes (PDGRFβ in green) with basement membrane protein Collagen IV (magenta). Nuclei are stained with DAPI (blue) (B). Scale bars = 600µm (A), 100µm (B).

Our second optimization for blood vessel formation included endothelial cell to pericyte (EC:PC) ratio in the chip. Pericyte coverage is associated with tightness of the blood vessels, with EC:PC ratios ranging from 1:1 to 1:10 (Armulik, Genové, Betsholtz, 2011). In central nervous system, and especially in retina, due to the barrier properties of the capillaries, this ratio is estimated to be 1:1, with the highest pericyte coverage in the human blood vessels (Frank, Turczyn, and Das 1990).

To see the effect of different EC:PC ratios, we have loaded chips with 3:1, 2:1 and 1:1 ratio (Fig. 21A). In 3:1 and 2:1 ratio, blood vessels were formed but were significantly larger compared to vessels in 1:1 ratio. The optimal blood vessel formation was observed in 1:1 ratio, as blood vessels were formed more branched than 3:1 and 2:1 ratios. It is postulated that in 3:1 and 2:1 ratios, pericyte numbers were not sufficient for blood vessel maturation and relatively high endothelial cell numbers caused blood vessels to enlarge.

Secondly, to ensure that the cells did not proliferate in an uneven manner after being loaded onto the chip, they were examined on D7. Chips were stained with Erg-1/2/3 and DAPI for nuclei staining (Fig. 21B). Since Erg (ETS related gene) is an endothelial cell-specific transcription factor (Birdsey et al., 2008), number of Erg-1/2/3-positive cells have been compared with overall nuclear (DAPI) staining. On average, 50,66% of the cells in chip were endothelial cells on D7, which indicated that the EC:PC ratio has not been changed during the culture.

A



B

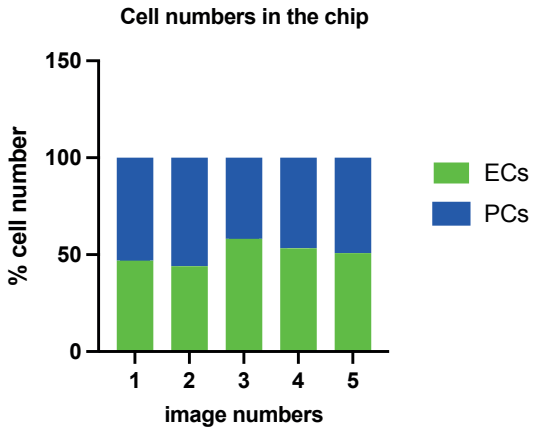


Figure 21: Endothelial cell:pericyte ratio test in 3D cell culture chip. Endothelial cells and pericytes have been loaded in 3:1, 2:1 and 1:1 ratios, keeping the total number of the cells equal. Endothelial cells are expressing mCherry (red), fluorescence images were taken on D5 (A). Cell number distribution in the chip after chip loading. Nuclei of endothelial cells were counted with Erg-1/2/3 staining and compared to DAPI staining of the nuclei of pericytes. SD ± 5,5 (B). Scale bars = 300µm.

3.2.2. Formation of a microvascular network

Microvascular network formation was visualized with fluorescence imaging of endothelial cells with 24-hour intervals from D1 to D7 (Fig. 22). On D1, endothelial cells are organized evenly throughout the chip and start to form small-sized vessels. Vessel scaffolds are being apparent on D2 and follow to be matured towards D3 and D4. From D5 on, blood vessels did not show any morphological change, and chips were usually used for analysis on D5 or D6.

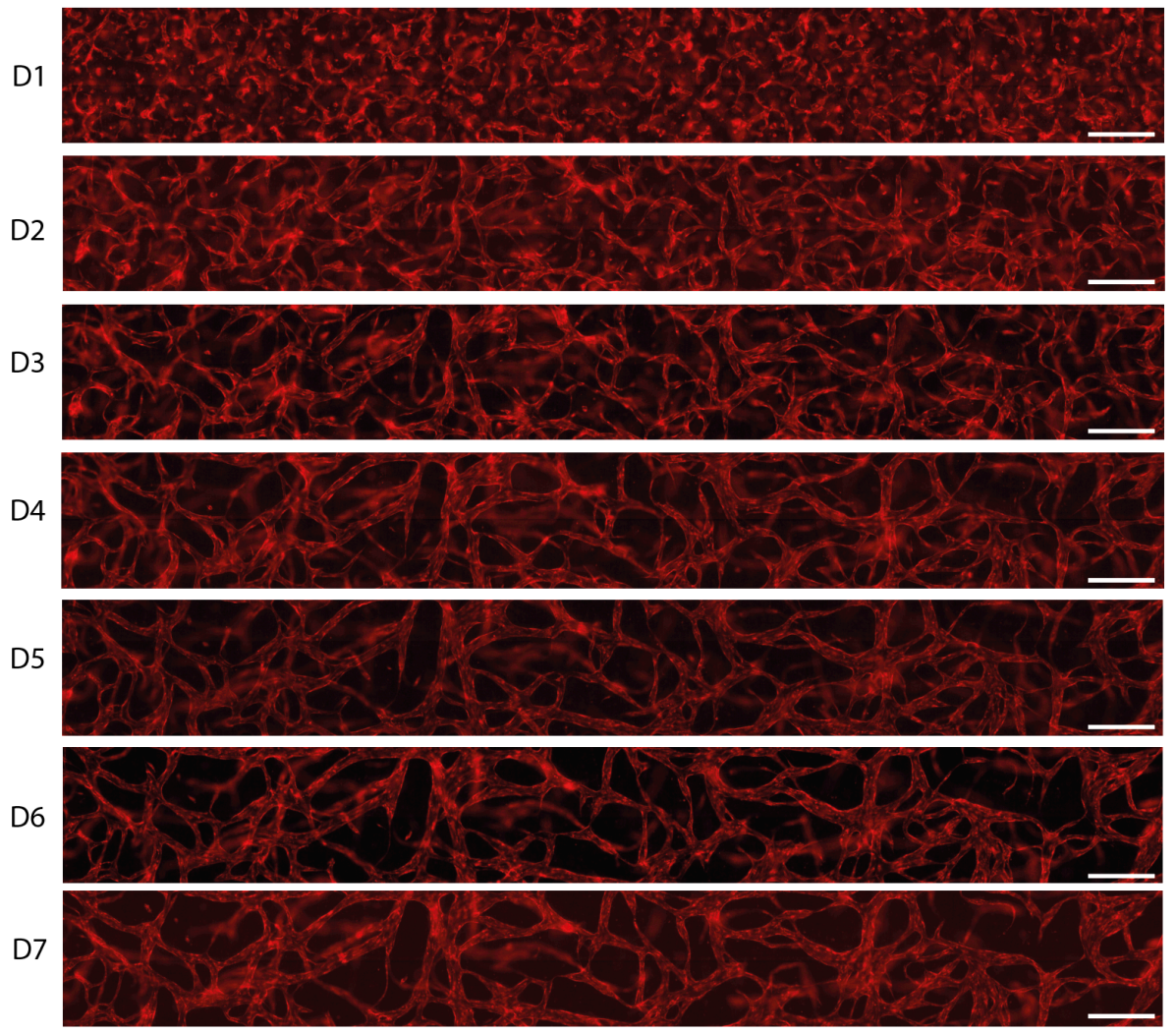


Figure 22: Formation of microvascular network in the chip from D1-D7. Endothelial cells express mCherry (red). Unorganized cells on D1 form microvascular networks with lumens until D5 and mature towards D7. Scale bar = 400µm.

Blood vessels formed with endothelial cells and pericytes also had lumens. Figure 23A displays a 2D view of a Z-stack image (xy view) of a representative blood vessel with its branches. In

xz and yz views, one can observe the round blood vessel shape that has lumens. Calculation of the lateral and transverse diameter (Fig. 23B) of the blood vessel was done using pixel intensity of the xz view of the 3D image and is shown to be 50,2 µm (lateral) and 28,2 µm (transverse) (Fig. 23C).

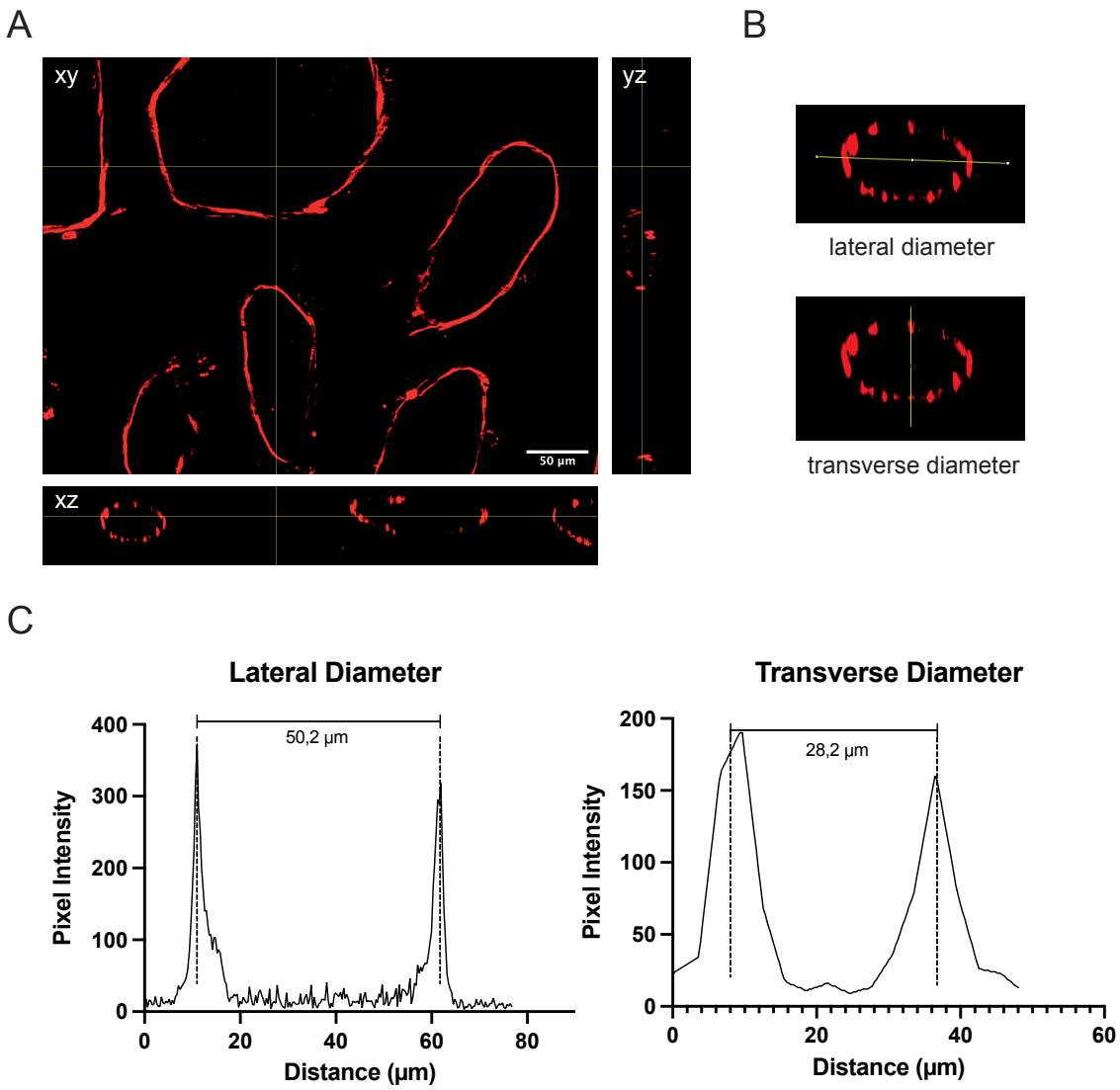


Figure 23: Lumen formation in the blood vessels. Z-stack image of a respresentative blood vessel (CD31, red) shows lumen formation in xz and yz layers (A). Lateral and transverse diameters of one branch (leftmost vessel in xz view) (B). Plotted pixel intensity is shown to measure lateral and transverse diameters of the blood vessel shown in B (C).

3.2.3. Perfusion assay of blood vessels

Functional endothelial cells must be perfused upon blood vessel formation. As blood is flowing from the vessels, influx and efflux is controlled via transporter proteins within the cell membrane, which determines the tightness. Blood vessels in the central nervous system, especially in the retina are known to be very impermeable in order to ensure a highly controlled influx and efflux (Runkle and Antonetti, 2011). This means that even very small molecules do not cross the inner blood-retinal-barrier. Therefore, a functional iBRB would show no leakiness of the blood vessels in healthy conditions.

Therefore, the perfusion and leakiness of our blood vessels were analysed with 40 kDa FITC-dextran. Blood vessels were perfused with dextran and fluorescence images were taken every minute to observe and then quantify the leakiness (Fig. 24A). A portion of every image was taken to ensure the quantification of blood vessels with clear borders (Fig. 24B). Dextran started to penetrate the blood vessels within the first minute (Fig. 24C, intravessel) and has shown the highest intensity in the 3rd minute inside the vessel. After the 4th minute, dextran started to leak from the vessels, as the intravessel intensity started to decrease and extravessel intensity increased.

Blood vessels with endothelial cells and pericytes were therefore perfusable, although leakiness was observed after the 3rd minute.

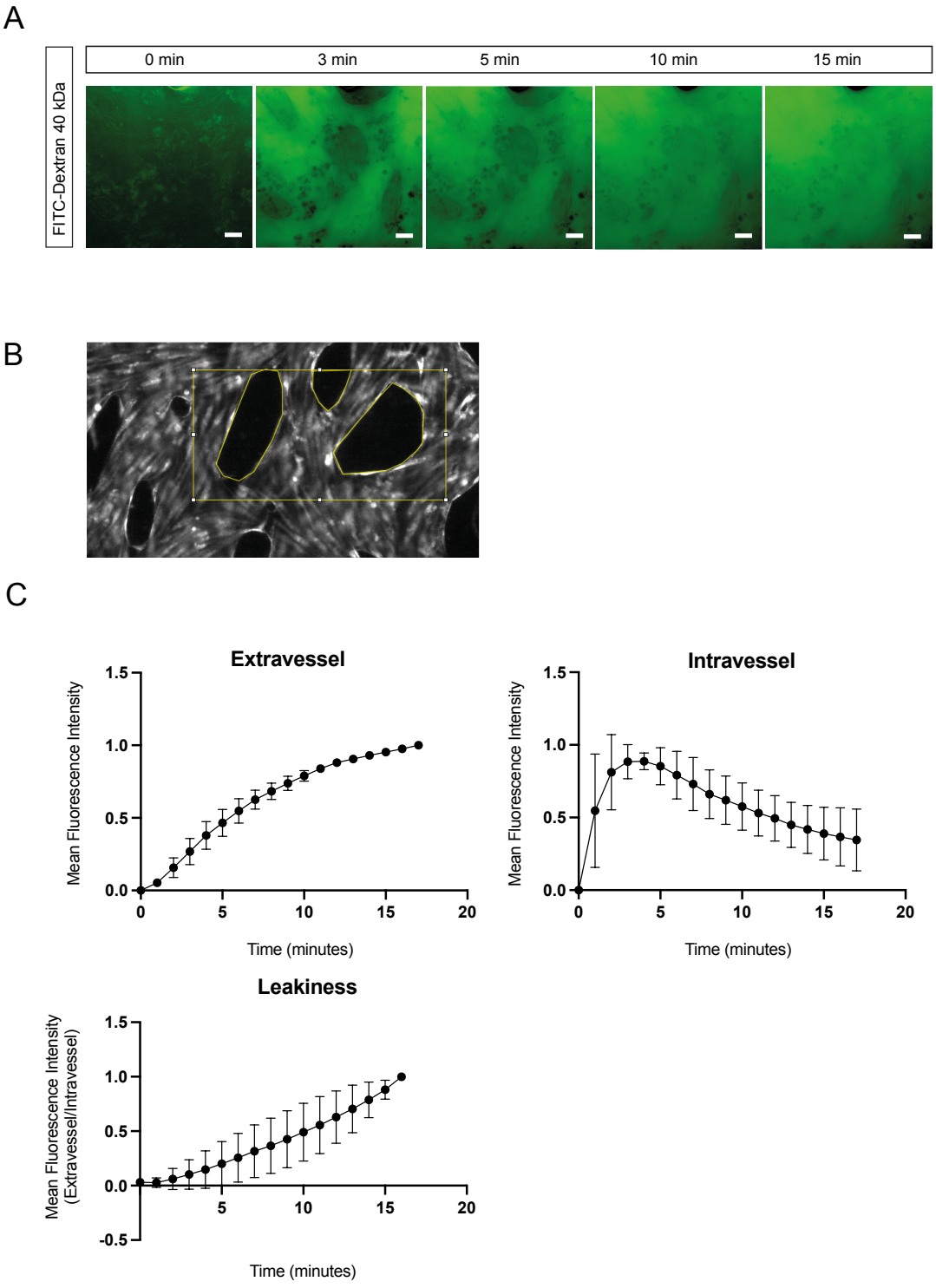


Figure 24: Perfusion of blood vessels with 40 kDa dextran. Representative fluorescence images of perfused chips after perfusion with 40 kDa dextran (A). Region of interest (ROI) example of vessels with defined borders (B). Time-lapsed quantification of mean fluorescence intensity of extra-, and intravessels. Leakiness is indicated as extravessel/intravessel mean fluorescence intensity, n=3, ±SD (C). Scale bar = 50 µm.

3.3. Induction of diabetes in 3D microfluidic chip on blood vessels

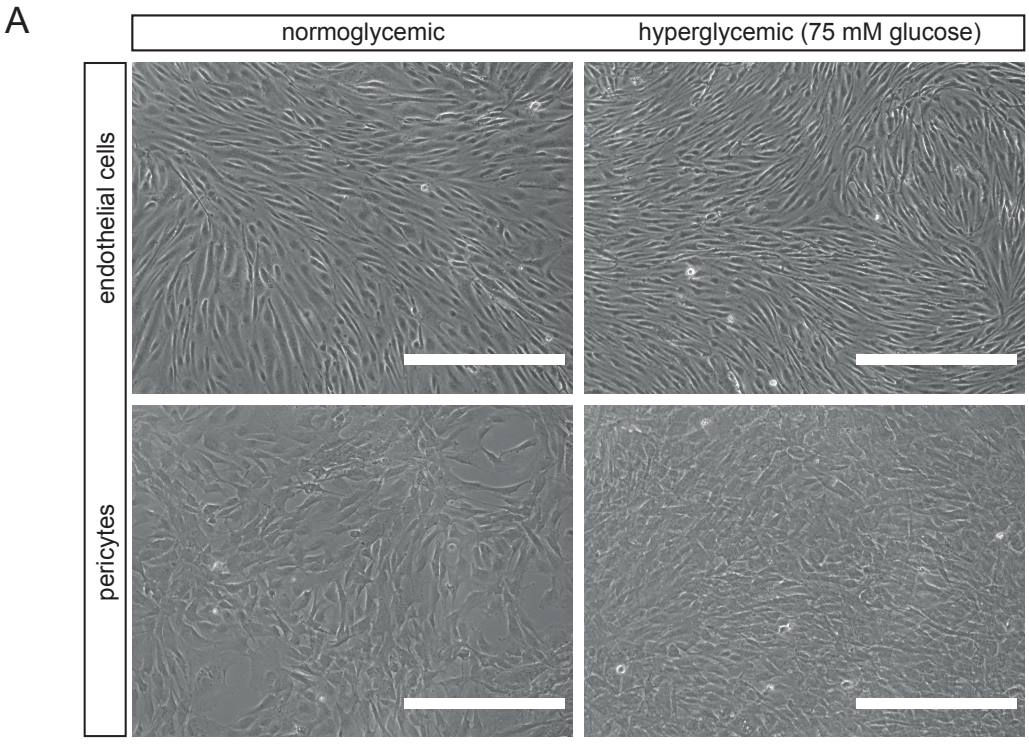
After the generation of a functional blood vessel model in the chip, I have tested several approaches to induce diabetes in blood vessels. Since high blood glucose level is the major manifestation of diabetes, hyperglycemic (28 mM or 78 mM glucose) culture medium was used to mimic that *in vitro*. Another approach was to use AGE-precursor methylgloxal (MGO) in culture medium, whose concentration is elevated in diabetic patients and cause vascular dysfunction (Shamsaldeen et al. 2016). Both approaches and their combinations have been tested on adherently cultured cells. After the determination of the optimal conditions for diabetes induction, blood vessels in the chips have been incubated with those conditions.

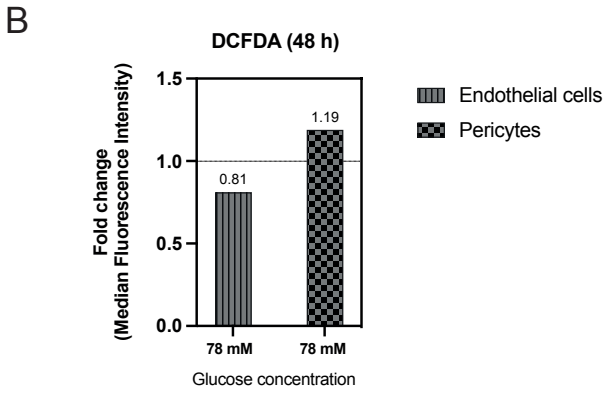
3.3.1. Reactive oxygen species (ROS) production in hyperglycemic conditions

As the first approach to induce diabetes in blood vessels, adherent endothelial cells and pericytes have been grown in hyperglycemic culture medium. Both control ECs and PCs were grown in normoglycemic culture medium, which had 8 mM glucose. We have tested two different levels of glucose: 28 mM and 78 mM. Morphologically, both endothelial cells and pericytes did not show any abnormality (Fig. 25A). However, we have observed an increased proliferation rate in both cell types after upon hyperglycemia.

Since we have not seen any morphological change, we wanted to test the ROS level in ECs, PCs, and additionally Müller glia cells, as there is a correlation with high glucose levels and intracellular ROS levels (Kowluru and Chan, 2007). For this purpose, 2',7' –dichlorofluorescin diacetate (DCFDA) assay was performed. DCFDA is a compound that enters the live cells and turns fluorescent upon oxidation by ROS within the cells. Therefore, the changes of ROS can be quantitively compared in different groups with flow cytometry analysis.

Fig. 25 shows quantified levels of DCFDA fluorescence intensity of ECs, PCs, and Müller glia in hyperglycemic conditions after 24 h (Fig. 25C) and 48 h (Fig. 25B) of exposure. For each measurement, normoglycemic controls (8 mM for ECs and PCs, 25 mM for Müller glia) were measured with flow cytometry and the data was normalized to 1. Müller glia and pericytes have been tested in addition to endothelial cells because of their role in metabolizing the excretions from the ECs.





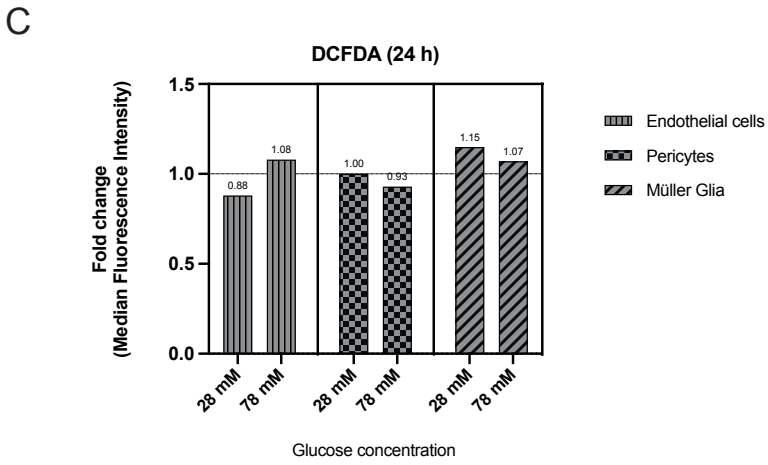


Figure 25: Induction of hyperglycemia in ECs and PCs and ROS detection in hyperglycemic ECs, PCs, and Müller glia. Phase-contrast images of ECs and PCs in normoglycemic vs hyperglycemic conditions

after 3 days (A). Scale bars = 400µm. DCFDA fluorescence intensity of 24 h (C) and 48 h (B) of exposure to hyperglycemia have been measured with flow cytometry and normalized to normoglycemic conditions of each cell type, n=2.

After 48 hours of exposure, as well as 24 hours, no significant changes of ROS levels have been observed neither in endothelial cells, pericytes, or Müller glia. Therefore, considering that they did not cause any detrimental effects on the morphology and viability of the cells, 78 mM glucose concentration have been used in chip experiments to induce diabetes.

3.3.2. MGO toxicity test via TUNEL assay

An alternative approach to induce diabetes in blood vessels was the AGE precursor methylgloxal (MGO) treatment. Diabetic patients have elevated levels of MGO in their plasma. As a metabolite derived from glucose, MGO also causes apoptosis in a wide range of cells including endothelial cells and pericytes (Matafome, Sena, and Seiça, 2013; Jang et al. 2017; Lee et al. 2020). Moreover, it is affecting vessel permeability in retina, which is the reason why we have chosen it as an inducer of diabetes in our disease model (Karachalias et al. 2003).

In order to test the sufficient MGO concentration for endothelial cells, TUNEL assay was performed (Fig. 26). Endothelial cells were treated with four different MGO concentrations (1,2 µM, 6,5 µM, 100 µM, and 300 µM) in normoglycemic (5,5 mM glucose) culture medium and stained with TUNEL dye. None of the MGO conditions displayed morphologic abnormalities prior to staining. Fig. 26 displays the TUNEL (green) and nuclei (blue) staining in four different MGO concentrations, and DNaseI control. Only one cell was positive for TUNEL in 1,2 µM MGO concentration, whereas two cells were positive for TUNEL in 300 µM condition. In 6,5 µM and 100 µM MGO conditions, there were no TUNEL-posivite cells. As none of the conditions significantly induced apoptosis in endothelial cells except for 300 µM condition, 100 µM MGO was determined as the concentration for diabetes induction in chip experiments.

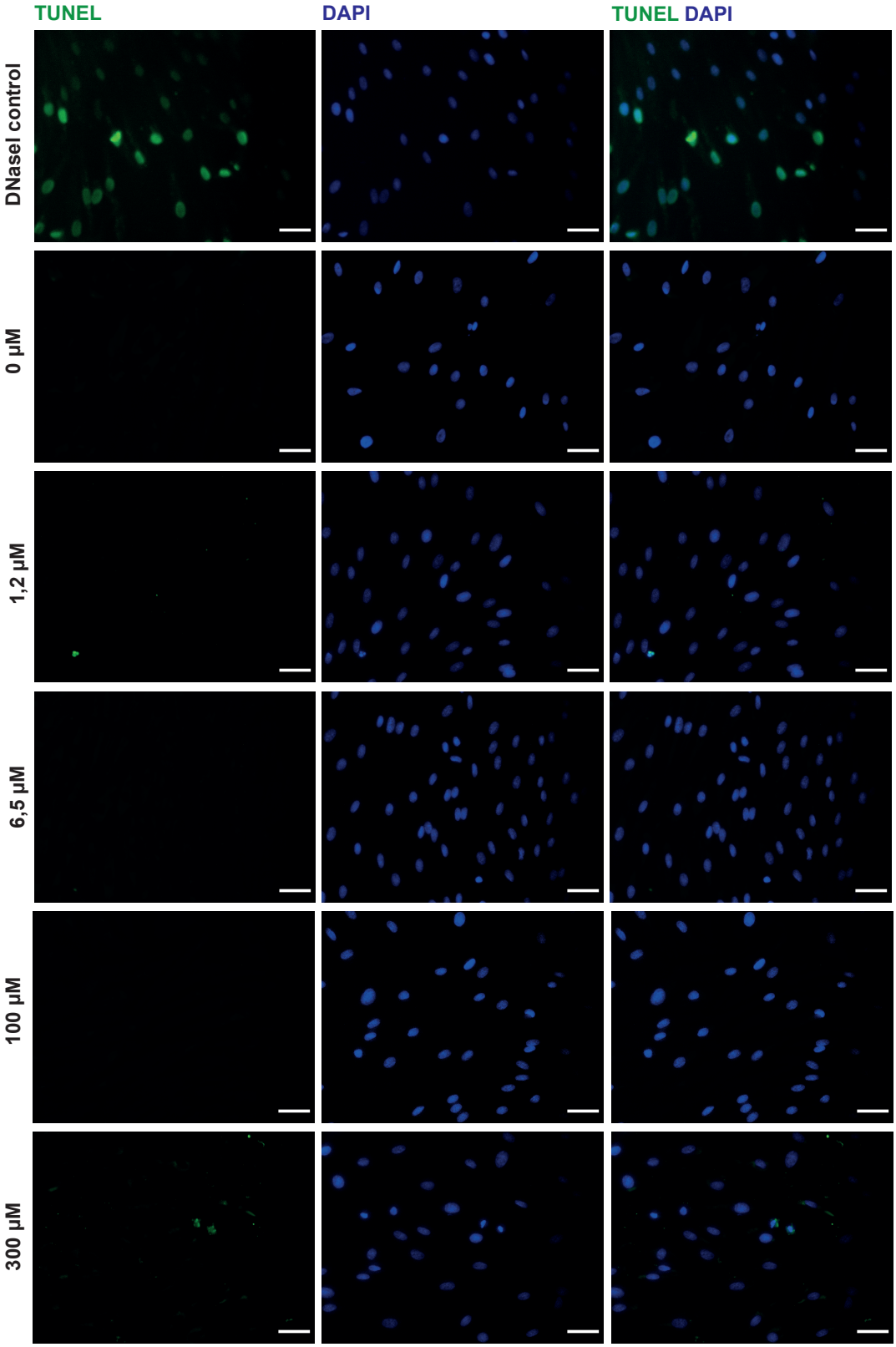


Figure 26: Apoptosis induction upon a range of MGO concentrations. Endothelial cells were stained with TUNEL (green) and nuclei were stained with DAPI (blue). Scale bars = 50µm.

3.4. Assessment of blood vessels on chip

Recapitulation of the inner blood-retinal barrier model has continued with the exposure of diabetic conditions in the 3D cell culture chip after the right approach has been chosen to mimic diabetes *in vitro*.

For this purpose, endothelial cells and pericytes have been loaded in chips in normal or diabetic (hyperglycemic or MGO treated) conditions. After 6-7 days of culture in respective conditions, blood vessels have been stained and using 3D images via Apotome (Fig. 27). CD31 staining was used to define blood vessel borders and blood vessel diameter and shape has been assessed and quantified.

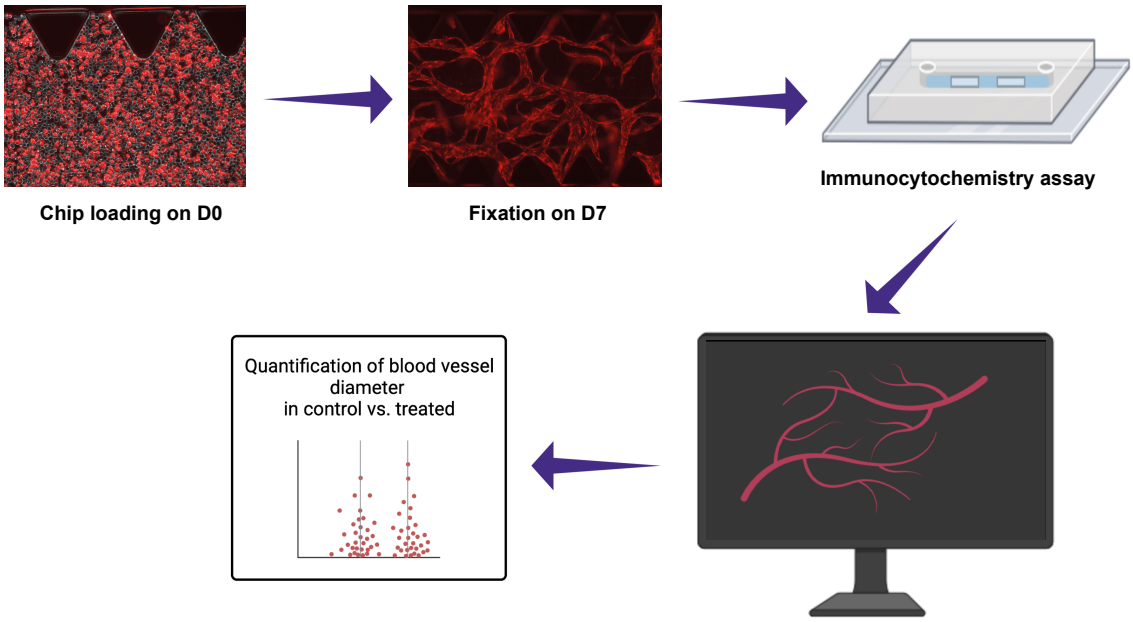


Figure 27: Schematic of quantification on blood vessels. Endothelial cells and pericytes have been loaded on chips (D0) and grown for a maximum of 7 days. Afterwards, immunocytochemistry assay has been carried out in the chip. Blood vessel diameter and shape was analyzed using Fiji.

3.4.1. Quantification of blood vessel diameter and shape

Diabetic retinopathy causes various changes in retinal vasculature (Chua et al. 2020). During diabetes, retinal blood vessels are enlarged, especially in venules (Klein et al. 2012; Silva et al. 2015; Drobnjak et al. 2017). Assessing the changes in retinal blood vessels during diabetes can therefore shed light onto the progression of the disease.

Feret's diameter in an object indicates the largest distance between two parallel planes. In blood vessels, that corresponds to the lateral diameter. We have compared diabetic vessels with control ones in terms of Feret's diameter (Fig. 28A), minimum Feret's diameter (Fig. 28B), and Feret's diameter/Minimum Feret's diameter (Fig. 28C). Compared to control (71.6 µm, SD±38.2), averaged Feret's diameter of hyperglycemic blood vessels was slightly smaller (65.5 µm, SD±37.4), though this change was not significant (Fig. 28A). However, MGO-treated blood vessels had significantly larger blood vessels with average Feret's diameter of 94.5 µm (SD ±41.4).

Minimum Feret's diameter of control vs. diabetic blood vessels is displayed on Fig. 28B. Hyperglycemic blood vessels have slightly smaller min. Feret's diameter with 22.2 µm (SD ±5.6) compared to control (24.5 µm, SD±7.7), whereas MGO-treated vessels have significantly larger min. Feret's diameter (31.7 µm, SD±10.6). Taking the information on Fig. 28A and 28B together, one can say that the MGO-induction caused the vessels to be enlarged, whereas hyperglycemic blood vessels have slightly smaller vessels in comparison to control ones.

Vessel shape was also quantified in diabetic vs. control blood vessels (Fig. 28C). The ratio of Feret's diameter/Min. Feret's diameter indicates the roundness of a blood vessel, with the ratio 1 indicating a perfectly round shape. We have assessed the vessel shape in all conditions, however, there was no significant difference between control vs. diabetic vessels (control: 2.9, SD±0.9; 75 mM glucose: 2.8, SD±1.1, 100 µM MGO: 3.0, SD±0.9).

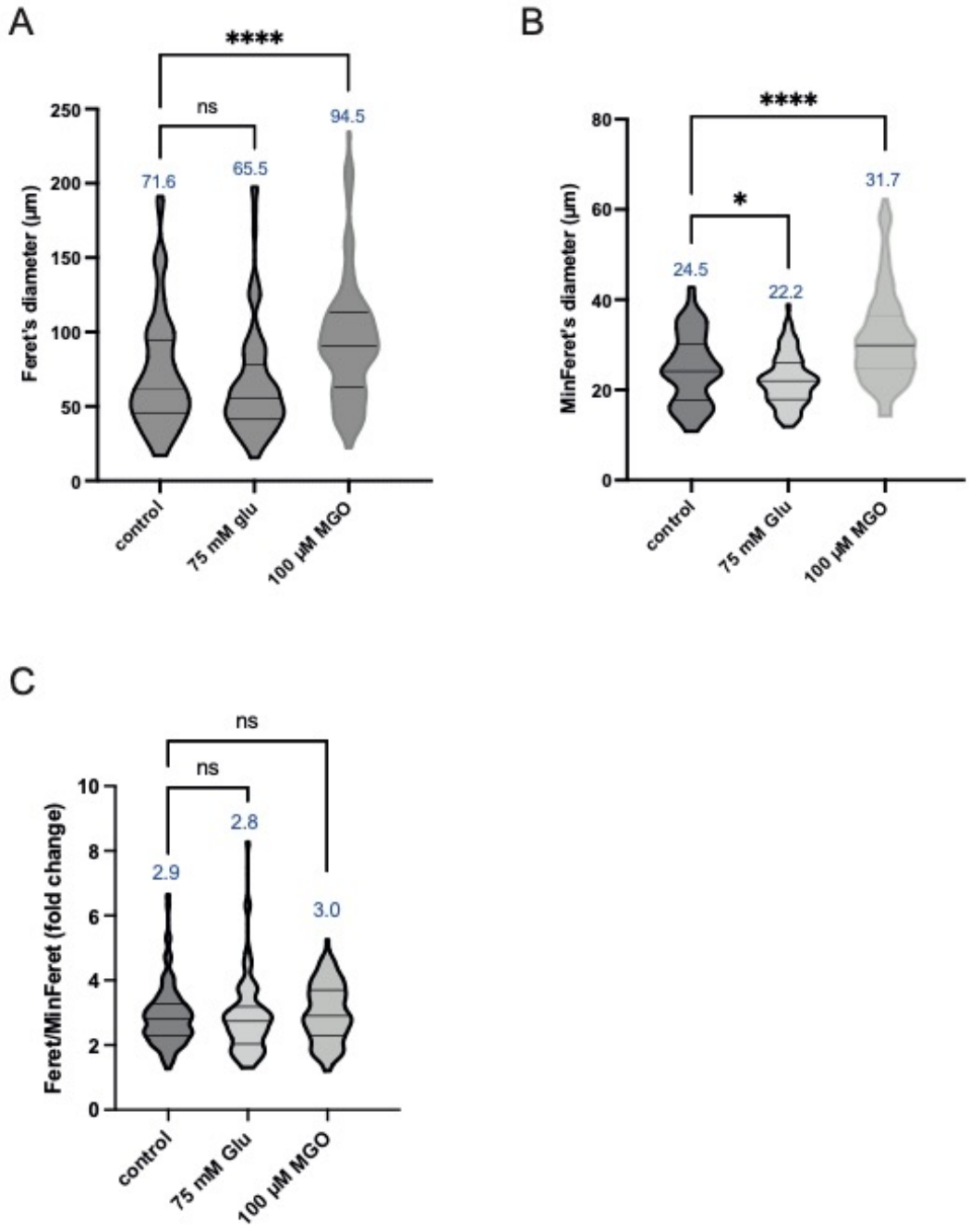


Figure 28: Diameters and shape in diabetic vs. control blood vessels. Feret's diameter (A), minimum Feret's diameter (B), and Feret's diameter/minimum Feret's diameter (C) have been compared between control (5.5 mM glucose), 75 mM glucose, 100 µM MGO-treated blood vessels in the chip. Non-significant (ns): p value > 0.05, *: p-value < 0.05, ****: p-value < 0.0001.

3.4.2. Effect of TGF-β pathway on blood vessel and shape

TGF-β signalling pathway controls many aspects of blood vessels in health and disease. For instance, TGF-β1 helps to decrease proliferation of endothelial cells and mature the blood

vessels (Sato and Rifkin, 1989). However, during diabetes, elevated levels of TGF-β disrupts blood-brain-barrier integrity (Shimizu et al. 2013). Considering the multifunctional aspect of TGF-β signalling, we have tested the influence of TGF-β1 and its inhibitor SB431542 in blood vessels.

Blood vessels were therefore cultured with 1 ng/ml TGF-β1 and 10 µM TGF-β inhibitor (SB431542) for 6 days in chip culture and Feret's diameter (Fig. 29A), minimum Feret's diameter (Fig. 29B), and blood vessel shape (Fig. 29C) have been assessed.

Interestingly, TGF-β1 treatment caused a significant decrease in Feret's diameter of blood vessels (control: 73.5 µm (SD±39.1), TGF-β1: 41.9 µm (SD±14.7). Minimum Feret's diameter has also been smaller (control: 24.5 µm (SD±7.7), TGF-β1: 16.5 µm (SD±3.3) in TGF-β1-treated blood vessels (Fig. 29B), which overall resulted in rounder vessel shape compared to control (Fig. 29C, control: 2.9 (SD±0.9), TGF-β1: 1.8 (SD±0.6).

TGF-β inhibitor resulted in the smallest and roundest blood vessels compared to all the other conditions with 30.8 µm Feret's diameter (SD±12.1) and Feret's/Minimum Feret's diameter ratio of 1.8 (SD±0.5).

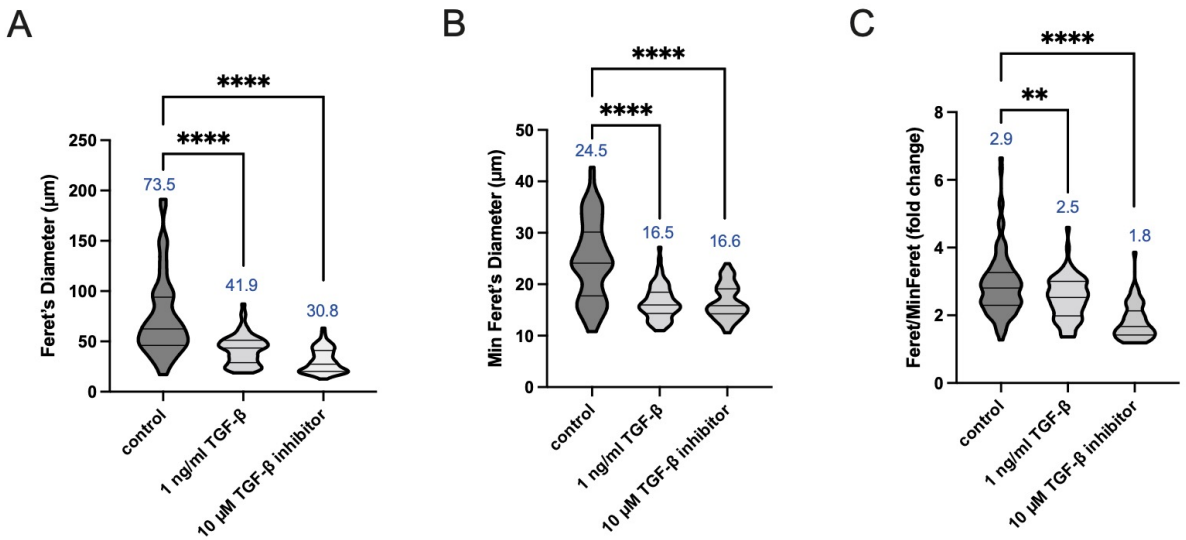


Figure 29: Effect of TGF-β pathway induction and inhibition on blood vessels. Non-significant (ns): p value > 0.05, *: p-value < 0.05, **: p-value < 0.01, ***: p-value < 0.001, ****: p-value < 0.0001.

3.5. Development of the disease model

Core components of the inner blood-retinal barrier have been established with endothelial cells and pericytes as mentioned in previous sections. As part of the neurovascular unit (NVU), glial cells (Müller glia, astrocytes, and microglia) also play a crucial role in keeping the barrier intact and regulated. Therefore, implementation of glial cells in iBRB model for diabetic retinopathy would be ideal. In this part of my PhD project, I have generated two glial components of the NVU (Müller glia and astrocytes) from hiPSCs. In addition to that, I have also performed preliminary experiments to pursue RNA-sequencing with the chip model for comparative gene expression analysis.

3.5.1. Müller glia extraction and addition to the blood vessel chip

In order to generate Müller glia, hiPSCs were initially differentiated into retinal organoids. Within the retinal organoids, Müller glia markers such as cellular retinaldehyde–binding protein (CRALBP) is expressed from D120 onwards. After that point, they are maintained in the ROs and can be extracted. ROs were dissociated using a neurosphere kit in order to singularize neurons and glia, and dissociated cells were plated on fibronectin-coated plates (Fig. 30). The aim was to selectively grow glial cells, since neurons did not survive on fibronectin coating and the only cell type observed in retinal organoids was Müller glia. Neurons however would attach to Müller glia in the culture and were washed off with DPBS several days after the plating. Eventually, only Müller glia would survive and expand on fibronectin coated plates. Cryopreservation was also possible when Müller glia reached confluency.

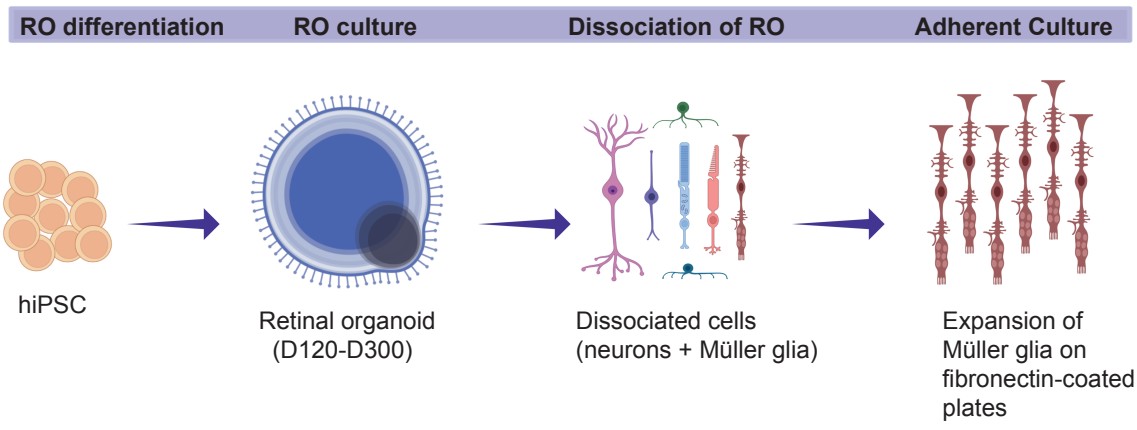


Figure 30: Generation of Müller glia from hiPSCs. ROs were generated from hiPSCs. Müller glial cells as well as other retinal neurons are apparent from D120. For adherent Müller glia culture, ROs between D120-D300 were dissociated with neuron dissociation kit and plated on fibronectin coating.

hiPSC-derived Müller glia were characterized by ICC (Fig. 31). Glia were positive for the common markers CD44, CRALBP, glutamine synthase and vimentin. Cells were also positive for the nuclear marker Sox9. However, unexpectedly, Müller glia were also positive for pericyte markers NG2 and PDGFRβ.

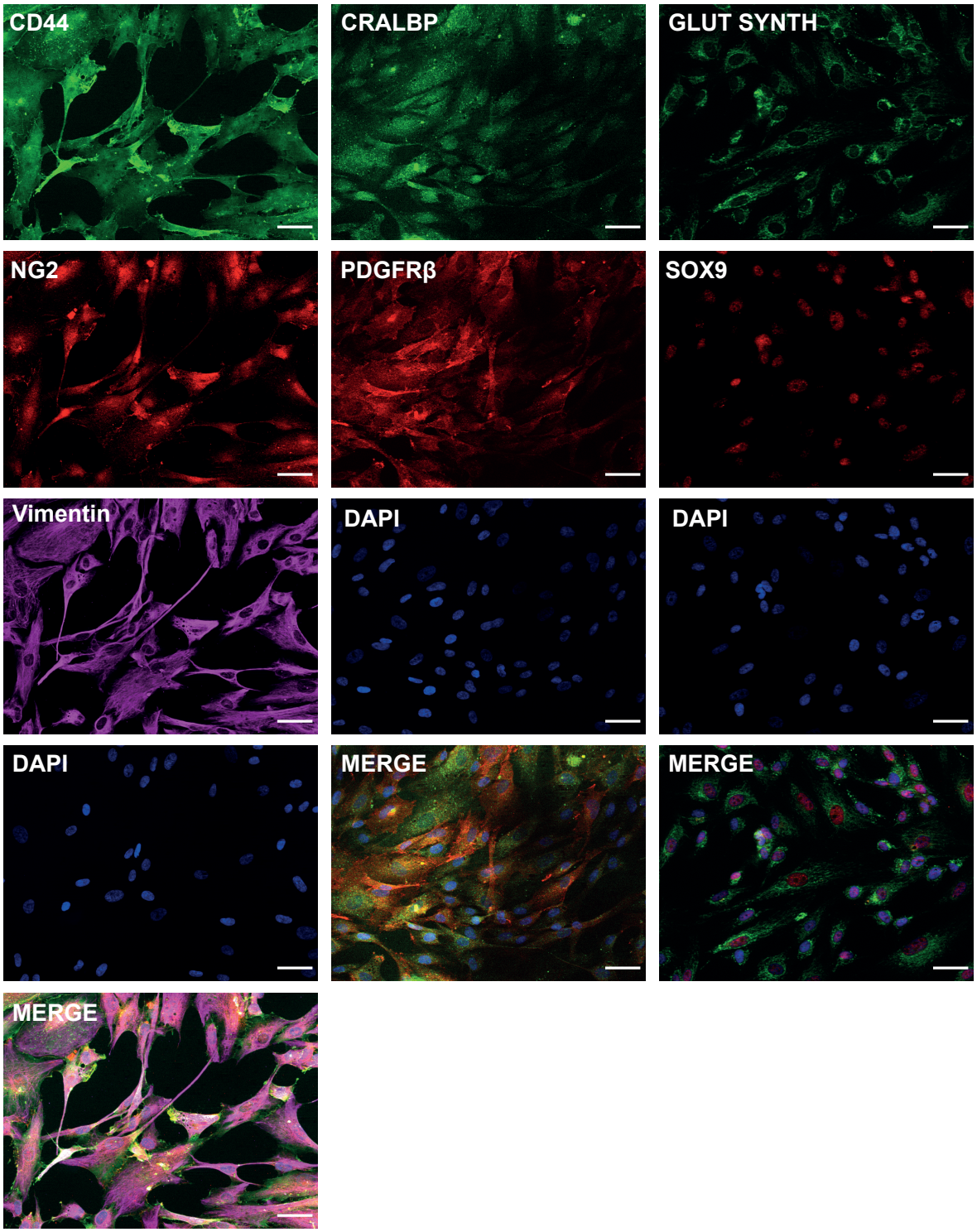


Figure 31: Müller glia characterization by immunocytochemistry. Scale bar = 50µm.

A test experiment has been conducted to see the interaction of Müller glia blood vessels in the chip model (Fig. 32). Endothelial cells (60.000 cells), pericytes (20.000 cells), and Müller glia cells (30.000 cells) were loaded in the chip and visualized on D6. We have clearly seen

that Müller glia (green) have been interacting with the endothelial cells (red). End-feet of Müller glial cells were located on endothelial cells in a similar fashion to inner blood-barrier barrier (white arrow in Fig. 32). However, blood vessels were not as branched as usual, and since the optimization and staining of each cell type posed a problem, further experiments were not performed.

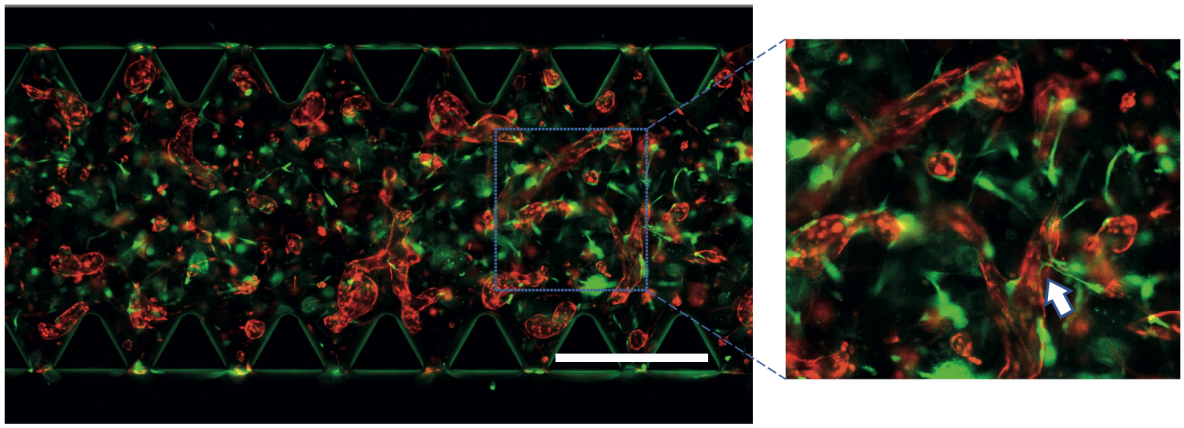


Figure 32: Müller glia incorporation into the microvasculature shows interaction with the blood vessels. Scale bars = 300 µm.

3.5.2. Generation of iPSC-derived astrocytes

Astrocytes are one of the glial components in the neurovascular unit in central nervous system and in retina. During development, they guide retinal angiogenesis by providing a scaffold for endothelial cells. And in adult retina, similar to Müller glia, they are part of the inner blood-retinal barrier. Retinopathies impact astrocytes as well as other cell types and cause disruption of iBRB permeability (Tao and Zhang, 2014). hiPSC-derived astrocytes therefore would be a great source to study diabetic retinopathy *in vitro*. With this aim, we have generated astrocytes from episomal hiPSCs line (E1) based on a current protocol (Krencik and Zhang, 2011) with minor modifications. The protocol is based on generation of neural rosettes within embryoid bodies from hiPSCs and consequent formation of astroglial progenitors in suspension culture. As shown in Fig. 33, from D90 onwards, astrospheres are plated onto fibronectin-coated plates and expanded.

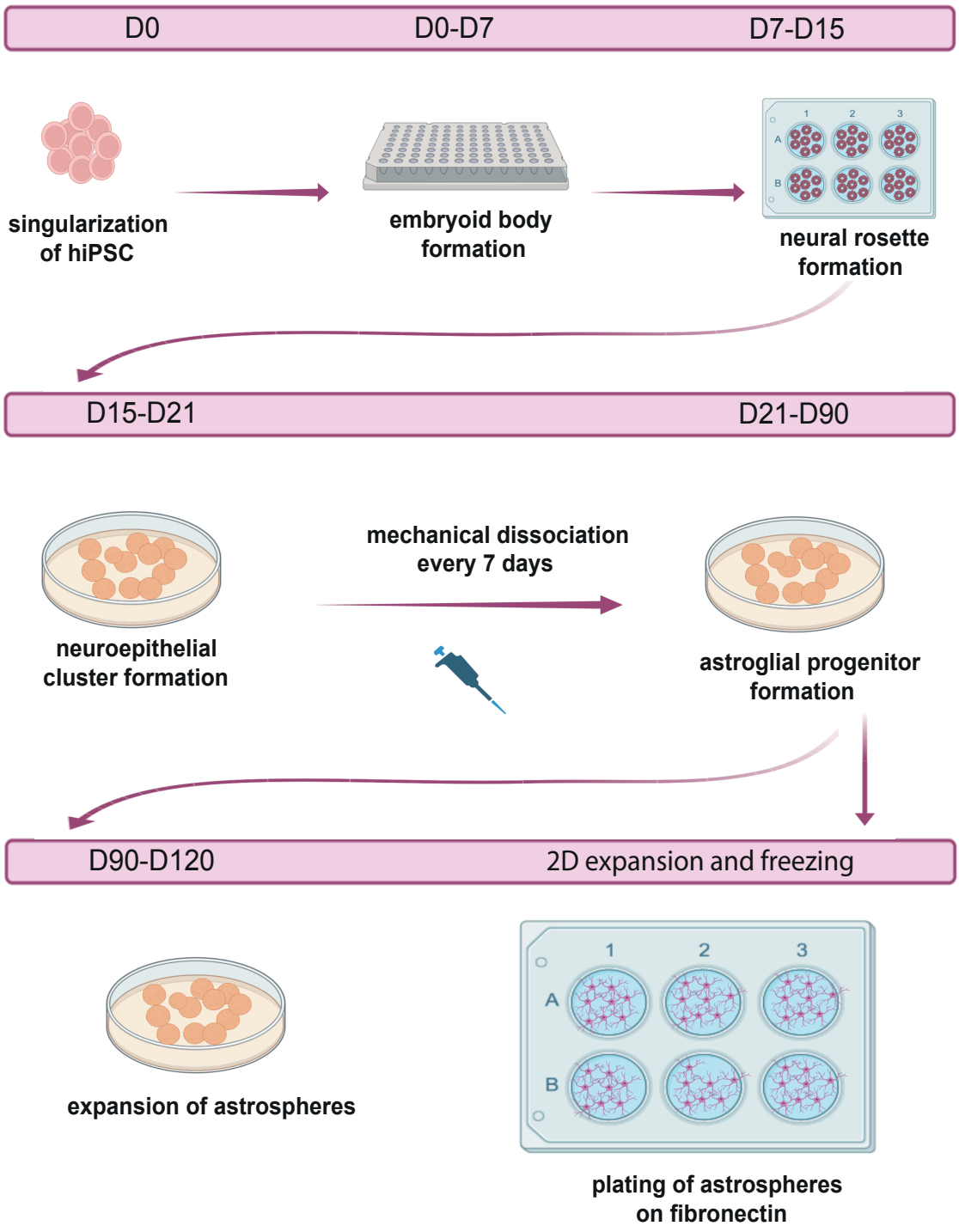
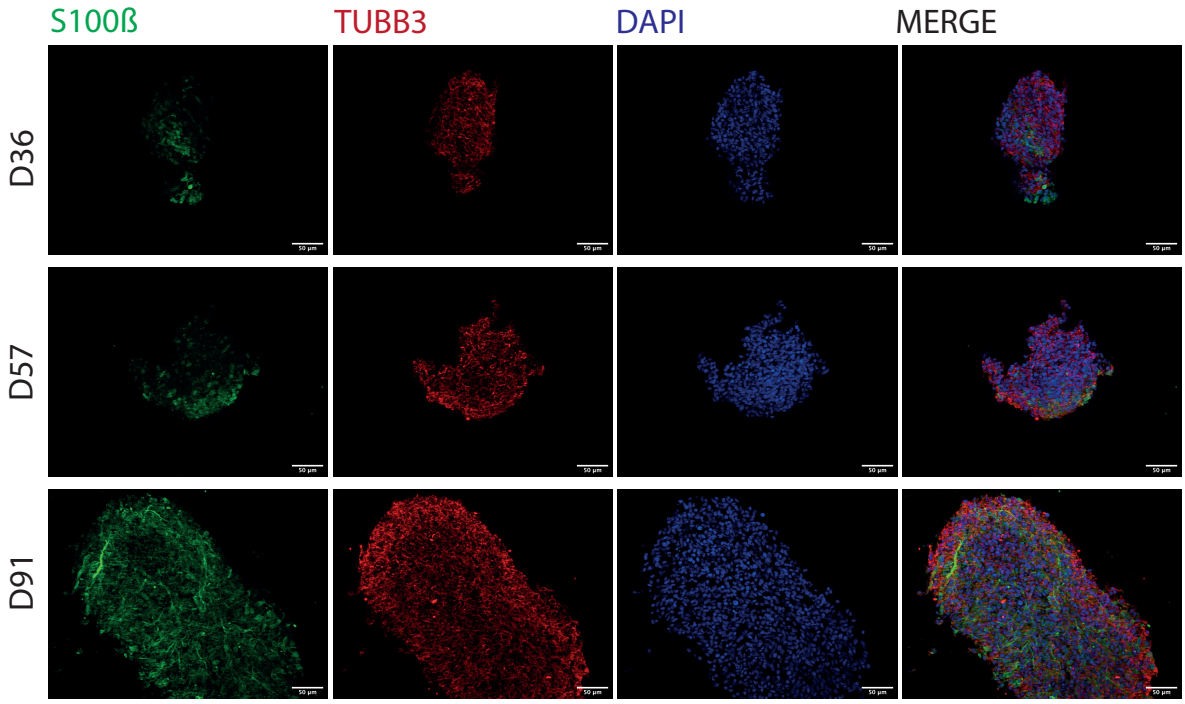


Figure 33: Astrocyte differentiation from hiPSC. Embryoid bodies are formed from hiPSC (D0-D7) and EBs are plated on GFR-Matrigel for neural rosette formation for 7 more days. On D15, once neural

rosettes are formed, they are manually picked and cultured in suspension culture in N2 medium. Neurepithelial clusters are cultured until astroglial progenitors appear (D15-D90). During this time, spheres are mechanically dissociated to disrupt the domination of neural progenitors. Between D90-D120, astroglial progenitors are plated on fibronectin-coated plates and expanded.

Spheres during three different stages of astrocyte differentiation (Day 36, Day 57, Day 91) have been collected and stained for their markers (Fig. 34). S100β was observed as early as Day 36 of differentiation, however the expression profile was observed in a portion of the sphere. GFAP expression was apparent at Day 91, as expected. Spheres were positive for Pax6 and β-tubuline class III (TUBB3) all through the differentiation, as well as vimentin. CD44 was never expressed in any stage of the differentiation.



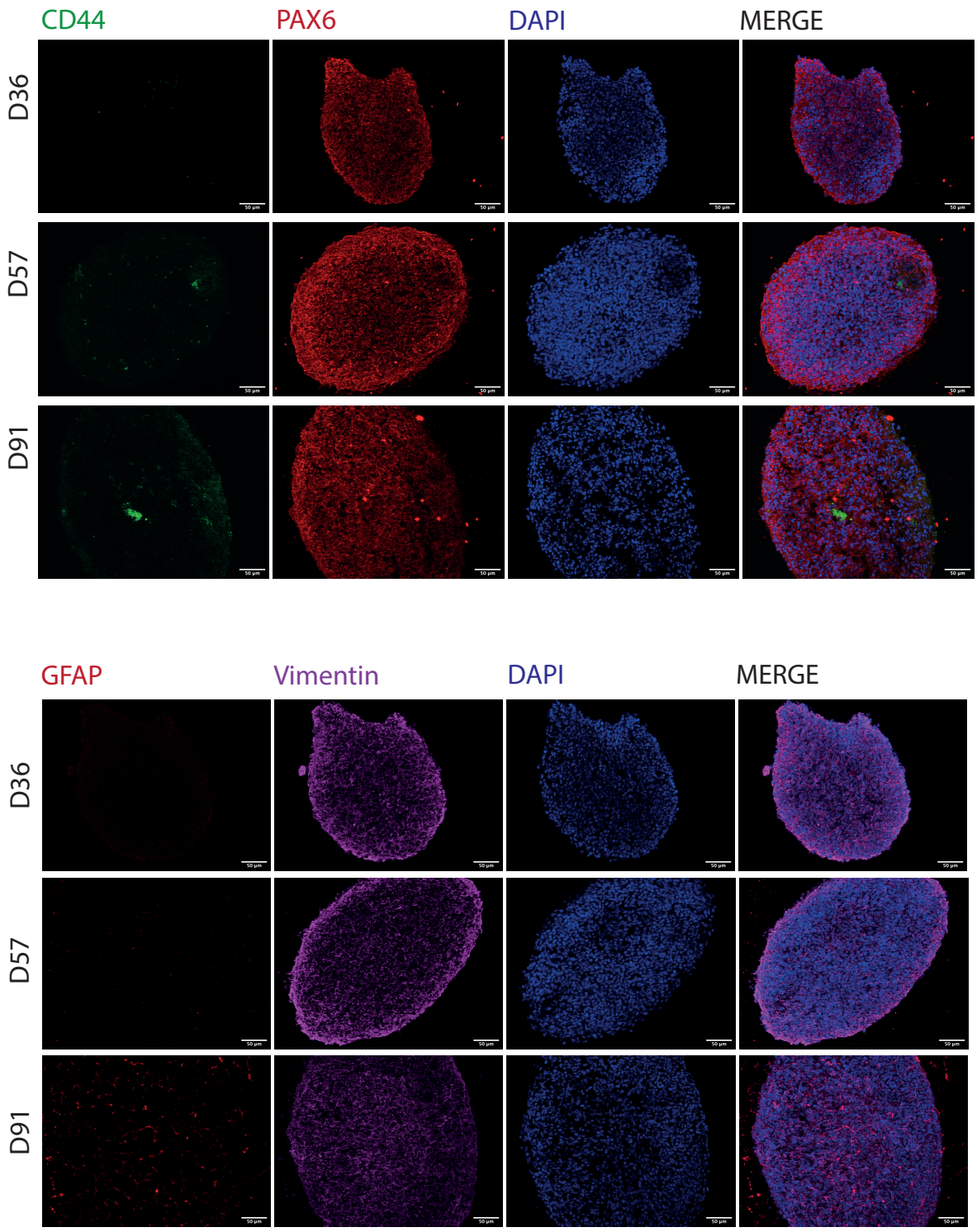


Figure 34: hiPSC-derived astrocyte characterization my immunofluorescence.

3.5.3. FACS of chips for RNA sequencing plan

The duration of this project was limited to the experiments above. However, a portion of the future experimental designs could be followed by the scientists in our lab.

In order to achieve a comparative gene analysis, RNA-sequencing of the cells within the chips were planned. Fig. 35A depicts an overall plan; diabetic vs. control blood vessels are collected from the 3D cell culture chip, sorted via FACS as endothelial cells and pericytes by CD31 and RNA extraction follows. With this plan, it is expected to see the differential gene expression profiles of endothelial cells and pericytes in diabetic vs. control conditions. There were several optimization steps in this plan and during the course of this thesis, only a few steps could be optimized, and the plan was not finalized. The first optimization step was required for the detachment of cells from the chip; since endothelial cells and pericytes were embedded on a fibrin gel, which was polymerized and robust, it was challenging to dissolve it with cell detachment agents. Cell detachment with TrypLE and AccuMAX was tried and both agents were successful. To increase the surface area of the chip with dissociation agents, chip was detached from its plastic film at the bottom and agents were applied directly on top of the vessels, instead of using media channels. This method also fastened the detachment process. Fig. 35B shows the FACS result of the first step experiment; live cells were selected with DAPI and double positive cells for CD31 and mCherry were collected as endothelial cells whereas double negative cells (CD31 and mCherry negative) were collected as pericytes. Both cell fractions were collected in RLT buffer in microcentrifuge tubes for further RNA extraction and frozen on dry ice upon collection from FACS machine. The separation of endothelial cells and pericytes were very distinct and ensured that the live staining was working efficiently. However, in the next step of optimizations, mCherry endothelial cells were not used in order to prevent the domination of highly abundant mCherry protein in RNA sequencing analysis. Therefore, non-mCherry endothelial cells were generated from episomal hiPSC source and the chip loading and cell detachment was repeated (Fig. 35C). It is important to note that in the second trial, TrypLE was used as a cell detachment agent and cell survival was similar to the AccuMAX detachment. Separation was based on CD31 expression only. Similar to the previous experiments, the separation of endothelial cells from pericytes were very clear, however, the quantity of endothelial cells was lower than pericytes.

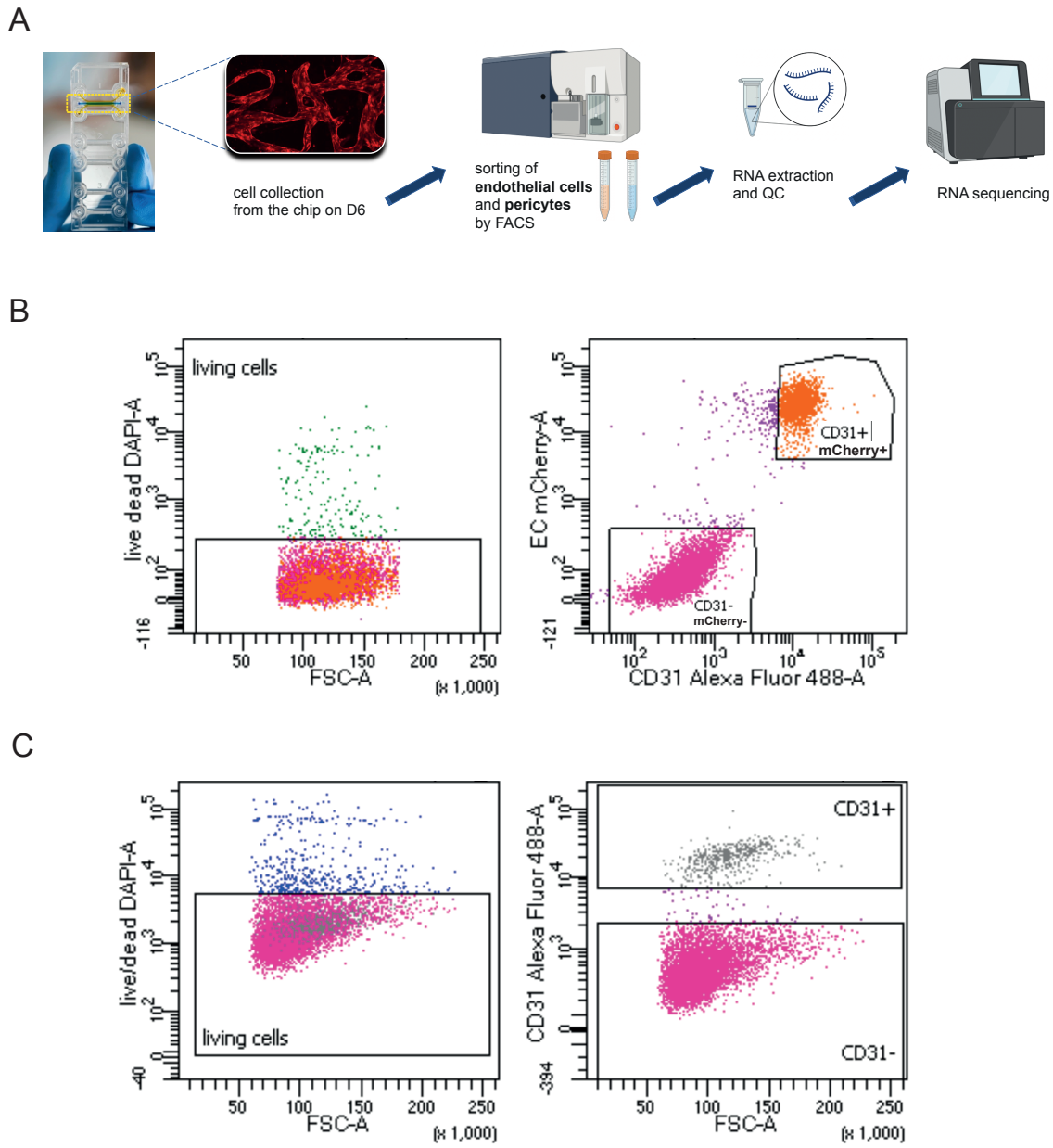


Figure 35: RNA sequencing plan of endothelial cells and pericytes. Future development of the chip includes RNA-sequencing of endothelial cells and pericytes that have been sorted by FACS after chip loading, ideally on D6 (A). DAPI staining shows the majority of cells are alive after detachment and staining procedures, and a distinct separation of ECs and PCs based on CD31 and mCherry staining (B). The use of non-mCherry ECs as the next improvement step shows a similar result, with low cell death as well as a distinct separation of ECs and PCs (C).

4. Discussion

4.1. Recapitulation of iBRB using hiPSC-derived endothelial cells and pericytes

Generating human *in vitro* disease models can replace animal models allowing to study processes specific for human organism, overcoming the ethical concerns, making high-throughput screenings for diagnostic and therapeutic targets cheaper. Since retinal microvasculature is affected by diabetic retinopathy and is responsible for edema and blindness via iBRB disruption and neovascularization, I focused on vascular component of the retina to model the disease. Therefore, I recapitulated iBRB with hiPSC-derived cells on a 3D cell culture chip. In this section, I will discuss the generation and characterization of hiPSC-derived cell types that are forming the neurovascular unit for iBRB. HIPSC is an invaluable tool for personalized medicine approach, since disease modelling and drug testing can be done with patient specific cell lines that would include the genetic make-up of an individual.

4.1.1. hiPSC-derived endothelial cells

Endothelial cells are structurally and functionally the most important component of the neurovascular unit. HiPSC-derived endothelial cells hold the most potential for vascular network formation with unlimited proliferation capacity, their use in translational research, and the ability to generate organ specific ECs. In 77% of the vascular network studies performed between 2013-2018, primary human cells such as HUVECs have been used, compared to 9% of hPSC-derived ECs (Wang, Lin, and Martin, 2019). Although the trend is in favor of hiPSC-derived ECs, the lack of efficient and reproducible EC generation protocols is an obstacle. Therefore, a reproducible and efficient differentiation protocol and *in vitro* culture was crucial for my project. Among many EC differentiation protocols, I have tested several of them (Orlova et al., 2014; Patsch et al.; 2015; Wimmer et al., 2019). However, differentiation protocols based on adherent culture of hiPSCs resulted in extremely low yield, with or without a purification method such as FACS. To add, optimizations to the protocols were also tested such as initial hiPSC number and various culture plate coatings, which did not increase the yield (data not shown). Simultaneously, we have generated 3D vascular organoids from a published protocol (Wimmer et al., 2019). Vascular organoid differentiation was based on embryoid body formation from hiPSCs, followed by EC differentiation via small

molecules indicated in the protocol by Patsch and colleagues. Therefore, in an attempt to increase our EC yield, we have combined and improved the two protocols and published a novel EC differentiation protocol (Pars et al., 2021). This novel protocol included an initial EB formation stage and consequent suspension culture for 5 days, followed by adherent culture and MACS separation with CD31 beads on D9 or D10 (Fig. 8). Initial EB formation when mesodermal lineage is induced can be crucial since 3D environment and cell-cell interactions are mimicked similar to the developmental mesoderm formation (Han et al., 2018). Two-step differentiation protocols using initial EB formation followed by monolayer differentiation was performed by other groups as well (Mulfaul et al., 2020; Garcia-Alegria et al., 2021). In a zebrafish endothelial cell generation study, EB-based endothelial cell differentiation from blastocysts were shown to be more efficient in induced EC markers compared to monolayer differentiation (Ibrahim, Xie, and Richardson, 2020).

Separation by MACS at the end of differentiation ensured the purity and enrichment of generated endothelial cells. The use of magnetic beads, compared to FACS separation also increased cell survival. Following MACS separation, obtained % of ECs differed significantly between E1 and K5 line, as measured 8% and 55%, respectively (Fig. 10A). However, when EC/hiPSC ratio (number of ECs generated per number of hiPSCs used on D0) was calculated for two of the lines E1 and K5, the efficiency is measured as 1 and 2, respectively (Fig. 10B). This demonstrates that even for the least efficient line, EC yield per hiPSC was 50%.

Morphologically, generated ECs resemble primary brain endothelial cells with their long and thin morphologies (Fig. 9C). Due to their tight junctions, brain and presumably retinal endothelial cells show a tightly packed assembly in cell culture (Fig. 13A), which indicates that their barrier property can be observed even in monolayer culture, similar to our observation (Craig et al., 1998). Compared to usual round and cobble-stone shape of cultured primary ECs, hiPSC-derived ECs generated with this protocol resemble their *in vivo* counterparts (Krüger-Genge et al., 2019). Cryopreservation of hiPSC-derived cells with this protocol is also efficient, since cells can be thawed similar to immortalized lines and cell death is minimal (~9%) (Fig. 10C).

Marker expressions of hiPSC-derived ECs were also confirmed with immunocytochemistry and flow cytometry. For instance, for K5 line, 50% of cells in D10 of differentiation (prior to MACS separation) were positive for CD31 and VE-cadherin in flow cytometry analysis (Fig. 12). When sorted with CD31 beads, CD31 and VE-cadherin was expressed in all cells, and CD31 expression was retained until at least passage 2 (Fig. 13B).

Tight junction complex markers, ZO-1 and retina-specific claudin-5 expression was also observed in majority of ECs, which indicates that hiPSC-derived ECs express markers found in retinal endothelial cells (Fig. 10). Similarly, CD146 was also expressed in majority of the cells, which is essential in BBB maturity, since it is expressed in brain ECs during BBB development and downregulated by pericytes upon barrier formation (Chen et al., 2017; Abu El-Asrar et al., 2021). CD34, which is expressed in hematopoietic stem cells and endothelial progenitor cells, were also expressed in a portion of our generated ECs. Although in HUVECs, CD34 expression is associated with tip cells and low proliferation capacity, CD34+ cells in brain ECs were associated with repairing vascular injuries (Siemerink et al., 2012; Abdulkadir et al., 2020; Loiola et al., 2021).

EC functionality was proved by several methods. Initially, a tube formation assay was performed. ECs cultured in on thick Matrigel formed tubes within 16 hours, which was confirmed with Calcein-AM staining (Fig. 15). However, tube formation assay is not a 100% accurate method for proving EC functionality, since other cell types such as tumor cell lines from various tissues as well as fibroblasts were found to form tubes on Matrigel as well (Auerbach et al., 2003; Francescone, Faibish, and Shao, 2011).

Therefore, we used another method involved in inflammation response of ECs. Upon inflammation, ECs increase their ICAM-1 expression to facilitate transendothelial leukocyte migration. Upregulation of ICAM-1 increases the permeability of both iBRB and BBB, which is also associated with diabetic retinopathy (Khalfaoui et al., 2008; Yao et al., 2019). Therefore, we exposed adherent ECs to TNF-α and measured protein levels of ICAM-1 using western blot. Quantified results showed that ECs overexpressed ICAM-1 in a dose-dependent manner when subjected to 10 ng/ml and 100 ng/ml TNF-α (Fig. 16). CD31 was used as a standard for quantification, since its expression is not known to be changed even though it has a role in ICAM-1 signaling (Couty et al., 2007).

Lastly, we cultured endothelial cells in 3D culture chip for blood vessel formation. Blood vessels were formed within 24 hours and immunocytochemistry with Z-stacks showed lumen formation (Fig. 23), which strongly proved functionality.

Taken together, hiPSC-derived endothelial cells could be readily generated, expressed key cell markers, and were functional. After the generation of the first important component of iBRB, generation of pericytes were performed, which will be discussed in the next section.

4.1.2. Neural-crest stem cell-derived pericytes

In the experiments conducted within the scope of these thesis, two types of pericytes have been generated: mesodermal PCs and NC-derived PCs. Mesodermal PCs were generated using the same hiPSC-derived EC protocol (Pars et al., 2021). They expressed pericyte markers PDGFRβ, NG2, and SMA in immunocytochemistry assays (Fig. 14) and with flow cytometry analysis. Handling and culture of mesodermal PCs are also straightforward since they can be cultured up to passage 6 and cryopreserved with minimal cell death. Occasionally, endothelial cell contamination in pericyte culture would be observed, which caused purity problems. Mesodermal PCs have been used in early optimization experiments for the chip culture, however, mainly due to their embryonic resemblance to retinal pericytes, for generating the disease model, NC-derived PCs were used as perivascular cells, which were differentiated from hiPSC in a two-step protocol (Fig. 17) (Gastfriend et al., 2021).

Majority of NC-derived PCs expressed PDGFRβ and NG2 in flow cytometry analysis, with 88% and 86%, respectively (Fig. 19). Although in the original protocol, neither NCSC nor NC-derived PCs were recommended to be cryopreserved, we could manage to cryopreserve both cell types after several optimizations. For NC-derived PCs, death rate was 27% on average post-thaw (Table 17). However, due to the low amount of hiPSCs needed initially for the protocol, one could generate a large batch of NCSCs and cryopreserve them to compensate for high death rate upon thawing.

Although there is no universal pericyte marker, PDGFRβ is known to be expressed in many healthy retinal pericytes (Xiang et al., 2019; Rangasamy et al., 2020). We observed the

expression of PDGFRβ in the majority of NC-derived PCs in immunocytochemistry assay (Fig. 18). Since pericyte characterization considers their location on the vascular wall in addition to cell markers, we performed microvascular network formation by co-culturing PCs with endothelial cells in the chip culture. Immunocytochemistry revealed PDGFRβ expression located in close contact to ECs, similar to retinal capillaries (Dreisig, Blixt, and Warfvinge, 2018). Another important marker, basement membrane protein collagen IV was expressed in all cells as well. Overexpression of collagen IV is associated with hyperglycemia and diabetic retinopathy; however, it is known that retinal pericytes express collagen IV also in healthy retinas in many species (Wakisaka et al., 1997; Dimaio et al., 2008). Additionally, even in homeostasis, basement membrane bridges that are positive for collagen IV, are observed in murine retinal vasculature (Corliss et al., 2020). NG2, a glial marker, is also found to be expressed in majority of pericyte types, and its expression in majority of cells in immunostaining is consistent with the flow cytometry analysis. However, unexpectedly, CD146 expression was also observed in a portion of pericytes. In murine retina, pericytes, especially in branching vessels had CD146 expression, although this was not observed in capillaries (Wittig et al., 2013). However, in human retinal pericytes, CD146 expression was detected, although the expression was more abundant in retinal VSMCs (Smyth et al., 2018).

4.1.3. Müller glia and astrocytes – additional components of iBRB

The generated disease model of DR included endothelial cells and pericytes. However, macroglial components of neurovascular unit are known to be associated with barrier homeostasis as well (Tout et al., 1993). Müller glia, as well as astrocytes have buffering effects of water and ions through the retinal capillaries. Therefore, in studying diabetic retinopathy, which is caused by various metabolic changes in retina, glial cells would be interesting to be incorporated to the disease model.

With this aim, I generated Müller glia and astrocytes from the same hiPSC source as ECs and PCs and characterized them.

Astrocytes were generated from hiPSCs based on a published protocol with some modifications (Fig. 33) (Krencik et al., 2011). Since astrocytes are confined in RGL and optic nerve of retina, their role in iBRB is not fully understood. However, they share some

similarities with Müller glia, and their incorporation would shed light on physiological and pathological processes of the retinal blood vessels and neurons.

Immunocytochemistry assay revealed cell markers that are expressed during astrocyte differentiation (Fig. 34). CD44 was never observed at any stage of differentiation, whereas neuronal marker Pax6, and vimentin were consistently expressed during differentiation, whereas another neuronal marker TUBB3 was unexpectedly observed in all stages. This could be explained because of unspecific binding of TUBB3 antibodies or the existence of neural progenitors. As a neural progenitor marker, Pax6 expression is expressed in optic cup. However, since retinal astrocytes are formed within the optic disc, which is in close proximity to the optic cup, $Pax6^+$ cells still may hold potential for astrocyte fate (Paisley and Kay, 2021). Expressions of S100β, GFAP and vimentin are consistent with astrocyte expression patterns. In rodent retinae, astrocyte precursors express vimentin, which is reduced once astrocytes mature upon contact with blood vessels, whereas S100β and GFAP expressions are absent in precursor stage and arise toward maturation (Sheef et al., 2005; Chan-Ling et al., 2009).

Müller glia generation was conducted with isolation from >120 day-old ROs via single cell dissociation (Fig. 30). Although this method is easy to conduct, there may be variances between ROs that are manually chosen. However, once Müller glia are transferred to 2D culture, their expansion rate, robustness, and low death ratio after cryopreservation make them suitable for routine use. For instance, in primary porcine retinal astrocyte culture, glutamine synthase and CRALBP expression is known to be downregulated over time in 2D culture, whereas in our culture, both markers were expressed in most cells (Hauck, Suppmann, and Ueffing, 2003).

Generated Müller glia also expressed CD44, vimentin and Sox9 (Fig. 31), similar to the human Müller glia generated from ROs in another study (Eastlake et al., 2019). NG2, as a glial marker, was also observed in Müller glia immunostainings, expressed by some cells. Although NG2-expressing glia are usually found in CNS and are precursors of oligodendrocytes, their transcriptome is highly different than oligodendrocyte-associated genes, which may suggest that they may be involved in differentiation of other cell types (Du et al., 2021). However, unexpectedly, some Müller glia expressed PDGFRβ, which is a pericyte marker. Since Müller

glia are known to express another subunit of PDGFRβ, namely PDGFRα, the expression can be explained because of the cross-reactivity of PDGFRα. Alternatively, the signal could be specific, since there are recent mouse studies showing PDGFRβ expression in Müller glia in gene level (Díaz-Lezama et al., 2021; Mayr et al., 2022). Nevertheless, this made the co-culturing of blood vessels with Müller glia harder since pericytes and Müller glia could not be easily distinguishable upon co-culturing. However, investigating PDGFRβ signaling in Müller glia could be further investigated to see the cell-cell interaction between pericytes and Müller glia and its implications in iBRB.

After the generation and characterization of Müller glia, I have also conducted preliminary experiments with tricellular co-cultures of ECs, PCs, and Müller glia. According to our knowledge, human Müller glia were not included in any disease modelling study of DR. When co-cultured with endothelial cells and pericytes, Müller glia were shown to wrap blood vessels and acquired their specific elongated and thin shape (Fig. 32). In some parts of the chip, end-feet of Müller glia could also be observed. On the other hand, blood vessels did not form their typical branched, capillary-like assembly upon the co-culture with Müller glia. Optimization steps to include an established tricellular co-culture were challenging and were not fully investigated during the course of my thesis. Some of these challenges included the hardships in labelling and distinguishing PCs from Müller glia after the chip co-culture, as well as cell the correct ratio of ECs:PCs:Müller glia. Since blood vessel formation with endothelial cells is highly dependent on cell density, adding additional components to the model will reduce the relative number of endothelial cells per chip, which reduces or halts the blood vessel formation. Also, adding Müller glia to the chip culture after the vasculature is formed could be tested, since Müller glia would help mature the already existent vessels. However, once these challenges are solved, adding of Müller glia to the existing model holds potential for investigating retinopathies.

4.2. Self-assembly of blood vessels in 3D chip shows retinal capillary-like properties

We have recapitulated the iBRB considering its crucial aspects. Endothelial cells that expressed tight junction proteins formed blood vessels and were perfusable in chip culture. Pericytes were co-cultured with ECs in 1:1 ratio as in retinal capillaries and matured the

microvasculature by possibly inhibiting EC proliferation. The formed microvasculature network also had a basement membrane and was stable for up to 7 days in culture.

4.2.1. Microvascular network formation in chip resembles physiological blood vessel formation

Retinal-like microvasculature was formed within 1:1 ratio of endothelial cells and pericyte in chip culture. Generated blood vessels were assessed with immunostaining and perfusion test. Microvascular network formation was initiated within 6-12 hours of cell loading in the chip. The 7-day time lapse images showed the initial formation of blood vessels within 24 hours, where endothelial cells formed tubes with lumens, and pericytes wrapped up the vessels after this point (Fig. 22). Blood vessels were labelled with endothelial cell marker CD31, pericyte marker PDGFRβ and basement membrane marker Col. IV, which clearly showed a capillary-like structure. Since DR affects capillaries the most and many vessels within the retina are capillaries, this relevance was of great importance (Burns, Elsner, and Gas, 2021).

Lumen formation of blood vessels were visualized with Z-stacks, and lateral diameter of 50 µm and transverse diameter of 28 µm show a slightly larger vessel size than capillaries (Fig. 23). However, we have seen that the vessel size is affected by many variables of chip culture and would show differences between experiments. Some of these included cell loading in the chip in total volume of 10 µl which would polymerize within 10 seconds and state of ECs. Different passage numbers of ECs, PCs, and their doubling time could be affecting microvasculature formation. To overcome this challenge, while collecting quantitative data, we have performed experiments with triplicates per chip set, and on different time points.

Functionality of blood vessels were displayed with 40 kDa FITC-dextran (Fig. 24). Although generated blood vessels were perfusable, the leakage followed after 3 minutes (Fig. 24A). Despite the leakage, parts of vessels that anastomosed, even after 15 minutes, darker spots could be seen, which did not leak as much as the rest. However, it is important to note that in order to perform perfusion assay, side channels of the chip had to be fully connected to the microvasculature in the middle part, which was challenging. Therefore, unconnected parts of the side channels to the middle channel may have caused the flow of dextran directly

to the gel layer. Confocal imaging with a better resolution and Z-stacks would be more suitable for the assessment of perfusion.

For our model, as a hydrogel in the chip, we used fibrin gel. Fibrin is known to induce capillary formation of endothelial cells via VE-cadherin *in vitro* (Bach et al., 1998; Martinez et al., 2001). In microfluidic chips, fibrin is widely used for microvasculature formation because of its strength to withstand pressure better than collagen-I and its stability in culture (Park et al., 2014; Koroleva et al., 2016; Zhang, Wan, and Kamm, 2021). However, fibrin also induces inflammatory cytokine release in a variety of tissues and linked to increased expression of ICAM-1 in endothelial cells (Luyendyk, Schoenecker, and Flick, 2019). Fibrinogen could also induce angiogenesis. In an *in vitro* study conducted with HUVECs, fibrinogen was found to increase cells proliferation compared to cells without fibrinogen, which is one of the two components in fibrin gel (Sahni, Sporn, and Francis, 1999). For a more physiological model, other gel compositions could also be tested. Basement membrane (BM) of retinal capillaries consists of several extracellular matrix components such as collagen IV, laminin, perlecan, nidogen, and fibronectin. These components play crucial rules in retinal vessels in providing a scaffold for them and by regulating cell adhesion and migration. For instance, retinal angiogenesis requires the degradation of collagen IV in BM for angiogenic sprouts to grow (Spuul et al., 2016). Additionally, retinal BM contributes to the assembly of tight junctions and helps to regulate the blood flow of retinal vessels (Roy and Kim, 2021). As retinal BM is affected and is thickened in DR, mimicking physiological retinal BM could improve the disease model of diabetic retinopathy.

4.2.2. Pericytes are crucial for vessel coverage and maturing endothelial cells

Endothelial cells derived from hiPSCs had the capability to form blood vessels in 3D chip culture. However, formed blood vessels with ECs alone had a significantly larger diameter than those co-cultured with pericytes and did not resemble capillary structures. It is known that increased EC density causes increased capillary diameter in retinal vessels (Watson et al., 2016). In comparison, when ECs are cultured alone to form microvasculature, even though lumen formation occurs during the first 48 hours, due to ECs proliferation, blood vessels cannot mature, and capillary diameter increases over time (data not shown). The addition of

pericytes to the vessel model significantly improved the vessel formation, as it can be observed with a reduced vessel diameter (Fig. 20A). This result has previously been shown in another study, where brain pericytes were co-cultured with ECs in 3D chip culture and capillary diameter was significantly reduced compared to ECs cultured alone (Campisi et al., 2018). When primary pericytes have been used in EC co-culture, along with astrocytes, blood vessel leakage has been significantly reduced as well (Vatine et al., 2019). Pericytes in retinal and brain capillaries are known to influence blood vessel diameter to regulate blood flow, especially at the branching points (Peppiatt et al., 2006; Hamilton, Attwell, and Hall, 2010; Gonzales et al., 2020). This is in line with *in vivo* function of pericytes that suppress endothelial cell proliferation and help blood vessels to mature upon blood vessel formation. In a mice study where retinal vasculogenesis was observed, retinal vessel diameter has been shown to significantly reduced in vessels, especially in capillaries (Ehling et al., 2013).

We have generated pericytes from mesodermal and ectodermal lineages and due to the tissue-specificity of our model, established the iBRB model with ectodermal (neural crest-derived) pericytes. The generation of tissue-specific cell types is very crucial for an accurate recapitulation of a disease model, especially in the case of diabetic retinopathy, where pericyte loss is one of the earlier symptoms. Additionally, pericytes have regenerative properties upon injury, and therefore are a potential therapeutic target for brain vasculopathies (Geranmayeh, Rahbarghazi, and Farhoudi, 2019). However, this regenerative capacity is not observed in all subtypes of pericytes, which emphasizes the importance of tissue specificity (Ferland-McCollough et al., 2017; Nwadozi, Rudnicki, and Haas, 2020).

Similar to the capillaries of blood-retinal-barrier, ECs and PCs were cultured in 1:1 ratio, and formed the smallest vessels in diameter, compared to higher EC:PC ratios.
An interesting point was also that the EC and PC ratio within the chip remained the same after 7 days of culture, confirmed with nuclei staining using ERG-1/2/3 for ECs (Fig. 21B). This could show that the pericytes are stabilizing the vessel formation and blood vessels do not undergo angiogenesis. Consistent with this observation is that, in the absence of pericytes, blood vessel forms larger vessels with sparse lumens.

Taken together, in our blood vessel model in a 3D chip, we have recapitulated the iBRB and physiologically relevant pericytes greatly improved the retinal-like capillary formation and stabilization.

4.3. Induction of diabetes in iBRB *in vitro*

Complexity of DR make it hard to mimic *in vitro* compared to *in vivo* animal models. We have assessed two ways of diabetes induction: hyperglycemia and MGO-treatment. In order to find an optimal concentration of diabetes induction method, ROS production and TUNEL assay have been conducted. However, no significant difference between controls and diabetes-induced cells have been observed in monolayer culture.

4.3.1. Hyperglycemia and MGO treatment on blood vessels

Diabetes is a systemic disease that affects many parts of cellular metabolism in various organs, including the eye. Disease modelling of diabetes *in vivo* is often performed with STZ treatment for pancreatic β-cell destruction or dietary change in rodents (Dewangan et al., 2017). However, mimicking the disease *in vitro* is a challenge due to its complexity.

In our disease model, we used two approached to induce diabetes: hyperglycemic medium and AGE-precursor methylgloxal (MGO) treatment of blood vessels in the chip. Hyperglycemia is widely used in *in vitro* studies to mimic diabetes. The expression of tight junction complex proteins such as claudin-5 and occludin were reduced and an increased permeability was observed in retinal endothelial cells *in vitro* (Saker et al., 2014). Similarly, HUVECs exposed to hyperglycemic medium displayed increased ROS production (Dymkowska et al., 2014). However, the use of hyperglycemic medium approach comes with disadvantages. Firstly, most stem cell media used in cell culture contain high glucose levels, and hiPSCs grown in these media could have a metabolic memory when differentiated into other cell types, including ECs and PCs (Roberts and Porter, 2013). Metabolic memory is the persistence of metabolism-associated effects in cells, even after the initial exposure is retracted. In the case of hyperglycemic exposure, its effects are observed both *in vivo* and *in vitro* in ECs such as persistent ROS production, AGE formation, and possible epigenetic changes (Zeeuw, Wong, and Charmaliet, 2015). Also, glucose response in ECs of different tissue origins can vary. Also,

the downstream effects of hyperglycemia may not be reflected *in vivo* since daily medium change may not allow for accumulation of metabolites associated with hyperglycemia and diabetes. Considering the points above, we have used another approach for diabetes induction in addition to hyperglycemic medium.

MGO was shown to be an alternative indicator of diabetes compared to hyperglycemia, which has higher concentrations in patients' blood compared to individuals without DR (Groener et al., 2019; Bhat et al., 2019). Also, considering that MGO is a downstream metabolite of glucose metabolism, as it is formed with glycation of proteins and lipids, and is associated with iBRB disruption, it was chosen as an alternative for disease modelling of diabetic retinopathy. Methylgloxal administration has been used in rodents and *Drosophila* models as well as in *in vitro* cultures and resulted in vasculopathies attributed to diabetic retinopathy (Moraru et al., 2018; Hammes, 2018; Schalkwijk and Stehouwer, 2020).

4.3.2. ROS production and toxicity assays

I have assessed ROS induction in hyperglycemia and MGO-treated ECs and PCs, as they are known to cause enhanced oxidation. However, there was no significant change in treated versus control cells in any cell type and way of diabetes induction.
This could be explained by the rapid response of cells to metabolic changes and the insensitivity of DCFDA analysis. Since only 24h and 48h responses were measured (Fig. 25B-C), early responses of cells could be missed. Another possible explanation is that the normoglycemic cells that were used as controls could still have a metabolic memory and an increased ROS production. A study with HUVECs that quantified DCFDA staining have shown that initial hyperglycemic medium exposure followed by normoglycemic culture causes an increased ROS production compared to cells grown in only normoglycemic medium (Schisano et al., 2011).

Similarly, TUNEL assay in MGO-induced endothelial cells did not show any significant difference between control versus various concentrations of MGO-treatment (Fig. 26). Even though MGO is known to induce apoptosis in endothelial cells, there are other possibilities of cell death such as necrosis. In a study where HUVECs were co-exposed to hyperglycemia and MGO, the higher concentration of glucose (>25 mM) favored apoptotic cell death associated

with higher ROS levels, compared to lower levels of glucose, which favored necrosis (Chan and Wu, 2008).

Taken together, there were no quantitatively significant responses in monolayer cultures of ECs and PCs to hyperglycemia. Considering the possibility that responses of ECs and PCs to diabetes may differ between 2D and 3D culture, we carried on with our diabetes induction method directly in blood vessels in order to see its effects. In the next sections, these effects on blood vessels will be discussed.

4.4. Effect of diabetes on blood vessel diameter and shape in diabetic vs. control blood vessels

4.4.1. Increased blood vessel diameter in diabetic blood vessels

Blood vessels subjected to diabetes conditions (hyperglycemic or MGO-treated culture medium) displayed unexpected results. MGO treatment resulted in enlarged vessels compared to control ones, with a larger Feret's diameter, as well as larger minimum Feret's diameter (Fig. 28A-B). However, unexpectedly, hyperglycemia did not cause an enlargement of the blood vessel diameter. On the contrary, minimum Feret's diameter of hyperglycemic blood vessels were slightly smaller than control. Vessel shape was not affected in diabetic vessels (Fig. 28C).

This result indicates that MGO is a better approach than hyperglycemic medium to induce diabetes in blood vessels on chip culture. MGO may have caused the diabetes-associated cellular changes faster than hyperglycemia, and more directly as it is a metabolite caused by chronic exposure to high glucose levels. Also, glucose metabolism is highly complex and the metabolic memory of ECs and PCs during hiPSC culture may have hindered the accurate comparison of blood vessels. It is also noteworthy to mention that the duration of hyperglycemia exposure could affect the response of blood vessels.

4.4.2. Pivotal role of TGF-β pathway in blood vessels

TGF-β pathway on blood vessels had a significant effect on blood vessels. Initially, exposure to TGF-β significantly reduced the vessel size in blood vessels (Fig. 29A) and resulted in

rounder vessels compared to control (Fig. 29C). Our observation is in line with an *in vitro* study showing that TGF-β responsiveness in bovine retinal ECs occurs through its downstream targets (ALK5 and ALK1), and retinal pericytes are more sensitive to TGF-β increase than in retinal ECs (van Geest et al., 2010). Surprisingly, when TGF-β pathway was inhibited with SB431542, blood vessel diameter and shape were measured to be ideal, as Feret's diameter were 30.8 µm on average, and the shape close to an idea blood vessel (Feret's diameter/min. Feret's diameter: 1.8 for SB431542). TGF-β inhibition induced a more capillary-like phenotype in blood vessels, as well as a rounder shape compared to control and TGF-β exposure. This is possibly caused by inhibition of EC proliferation and maturation of blood vessels. It is known that TGF-β pathway has crucial roles in endothelial cell-pericyte crosstalk and therefore regulates the iBRB stability. As TGF-β1 is used in pericyte maturation in 2D culture and is needed for pericyte recruitment during blood-retinal barrier formation, the timing of TGF-β pathway activation is crucial in iBRB. TGF-β inhibition is used to boost endothelial cell proliferation during differentiation, however, once blood vessels have formed, inhibition of TGF-β1 may be needed to increase the barrier properties and stabilization of vessels. It is known that TGF-β expression is elevated in diabetes (Smit-McBride et al., 2020; Gu et al., 2020). However, considering pericyte dropout in diabetic retinal vessels, this increase may be beneficial and should not be inhibited. In a mice study, where TGF-β pathway was inhibited with a Smad2 inhibitor in diabetic mice, expression of tight junction proteins was significantly reduced (Dagher et al., 2017). This study also indicates that a slight increase in TGF-β1 expression in diabetes may be needed for vessel health, and TGF-β inhibition worsens the vessel integrity.

4.5. Future developments of the disease model

4.5.1. Comparative gene analysis of diabetic vs. control blood vessels

A diabetic retinopathy disease model has been established within the scope of this thesis. There are several improvements that can be done in the next steps. Firstly, comparison of gene expressions of diabetes-associated genes would be valuable to discover novel diagnostic and therapeutic targets. For this purpose, RNA sequencing from the diabetic versus control chips have been planned (Fig. 35). However, retaining cells from the chip has been challenging

to achieve a significant RNA quantity for downstream applications. Detaching the cells from the chip with other enzymatic digestion methods could improve the cell amount retained.

4.5.2. 3D chip culture improvements & drug testing

Glial components of the iBRB are crucial for barrier maintenance. Therefore, adding Müller glia to the existing model would improve the disease model. In fact, it has been seen that in BBB vasculature model, addition of astrocytes to EC and PC co-culture significantly reduced the blood vessel diameter (Campisi et al., 2018). In our model, the use of iBRB components from the same-hiPSC line poses an advantage compared to existing models.

3D chip culture of vasculature can also be improved with perfusion, growth factor concentration adjustments, and standardization of EC and PC passages used in chips.

In order to improve the vascular health, and to reduce angiogenesis-associated effects on vessels, reduction of VEGF and addition of protective molecules such as substance P could be applied to reduce vascular permeability (Ou et al., 2019).

Improving the disease model with Müller glia is also planned with the other members of the lab. As Müller glia is an important component of iBRB via the regulation of metabolism and is associated with DR-induced impairment, disease modelling of DR could be advanced with a tricellular co-culture.

5. References

Abbott N. J. (2002). Astrocyte-endothelial interactions and blood-brain barrier permeability. *Journal of anatomy*, *200*(6), 629–638. https://doi.org/10.1046/j.1469-7580.2002.00064.x

Abbott, N. J., Patabendige, A. A. K., Dolman, D. E. M., Yusof, S. R., & Begley, D. J. (2010). Structure and function of the blood-brain barrier. *Neurobiology of Disease*, *37*(1), 13–25. https://doi.org/10.1016/J.NBD.2009.07.030

Abbott, N. J., Rönnbäck, L., & Hansson, E. (2006). Astrocyte-endothelial interactions at the blood-brain barrier. *Nature reviews. Neuroscience*, *7*(1), 41–53. https://doi.org/10.1038/nrn1824

Abdulkadir, R. R., Alwjwaj, M., Othman, O. A., Rakkar, K., & Bayraktutan, U. (2020). Outgrowth endothelial cells form a functional cerebral barrier and restore its integrity after damage. *Neural regeneration research*, *15*(6), 1071–1078. https://doi.org/10.4103/1673-5374.269029

Abu El-Asrar, A. M., Nawaz, M. I., Ahmad, A., Siddiquei, M. M., Allegaert, E., Gikandi, P. W., De Hertogh, G., & Opdenakker, G. (2021). CD146/Soluble CD146 Pathway Is a Novel Biomarker of Angiogenesis and Inflammation in Proliferative Diabetic Retinopathy. *Investigative ophthalmology & visual science*, *62*(9), 32. https://doi.org/10.1167/iovs.62.9.32

Achberger, K 2018, Human retinal organoids- Exploration of a human induced pluripotent stem cell- derived *in vitro* model, PhD thesis, University of Tübingen, Tübingen.

Armulik, A., Genové, G., & Betsholtz, C. (2011). Developmental Cell Review Pericytes: Developmental, Physiological, and Pathological Perspectives, Problems, and Promises. *Developmental Cell*, *21*, 193–215. https://doi.org/10.1016/j.devcel.2011.07.001

Armulik, A., Genové, G., Mäe, M., Nisancioglu, M. H., Wallgard, E., Niaudet, C., He, L., Norlin, J., Lindblom, P., Strittmatter, K., Johansson, B. R., & Betsholtz, C. (2010). Pericytes regulate the blood-brain barrier. *Nature*, *468*(7323), 557–561. https://doi.org/10.1038/NATURE09522
Auerbach, R., Lewis, R., Shinners, B., Kubai, L., & Akhtar, N. (2003). Angiogenesis assays: a critical overview. *Clinical chemistry*, *49*(1), 32-40.

Bach, T. L., Barsigian, C., Chalupowicz, D. G., Busler, D., Yaen, C. H., Grant, D. S., & Martinez, J. (1998). VE-Cadherin mediates endothelial cell capillary tube formation in fibrin and collagen gels. *Experimental cell research*, *238*(2), 324–334. https://doi.org/10.1006/excr.1997.3844

Bandopadhyay, R., Orte, C., Lawrenson, J. G., Reid, A. R., De Silva, S., & Allt, G. (2001). Contractile proteins in pericytes at the blood-brain and blood-retinal barriers. *Journal of neurocytology*, *30*(1), 35–44. https://doi.org/10.1023/a:1011965307612

Bell, R. D., Winkler, E. A., Sagare, A. P., Singh, I., Larue, B., Deane, R., & Zlokovic, B. v. (2010). Article Pericytes Control Key Neurovascular Functions and Neuronal Phenotype in the Adult Brain and during Brain Aging. *Neuron*, *68*, 409–427. https://doi.org/10.1016/j.neuron.2010.09.043

Benfey, N., Foubert, D., & Ruthazer, E. S. (2022). Glia Regulate the Development, Function, and Plasticity of the Visual System From Retina to Cortex. *Frontiers in neural circuits*, *16*, 826664. https://doi.org/10.3389/fncir.2022.826664

Bergers, G., & Song, S. (2005). The role of pericytes in blood-vessel formation and maintenance. *Neuro-Oncology*, *7*(4), 452–464. https://doi.org/10.1215/S1152851705000232

Birdsey, G. M., Dryden, N. H., Amsellem, V., Gebhardt, F., Sahnan, K., Haskard, D. O., Dejana, E., Mason, J. C., & Randi, A. M. (2008). Transcription factor Erg regulates angiogenesis and endothelial apoptosis through VE-cadherin. *Blood*, *111*(7), 3498–3506. https://doi.org/10.1182/BLOOD-2007-08-105346

Bringmann, A., & Wiedemann, P. (2011). Müller glial cells in retinal disease. In *Ophthalmologica* (Vol. 227, Issue 1, pp. 1–19). https://doi.org/10.1159/000328979

Bringmann, A., Pannicke, T., Grosche, J., Francke, M., Wiedemann, P., Skatchkov, S. N., Osborne, N. N., & Reichenbach, A. (2006). Müller cells in the healthy and diseased retina. *Progress in Retinal and Eye Research*, *25*(4), 397–424. https://doi.org/10.1016/J.PRETEYERES.2006.05.003

Brown, M. E., Rondon, E., Rajesh, D., Mack, A., Lewis, R., Feng, X., Zitur, L. J., Learish, R. D., & Nuwaysir, E. F. (2010). Derivation of induced pluripotent stem cells from human peripheral blood T lymphocytes. *PloS one*, *5*(6), e11373. https://doi.org/10.1371/journal.pone.0011373

Bui, T. M., Wiesolek, H. L., & Sumagin, R. (2020). ICAM-1: A master regulator of cellular responses in inflammation, injury resolution, and tumorigenesis. *Journal of leukocyte biology*, *108*(3), 787–799. https://doi.org/10.1002/JLB.2MR0220-549R

Burns, S. A., Elsner, A. E., & Gast, T. J. (2021). Imaging the Retinal Vasculature. In *Annual Review of Vision Science* (Vol. 7, pp. 129–153). Annual Reviews Inc. https://doi.org/10.1146/annurev-vision-093019-113719

Campbell, J. P., Zhang, M., Hwang, T. S., Bailey, S. T., Wilson, D. J., Jia, Y., & Huang, D. (2017). Detailed Vascular Anatomy of the Human Retina by Projection-Resolved Optical Coherence Tomography Angiography. *Scientific Reports*, *7*. https://doi.org/10.1038/srep42201

Campisi, M., Shin, Y., Osaki, T., Hajal, C., Chiono, V., & Kamm, R. D. (2018). 3D self-organized microvascular model of the human blood-brain barrier with endothelial cells, pericytes and astrocytes. *Biomaterials*, *180*, 117–129. https://doi.org/10.1016/j.biomaterials.2018.07.014

Chan-Ling, T., Chu, Y., Baxter, L., Weible II, M., & Hughes, S. (2009). In vivo characterization of astrocyte precursor cells (APCs) and astrocytes in developing rat retinae: differentiation, proliferation, and apoptosis. *Glia*, *57*(1), 39-53.

Chan, W. H., & Wu, H. J. (2008). Methylglyoxal and high glucose co-treatment induces apoptosis or necrosis in human umbilical vein endothelial cells. *Journal of Cellular Biochemistry*, *103*(4), 1144–1157. https://doi.org/10.1002/JCB.21489

Chang, C.-Y., Ting, H.-C., Liu, C.-A., Su, H.-L., Chiou, T.-W., Lin, S.-Z., Harn, H.-J., & Ho, T.-J. (2020). *molecules Induced Pluripotent Stem Cell (iPSC)-Based Neurodegenerative Disease Models for Phenotype Recapitulation and Drug Screening*. https://doi.org/10.3390/molecules25082000

Chen, J., Luo, Y., Hui, H., Cai, T., Huang, H., Yang, F., Feng, J., Zhang, J., & Yan, X. (2017). CD146 coordinates brain endothelial cell-pericyte communication for blood-brain barrier development. *Proceedings of the National Academy of Sciences of the United States of America*, *114*(36), E7622–E7631. https://doi.org/10.1073/pnas.1710848114

Chen, J., Ma, L., Wang, S., Wang, X., Sun, Y., Gao, L., Li, J., & Zhou, G. (2017). Analysis of expression of transcription factors in early human retina. *International Journal of Developmental Neuroscience*, *60*, 94–102. https://doi.org/10.1016/J.IJDEVNEU.2017.01.015

Chow, B. W., & Gu, C. (2017). Gradual Suppression of Transcytosis Governs Functional Blood-Retinal Barrier Formation. *Neuron*, *93*(6), 1325-1333.e3. https://doi.org/10.1016/j.neuron.2017.02.043

Chua, J., Sim, R., Tan, B., Wong, D., Yao, X., Liu, X., Ting, D. S. W., Schmidl, D., Ang, M., Garhöfer, G., & Schmetterer, L. (2020). Optical Coherence Tomography Angiography in Diabetes and Diabetic Retinopathy. *Journal of Clinical Medicine*, *9*(6), 1–23. https://doi.org/10.3390/JCM9061723

Coorey, N. J., Shen, W., Chung, S. H., Zhu, L., & Gillies, M. C. (2012). The role of glia in retinal vascular disease. *Clinical & Experimental Optometry*, *95*(3), 266–281. https://doi.org/10.1111/J.1444-0938.2012.00741.X

Corliss, B. A., Ray, H. C., Doty, R. W., Mathews, C., Sheybani, N., Fitzgerald, K., Prince, R., Kelly-Goss, M. R., Murfee, W. L., Chappell, J., Owens, G. K., Yates, P. A., & Peirce, S. M. (2020). Pericyte Bridges in Homeostasis and Hyperglycemia. *Diabetes*, *69*(7), 1503–1517. https://doi.org/10.2337/db19-0471

Couty, J. P., Rampon, C., Leveque, M., Laran-Chich, M. P., Bourdoulous, S., Greenwood, J., & Couraud, P. O. (2007). PECAM-1 engagement counteracts ICAM-1-induced signaling in brain vascular endothelial cells 2. *Journal of neurochemistry*, *103*(2), 793-801.

Craig, L. E., Spelman, J. P., Strandberg, J. D., & Zink, M. C. (1998). Endothelial cells from diverse tissues exhibit differences in growth and morphology. *Microvascular research*, *55*(1), 65-76.

Cunha-Vaz, J. (2009). The Blood–Retinal Barrier in Retinal Disease. *European Ophthalmic Review*, *03*(02), 105. https://doi.org/10.17925/EOR.2009.03.02.105

da Silva, A. V. B., Gouvea, S. A., da Silva, A. P. B., Bortolon, S., Rodrigues, A. N., Abreu, G. R., & Herkenhoff, F. L. (2015). Changes in retinal microvascular diameter in patients with diabetes. *International Journal of General Medicine*, *8*, 267–273. https://doi.org/10.2147/IJGM.S83749

Dagher, Z., Gerhardinger, C., Vaz, J., Goodridge, M., Tecilazich, F., & Lorenzi, M. (2017). The Increased Transforming Growth Factor-β Signaling Induced by Diabetes Protects Retinal Vessels. *The American Journal of Pathology*, *187*(3), 627–638. https://doi.org/10.1016/J.AJPATH.2016.11.007

Daneman, R., & Prat, A. (2015). The blood-brain barrier. *Cold Spring Harbor perspectives in biology*, *7*(1), a020412. https://doi.org/10.1101/cshperspect.a020412

Dash, S., Siddam, A. D., Barnum, C. E., Janga, S. C., & Lachke, S. A. (2016). RNA-binding proteins in eye development and disease: implication of conserved RNA granule components. In *Wiley Interdisciplinary Reviews: RNA* (Vol. 7, Issue 4, pp. 527–557). Blackwell Publishing Ltd. https://doi.org/10.1002/wrna.1355

Davis-Silberman, N., & Ashery-Padan, R. (2008). Iris development in vertebrates; genetic and molecular considerations. *Brain Research*, *1192*, 17–28. https://doi.org/10.1016/J.BRAINRES.2007.03.043

de Zeeuw, P., Wong, B. W., & Carmeliet, P. (2015). Metabolic adaptations in diabetic endothelial cells. *Circulation Journal*, *79*(5), 934–941. https://doi.org/10.1253/circj.CJ-15-0230

Dejana, E., Orsenigo, F., & Lampugnani, M. G. (2008). The role of adherens junctions and VE-cadherin in the control of vascular permeability. *Journal of Cell Science*, *121*(13), 2115–2122. https://doi.org/10.1242/jcs.017897

Dewangan, H., Tiwari, R. K., Sharma, V., Shukla, S. S., Satapathy, T., & Pandey, R. (2017). Past and Future of in-vitro and in-vivo Animal Models for Diabetes: A Review. *Indian Journal of Pharmaceutical Education and Research*, *51*(4S), s522-s530.

Dias Moura Prazeres, P. H., Sena, I. F. G., Borges, I. da T., de Azevedo, P. O., Andreotti, J. P. P., de Paiva, A. E., de Almeida, V. M., de Paula Guerra, D. A., Pinheiro dos Santos, G. S., Mintz, A., Delbono, O., & Birbrair, A. (2017). Pericytes are heterogeneous in their origin within the same tissue. *Developmental Biology*, *427*(1), 6–11. https://doi.org/10.1016/J.YDBIO.2017.05.001

Díaz-Coránguez, M., Ramos, C., & Antonetti, D. A. (2017). The inner blood-retinal barrier: Cellular basis and development. *Vision Research*, *139*, 123–137. https://doi.org/10.1016/j.visres.2017.05.009

Díaz-Lezama, N., Wolf, A., Koch, S., Pfaller, A. M., Biber, J., Guillonneau, X., ... & Grosche, A. (2021). PDGF Receptor Alpha Signaling Is Key for Müller Cell Homeostasis Functions. *International journal of molecular sciences*, *22*(3), 1174.

Dimaio, T. A., Wang, S., Huang, Q., Scheef, E. A., Sorenson, C. M., & Sheibani, N. (2008). Attenuation of retinal vascular development and neovascularization in PECAM-1-deficient mice. *Developmental biology*, *315*(1), 72–88. https://doi.org/10.1016/j.ydbio.2007.12.008

Dreisig, K., Blixt, F. W., & Warfvinge, K. (2018). Retinal Cryo-sections, Whole-Mounts, and Hypotonic Isolated Vasculature Preparations for Immunohistochemical Visualization of Microvascular Pericytes. *Journal of visualized experiments : JoVE*, (140), 57733. https://doi.org/10.3791/57733

Drobnjak, D., Munch, I. C., Glümer, C., Færch, K., Kessel, L., Larsen, M., & Veiby, N. C. B. B. (2017). Relationship between retinal vessel diameters and retinopathy in the Inter99 Eye Study. *Journal of Clinical & Translational Endocrinology*, *8*, 22. https://doi.org/10.1016/J.JCTE.2017.03.002

Du, X., Zhang, Z., Zhou, H., & Zhou, J. (2021). Differential Modulators of NG2-Glia Differentiation into Neurons and Glia and Their Crosstalk. *Cellular and molecular neurobiology*, *41*(1), 1–15. https://doi.org/10.1007/s10571-020-00843-0

Dymkowska, D., Drabarek, B., Podszywałow-Bartnicka, P., Szczepanowska, J., & Zabłocki, K. (2014). Hyperglycaemia modifies energy metabolism and reactive oxygen species formation in endothelial cells in vitro. *Archives of Biochemistry and Biophysics*, *542*, 7–13. https://doi.org/10.1016/J.ABB.2013.11.008

Eastlake, K., Luis, J., & Limb, G. A. (2020). Potential of Müller Glia for Retina Neuroprotection. In *Current Eye Research* (Vol. 45, Issue 3, pp. 339–348). Taylor and Francis Ltd. https://doi.org/10.1080/02713683.2019.1648831

Eastlake, K., Wang, W., Jayaram, H., Murray-Dunning, C., Carr, A. J., Ramsden, C. M., ... & Limb, G. A. (2019). Phenotypic and functional characterization of müller glia isolated from induced pluripotent stem cell-derived retinal organoids: improvement of retinal ganglion cell function upon transplantation. *Stem Cells Translational Medicine*, *8*(8), 775-784.

Ehling, M., Adams, S., Benedito, R., & Adams, R. H. (2013). Notch controls retinal blood vessel maturation and quiescence. *Development (Cambridge, England)*, *140*(14), 3051–3061. https://doi.org/10.1242/dev.093351

Etchevers, H. C., Vincent, C., le Douarin, N. M., & Couly, G. F. (2001). The cephalic neural crest provides pericytes and smooth muscle cells to all blood vessels of the face and forebrain. *Development (Cambridge, England)*, *128*(7), 1059–1068. https://doi.org/10.1242/DEV.128.7.1059

Fagiani, E., & Christofori, G. (2013). Angiopoietins in angiogenesis. *Cancer Letters*, *328*(1), 18–26. https://doi.org/10.1016/J.CANLET.2012.08.018

Ferland-McCollough, D., Slater, S., Richard, J., Reni, C., & Mangialardi, G. (2017). Pericytes, an overlooked player in vascular pathobiology. *Pharmacology & therapeutics*, *171*, 30–42. https://doi.org/10.1016/j.pharmthera.2016.11.008

Fields, M. A., del Priore, L. v., Adelman, R. A., & Rizzolo, L. J. (2020). Interactions of the choroid, Bruch's membrane, retinal pigment epithelium, and neurosensory retina collaborate to form the outer blood-retinal-barrier. In *Progress in Retinal and Eye Research* (Vol. 76). Elsevier Ltd. https://doi.org/10.1016/j.preteyeres.2019.100803

Fosmark, D. S., Torjesen, P. A., Kilhovd, B. K., Berg, T. J., Sandvik, L., Hanssen, K. F., Agardh, C. D., & Agardh, E. (2006). Increased serum levels of the specific advanced glycation end product methylglyoxal-derived hydroimidazolone are associated with retinopathy in patients with type 2 diabetes mellitus. *Metabolism: Clinical and Experimental*, *55*(2), 232–236. https://doi.org/10.1016/J.METABOL.2005.08.017

Francescone III, R. A., Faibish, M., & Shao, R. (2011). A Matrigel-based tube formation assay to assess the vasculogenic activity of tumor cells. *JoVE (Journal of Visualized Experiments)*, (55), e3040.

Frank, R. N., Turczyn, T. J., & Das, A. (1990). Pericyte coverage of retinal and cerebral capillaries. *Investigative ophthalmology & visual science*, *31*(6), 999–1007.

Fuhrmann, S. (2010). Eye Morphogenesis and Patterning of the Optic Vesicle. *Current Topics in Developmental Biology*, *93*(C), 61–84. https://doi.org/10.1016/B978-0-12-385044-7.00003-5

Furuse, M., Hirase, T., Itoh, M., Nagafuchi, A., Yonemura, S., Tsukita, S., & Tsukita, S. (1993). Occludin: a novel integral membrane protein localizing at tight junctions. *The Journal of Cell Biology*, *123*(6 Pt 2), 1777–1788. https://doi.org/10.1083/JCB.123.6.1777

Gallardo, V. E., Bovolenta, P., Wallace, V. A., Cayouette, M., & Waskiewicz, A. J. (2018). Positive and negative regulation of Shh signalling in vertebrate retinal development. *F1000Research 2018 7:1934*, *7*, 1934. https://doi.org/10.12688/f1000research.16190.1

Garcia-Alegria, E., Potts, B., Menegatti, S., & Kouskoff, V. (2021). *In vitro* differentiation of human embryonic stem cells to hemogenic endothelium and blood progenitors via embryoid body formation. *STAR protocols*, *2*(1), 100367. https://doi.org/10.1016/j.xpro.2021.100367
Gastfriend, B. D., Stebbins, M. J., Du, F., Shusta, E. v., & Palecek, S. P. (2021). Differentiation of Brain Pericyte-Like Cells from Human Pluripotent Stem Cell–Derived Neural Crest. *Current Protocols*, *1*(1). https://doi.org/10.1002/cpz1.21

Geranmayeh, M. H., Rahbarghazi, R., & Farhoudi, M. (2019). Targeting pericytes for neurovascular regeneration. In *Cell Communication and Signaling* (Vol. 17, Issue 1). BioMed Central Ltd. https://doi.org/10.1186/s12964-019-0340-8

Gerhardt, H., Liebner, S., Redies, C., & Wolburg, H. (1999). N-cadherin expression in endothelial cells during early angiogenesis in the eye and brain of the chicken: relation to

blood–retina and blood–brain barrier development*. *European Journal of Neuroscience*, *11*(4), 1191–1201. https://doi.org/10.1046/J.1460-9568.1999.00526.X

Giger, F. A., & Houart, C. (2018). The birth of the eye vesicle: When fate decision equals morphogenesis. *Frontiers in Neuroscience*, *12*(FEB), 87. https://doi.org/10.3389/FNINS.2018.00087/BIBTEX

Girolamo, F., de Trizio, I., Errede, M., Longo, G., d'Amati, A., & Virgintino, D. (2021). Neural crest cell-derived pericytes act as pro-angiogenic cells in human neocortex development and gliomas. *Fluids and Barriers of the CNS*, *18*(1). https://doi.org/10.1186/S12987-021-00242-7

Gonzales, A. L., Klug, N. R., Moshkforoush, A., Lee, J. C., Lee, F. K., Shui, B., Tsoukias, N. M., Kotlikoff, M. I., Hill-Eubanks, D., & Nelson, M. T. (2020). Contractile pericytes determine the direction of blood flow at capillary junctions. *Proceedings of the National Academy of Sciences of the United States of America*, *117*(43), 27022–27033. https://doi.org/10.1073/pnas.1922755117

Graca, A. B., Hippert, C., & Pearson, R. A. (2018). Müller glia reactivity and development of gliosis in response to pathological conditions. In *Advances in Experimental Medicine and Biology* (Vol. 1074, pp. 303–308). Springer New York LLC. https://doi.org/10.1007/978-3-319-75402-4_37

Graw, J. (2010). Eye development. In *Current Topics in Developmental Biology* (Vol. 90, Issue C, pp. 343–386). Academic Press Inc. https://doi.org/10.1016/S0070-2153(10)90010-0

Groener, J. B., Oikonomou, D., Cheko, R., Kender, Z., Zemva, J., Kihm, L., Muckenthaler, M., Peters, V., Fleming, T., Kopf, S., & Nawroth, P. P. (2019). Methylglyoxal and Advanced Glycation End Products in Patients with Diabetes - What We Know so Far and the Missing Links. *Experimental and Clinical Endocrinology and Diabetes*, *127*(8), 497–504. https://doi.org/10.1055/S-0043-106443/ID/R03-2017-0089-DIA-0020

Gu, C., Lhamo, T., Zou, C., Zhou, C., Su, T., Draga, D., Luo, D., Zheng, Z., Yin, L., & Qiu, Q. (2020). Comprehensive analysis of angiogenesis-related genes and pathways in early diabetic retinopathy. *BMC Medical Genomics*, *13*(1), 1–11. https://doi.org/10.1186/S12920-020-00799-6/FIGURES/6

Gui, F., You, Z., Fu, S., Wu, H., & Zhang, Y. (2020). Endothelial Dysfunction in Diabetic Retinopathy. In *Frontiers in Endocrinology* (Vol. 11). Frontiers Media S.A. https://doi.org/10.3389/fendo.2020.00591

Haase, K., & Kamm, R. D. (2017). Advances in on-chip vascularization. In *Regenerative Medicine* (Vol. 12, Issue 3, pp. 285–302). Future Medicine Ltd. https://doi.org/10.2217/rme-2016-0152

Hamilton, N. B., Attwell, D., & Hall, C. N. (2010). Pericyte-mediated regulation of capillary diameter: a component of neurovascular coupling in health and disease. *Frontiers in neuroenergetics*, *2*, 5. https://doi.org/10.3389/fnene.2010.00005

Hammes, H. P. (2018). Diabetic retinopathy: hyperglycaemia, oxidative stress and beyond. *Diabetologia*, *61*(1), 29–38. https://doi.org/10.1007/S00125-017-4435-8/FIGURES/5

Han, X., Chen, H., Huang, D., Chen, H., Fei, L., Cheng, C., Huang, H., Yuan, G. C., & Guo, G. (2018). Mapping human pluripotent stem cell differentiation pathways using high throughput single-cell RNA-sequencing. *Genome biology*, *19*(1), 47. https://doi.org/10.1186/s13059-018-1426-0

Hauck, S. M., Suppmann, S., & Ueffing, M. (2003). Proteomic profiling of primary retinal Müller glia cells reveals a shift in expression patterns upon adaptation to in vitro conditions. *Glia*, *44*(3), 251-263.

Heithoff, B. P., George, K. K., Phares, A. N., Zuidhoek, I. A., Munoz-Ballester, C., & Robel, S. (2021). Astrocytes are necessary for blood-brain barrier maintenance in the adult mouse brain. *Glia*, *69*(2), 436–472. https://doi.org/10.1002/glia.23908

Herculano-Houzel, S. (2011). Scaling of Brain Metabolism with a Fixed Energy Budget per Neuron: Implications for Neuronal Activity, Plasticity and Evolution. *PLOS ONE*, *6*(3), e17514. https://doi.org/10.1371/JOURNAL.PONE.0017514

Herrmann, M., Bara, J. J., Sprecher, C. M., Menzel, U., Jalowiec, J. M., Osinga, R., Scherberich, A., Alini, M., & Verrier, S. (2016). Pericyte plasticity - comparative investigation of the angiogenic and multilineage potential of pericytes from different human tissues. *European Cells & Materials*, *31*, 236–249. https://doi.org/10.22203/ECM.V031A16

Hoon, M., Okawa, H., della Santina, L., & Wong, R. O. L. (2014). Functional architecture of the retina: Development and disease. In *Progress in Retinal and Eye Research* (Vol. 42, pp. 44–84). Elsevier Ltd. https://doi.org/10.1016/j.preteyeres.2014.06.003

Hoshino, A., Ratnapriya, R., Brooks, M. J., Chaitankar, V., Wilken, M. S., Zhang, C., Starostik, M. R., Gieser, L., la Torre, A., Nishio, M., Bates, O., Walton, A., Bermingham-McDonogh, O., Glass, I. A., Wong, R. O. L., Swaroop, A., & Reh, T. A. (2017). Molecular Anatomy of the Developing Human Retina. *Developmental Cell*, *43*(6), 763-779.e4. https://doi.org/10.1016/j.devcel.2017.10.029

Howard, J., Blakeslee, B., & Laughlin, S. B. (1987). The intracellular pupil mechanism and photoreceptor signal: noise ratios in the fly Lucilia cuprina. *Proceedings of the Royal Society of London. Series B, Containing Papers of a Biological Character. Royal Society (Great Britain)*, *231*(1265), 415–435. https://doi.org/10.1098/rspb.1987.0053

Huang, H., Gandhi, J. K., Zhong, X., Wei, Y., Gong, J., Duh, E. J., & Vinores, S. A. (2011). TNFalpha is required for late BRB breakdown in diabetic retinopathy, and its inhibition prevents leukostasis and protects vessels and neurons from apoptosis. *Investigative Ophthalmology & Visual Science*, *52*(3), 1336–1344. https://doi.org/10.1167/IOVS.10-5768

Hughes, S., Yang, H., & Chan-Ling, T. (2000). Vascularization of the human fetal retina: roles of vasculogenesis and angiogenesis. *Investigative ophthalmology & visual science*, *41*(5), 1217–1228.

Ibrahim, M., Xie, B., & Richardson, M. K. (2020). The growth of endothelial-like cells in zebrafish embryoid body culture. *Experimental cell research*, *392*(2), 112032. https://doi.org/10.1016/j.yexcr.2020.112032

Jang, J. H., Kim, E. A., Park, H. J., Sung, E. G., Song, I. H., Kim, J. Y., Woo, C. H., Doh, K. O., Kim, K. H., & Lee, T. J. (2017). Methylglyoxal-induced apoptosis is dependent on the suppression of c-FLIPL expression via down-regulation of p65 in endothelial cells. *Journal of Cellular and Molecular Medicine*, *21*(11), 2720–2731. https://doi.org/10.1111/jcmm.13188

Jang, S., Collin de l'Hortet, A., & Soto-Gutierrez, A. (2019). Induced Pluripotent Stem Cell-Derived Endothelial Cells: Overview, Current Advances, Applications, and Future Directions. *The American journal of pathology*, *189*(3), 502–512. https://doi.org/10.1016/j.ajpath.2018.12.004

Jean, D., Ewan, K., & Gruss, P. (1998). Molecular regulators involved in vertebrate eye development. *Mechanisms of Development*, *76*(1–2), 3–18. https://doi.org/10.1016/S0925-4773(98)00117-8

Jia, T., Jacquet, T., Dalonneau, F., Coudert, P., Vaganay, E., Exbrayat-Héritier, C., Vollaire, J., Josserand, V., Ruggiero, F., Coll, J. L., & Eymin, B. (2021). FGF-2 promotes angiogenesis through a SRSF1/SRSF3/SRPK1-dependent axis that controls VEGFR1 splicing in endothelial cells. *BMC Biology*, *19*(1). https://doi.org/10.1186/s12915-021-01103-3

Joussen, A. M., Murata, T., Tsujikawa, A., Kirchhof, B., Bursell, S. E., & Adamis, A. P. (2001). Leukocyte-mediated endothelial cell injury and death in the diabetic retina. *The American journal of pathology*, *158*(1), 147–152. https://doi.org/10.1016/S0002-9440(10)63952-1

Joussen, A. M., Ricci, F., Paris, L. P., Korn, C., Quezada-Ruiz, C., & Zarbin, M. (2021). Angiopoietin/Tie2 signalling and its role in retinal and choroidal vascular diseases: a review of preclinical data. *Eye (London, England)*, *35*(5), 1305–1316. https://doi.org/10.1038/S41433-020-01377-X

Kaji, Y., Usui, T., Ishida, S., Yamashiro, K., Moore, T. C. B., Moore, J., Yamamoto, Y., Yamamoto, H., & Adamis, A. P. (2007). Inhibition of Diabetic Leukostasis and Blood-Retinal Barrier Breakdown with a Soluble Form of a Receptor for Advanced Glycation End Products. *Investigative Ophthalmology & Visual Science*, *48*(2), 858–865. https://doi.org/10.1167/IOVS.06-0495

Kambal, A., Mitchell, G., Cary, W., Gruenloh, W., Jung, Y., Kalomoiris, S., Nacey, C., McGee, J., Lindsey, M., Fury, B., Bauer, G., Nolta, J. A., & Anderson, J. S. (2011). Generation of HIV-1 resistant and functional macrophages from hematopoietic stem cell-derived induced pluripotent stem cells. *Molecular therapy : the journal of the American Society of Gene Therapy*, *19*(3), 584–593. https://doi.org/10.1038/mt.2010.269

Karachalias, N., Babaei-Jadidi, R., Ahmed, N., & Thornalley, P. J. (2003). Accumulation of fructosyl-lysine and advanced glycation end products in the kidney, retina and peripheral nerve of streptozotocin-induced diabetic rats. *Biochemical Society Transactions*, *31*(6), 1423–1425. https://doi.org/10.1042/BST0311423

Keller, G. M. (1995). In vitro differentiation of embryonic stem cells. *Current Opinion in Cell Biology*, *7*(6), 862–869. https://doi.org/10.1016/0955-0674(95)80071-9

Khalfaoui, T., Lizard, G., & Ouertani-Meddeb, A. (2008). Adhesion molecules (ICAM-1 and VCAM-1) and diabetic retinopathy in type 2 diabetes. *Journal of molecular histology*, *39*(2), 243-249.

Kirthi, V., Nderitu, P., Alam, U., Evans, J. R., Nevitt, S., Malik, R. A., Hopkins, D., & Jackson, T. L. (2022). The prevalence of retinopathy in prediabetes: A systematic review. *Survey of ophthalmology*, S0039-6257(22)00045-5. Advance online publication. https://doi.org/10.1016/j.survophthal.2022.04.002

Klaassen, I., van Noorden, C. J. F., & Schlingemann, R. O. (2013). Molecular basis of the inner blood-retinal barrier and its breakdown in diabetic macular edema and other pathological conditions. In *Progress in Retinal and Eye Research* (Vol. 34, pp. 19–48). https://doi.org/10.1016/j.preteyeres.2013.02.001

Klein, R., Myers, C. E., Lee, K. E., Gangnon, R., & Klein, B. E. K. (2012). Changes in Retinal Vessel Diameter and Incidence and Progression of Diabetic Retinopathy. *Archives of Ophthalmology*, *130*(6), 749. https://doi.org/10.1001/ARCHOPHTHALMOL.2011.2560

Klettner, A., Kaya, L., Flach, J., Lassen, J., Treumer, F., & Roider, J. (2015). Basal and apical regulation of VEGF-A and placenta growth factor in the RPE/choroid and primary RPE. *Molecular vision*, *21*, 736.

Koga, K., Yamagishi, S., Okamoto, T., Inagaki, Y., Amano, S., Takeuchi, M., & Makita, Z. (2002). Serum levels of glucose-derived advanced glycation end products are associated with the severity of diabetic retinopathy in type 2 diabetic patients without renal dysfunction. *International journal of clinical pharmacology research*, *22*(1), 13–17.

Korn, J., Christ, B., & Kurz, H. (2002). Neuroectodermal origin of brain pericytes and vascular smooth muscle cells. *The Journal of Comparative Neurology*, *442*(1), 78–88. https://doi.org/10.1002/CNE.1423

Koroleva, A., Deiwick, A., Nguyen, A., Narayan, R., Shpichka, A., Kufelt, O., Kiyan, R., Bagratashvili, V., Timashev, P., Scheper, T., & Chichkov, B. (2016). Hydrogel-based microfluidics for vascular tissue engineering. *BioNanoMaterials*, *17*(1–2), 19–32. https://doi.org/10.1515/BNM-2015-0026/PDF

Kowluru, R. A., & Chan, P. S. (2007). Oxidative stress and diabetic retinopathy. In *Experimental Diabesity Research* (Vol. 2007). https://doi.org/10.1155/2007/43603

Krencik, R., & Zhang, S. C. (2011). Directed differentiation of functional astroglial subtypes from human pluripotent stem cells. *Nature Protocols*, *6*(11), 1710–1717. https://doi.org/10.1038/nprot.2011.405

Krüger-Genge, A., Blocki, A., Franke, R. P., & Jung, F. (2019). Vascular endothelial cell biology: an update. *International journal of molecular sciences*, *20*(18), 4411.

Kumar, A., D'Souza, S. S., Moskvin, O. v., Toh, H., Wang, B., Zhang, J., Swanson, S., Guo, L. W., Thomson, J. A., & Slukvin, I. I. (2017). Specification and Diversification of Pericytes and Smooth Muscle Cells from Mesenchymoangioblasts. *Cell Reports*, *19*(9), 1902–1916. https://doi.org/10.1016/j.celrep.2017.05.019

Lamb, T. D., Collin, S. P., & Pugh, E. N. (2007). Evolution of the vertebrate eye: opsins, photoreceptors, retina and eye cup. *Nature Reviews Neuroscience 2007 8:12*, *8*(12), 960–976. https://doi.org/10.1038/nrn2283

Langen, U. H., Ayloo, S., & Gu, C. (2019). Development and Cell Biology of the Blood-Brain Barrier. *Annual review of cell and developmental biology*, *35*, 591–613. https://doi.org/10.1146/annurev-cellbio-100617-062608

Lee, J. H., Parveen, A., Do, M. H., Kang, M. C., Yumnam, S., & Kim, S. Y. (2020). Molecular mechanisms of methylglyoxal-induced aortic endothelial dysfunction in human vascular endothelial cells. *Cell Death and Disease*, *11*(5). https://doi.org/10.1038/s41419-020-2602-1

Li, Y., Zhao, Y., Sang, S., & Leung, T. (2019). Methylglyoxal-Induced Retinal Angiogenesis in Zebrafish Embryo: A Potential Animal Model of Neovascular Retinopathy. *Journal of Ophthalmology*, *2019*. https://doi.org/10.1155/2019/2746735

Liebner, S., Dijkhuizen, R. M., Reiss, Y., Plate, K. H., Agalliu, D., & Constantin, G. (2018). Functional morphology of the blood-brain barrier in health and disease. *Acta Neuropathologica*, *135*(3), 311–336. https://doi.org/10.1007/S00401-018-1815-1

Loiola, R. A., García-Gabilondo, M., Grayston, A., Bugno, P., Kowalska, A., Duban-Deweer, S., Rizzi, E., Hachani, J., Sano, Y., Shimizu, F., Kanda, T., Mysiorek, C., Mazurek, M. P., Rosell, A., & Gosselet, F. (2021). Secretome of endothelial progenitor cells from stroke patients promotes endothelial barrier tightness and protects against hypoxia-induced vascular leakage. *Stem cell research & therapy*, *12*(1), 552. https://doi.org/10.1186/s13287-021-02608-y

Lutty, G. A., & McLeod, D. S. (2018). Development of the hyaloid, choroidal and retinal vasculatures in the fetal human eye. In *Progress in Retinal and Eye Research*. https://doi.org/10.1016/j.preteyeres.2017.10.001

Luyendyk, J. P., Schoenecker, J. G., & Flick, M. J. (2019). *The multifaceted role of fibrinogen in tissue injury and inflammation*. http://ashpublications.org/blood/article-pdf/133/6/511/1750532/blood818211.pdf

Mäe, M. A., He, L., Nordling, S., Vazquez-Liebanas, E., Nahar, K., Jung, B., Li, X., Tan, B. C., Chin Foo, J., Cazenave-Gassiot, A., Wenk, M. R., Zarb, Y., Lavina, B., Quaggin, S. E., Jeansson, M., Gu, C., Silver, D. L., Vanlandewijck, M., Butcher, E. C., … Betsholtz, C. (2021). Single-Cell Analysis of Blood-Brain Barrier Response to Pericyte Loss. *Circulation Research*, E46–E62. https://doi.org/10.1161/CIRCRESAHA.120.317473

Mansour, S. E., Browning, D. J., Wong, K., Flynn, H. W., & Bhavsar, A. R. (2020). The evolving treatment of diabetic retinopathy. In *Clinical Ophthalmology* (Vol. 14, pp. 653–678). Dove Medical Press Ltd. https://doi.org/10.2147/OPTH.S236637

Marcelo, K. L., Goldie, L. C., & Hirschi, K. K. (2013). Regulation of endothelial cell differentiation and specification. *Circulation Research*, *112*(9), 1272–1287. https://doi.org/10.1161/CIRCRESAHA.113.300506/FORMAT/EPUB

Martinez, J., Ferber, A., Bach, T. L., & Yaen, C. H. (2001). Interaction of fibrin with VE-cadherin. *Annals of the New York Academy of Sciences*, *936*, 386–405. https://doi.org/10.1111/j.1749-6632.2001.tb03524.x

Matafome, P., Sena, C., & Seiça, R. (2013). Methylglyoxal, obesity, and diabetes. In *Endocrine* (Vol. 43, Issue 3, pp. 472–484). Humana Press Inc. https://doi.org/10.1007/s12020-012-9795-8

Matter, K., & Balda, M. S. (1999). Occludin and the functions of tight junctions. *International Review of Cytology*, *186*, 117–146. https://doi.org/10.1016/S0074-7696(08)61052-9

Maurissen, T. L., Pavlou, G., Bichsel, C., Villaseñor, R., Kamm, R. D., & Ragelle, H. (2022). Microphysiological Neurovascular Barriers to Model the Inner Retinal Microvasculature. In *Journal of Personalized Medicine* (Vol. 12, Issue 2). MDPI. https://doi.org/10.3390/jpm12020148

Mayr, D., Preishuber-Pflügl, J., Koller, A., Brunner, S. M., Runge, C., Ladek, A. M., Rivera, F. J., Reitsamer, H. A., & Trost, A. (2022). Characterization of the Two Inducible Cre Recombinase-Based Mouse Models NG2-CreER™ and PDGFRb-P2A-CreER^{T2} for Pericyte Labeling in the Retina. *Current eye research*, *47*(4), 590–596. https://doi.org/10.1080/02713683.2021.2002910

McLeod, D. S., Hasegawa, T., Prow, T., Merges, C., & Lutty, G. (2006). The initial fetal human retinal vasculature develops by vasculogenesis. *Developmental Dynamics*, *235*(12), 3336–3347. https://doi.org/10.1002/dvdy.20988

Mi, X. S., Yuan, T. F., Ding, Y., Zhong, J. X., & So, K. F. (2014). Choosing preclinical study models of diabetic retinopathy: Key problems for consideration. In *Drug Design, Development and Therapy* (Vol. 8, pp. 2311–2319). Dove Medical Press Ltd. https://doi.org/10.2147/DDDT.S72797

Miesfeld, J. B., & Brown, N. L. (2019). Eye organogenesis: A hierarchical view of ocular development. In *Current Topics in Developmental Biology* (Vol. 132, pp. 351–393). Academic Press Inc. https://doi.org/10.1016/bs.ctdb.2018.12.008

Milne, R., & Brownstein, S. (2013). Advanced glycation end products and diabetic retinopathy. *Amino Acids*, *44*(6), 1397–1407. https://doi.org/10.1007/S00726-011-1071-3

Mulfaul, K., Giacalone, J. C., Voigt, A. P., Riker, M. J., Ochoa, D., Han, I. C., Stone, E. M., Mullins, R. F., & Tucker, B. A. (2020). Stepwise differentiation and functional characterization of human induced pluripotent stem cell-derived choroidal endothelial cells. *Stem cell research & therapy*, *11*(1), 409. https://doi.org/10.1186/s13287-020-01903-4

Namkoong, S., Kim, C. K., Cho, Y. L., Kim, J. H., Lee, H., Ha, K. S., Choe, J., Kim, P. H., Won, M. H., Kwon, Y. G., Shim, E. B., & Kim, Y. M. (2009). Forskolin increases angiogenesis through the coordinated cross-talk of PKA-dependent VEGF expression and Epac-mediated PI3K/Akt/eNOS signaling. *Cellular Signalling*, *21*(6), 906–915. https://doi.org/10.1016/J.CELLSIG.2009.01.038

Naylor, A., Hopkins, A., Hudson, N., & Campbell, M. (2020). Tight junctions of the outer blood retina barrier. In *International Journal of Molecular Sciences* (Vol. 21, Issue 1). MDPI AG. https://doi.org/10.3390/ijms21010211

Nwadozi, E., Rudnicki, M., & Haas, T. L. (2020). Metabolic Coordination of Pericyte Phenotypes: Therapeutic Implications. *Frontiers in Cell and Developmental Biology*, *8*, 77. https://doi.org/10.3389/FCELL.2020.00077/BIBTEX

O'Rahilly, R. (1975). The prenatal development of the human eye. *Experimental Eye Research*, *21*(2), 93–112. https://doi.org/10.1016/0014-4835(75)90075-5

Orlova, V. V., van den Hil, F. E., Petrus-Reurer, S., Drabsch, Y., Ten Dijke, P., & Mummery, C. L. (2014). Generation, expansion and functional analysis of endothelial cells and pericytes derived from human pluripotent stem cells. *Nature protocols*, *9*(6), 1514–1531. https://doi.org/10.1038/nprot.2014.102

Ou, K., Mertsch, S., Theodoropoulou, S., Wu, J., Liu, J., Copland, D. A., Schrader, S., Liu, L., & Dick, A. D. (2019). Restoring retinal neurovascular health via substance P. *Experimental Cell Research*, *380*(2), 115–123. https://doi.org/10.1016/j.yexcr.2019.04.008

Paisley, C. E., & Kay, J. N. (2021). Seeing stars: Development and function of retinal astrocytes. *Developmental biology*, *478*, 144-154.

Pandit, T., Jidigam, V. K., Patthey, C., & Gunhaga, L. (2015). Neural retina identity is specified by lens-derived BMP signals. *Development*, *142*(10), 1850–1859. https://doi.org/10.1242/DEV.123653

Park, D. Y., Lee, J., Kim, J., Kim, K., Hong, S., Han, S., Kubota, Y., Augustin, H. G., Ding, L., Kim, J. W., Kim, H., He, Y., Adams, R. H., & Koh, G. Y. (2017). Plastic roles of pericytes in the blood-retinal barrier. *Nature Communications*, *8*. https://doi.org/10.1038/NCOMMS15296

Park, Y. K., Tu, T.-Y., Lim, S. H., Clement, I. J. M., Yang, Y., & Kamm, R. D. (2014). In Vitro Microvessel Growth and Remodeling within a Three-dimensional Microfluidic Environment. *Cell Mol Bioeng*, *7*(1), 15–25. https://doi.org/10.1007/s12195-013-0315-6

Pars, S., Achberger, K., Kleger, A., Liebau, S., & Pashkovskaia, N. (2021). Generation of functional vascular endothelial cells and pericytes from keratinocyte derived human induced pluripotent stem cells. *Cells*, *10*(1), 1–13. https://doi.org/10.3390/cells10010074

Patsch, C., Challet-Meylan, L., Thoma, E. C., Urich, E., Heckel, T., O'Sullivan, J. F., Grainger, S. J., Kapp, F. G., Sun, L., Christensen, K., Xia, Y., Florido, M. H., He, W., Pan, W., Prummer, M., Warren, C. R., Jakob-Roetne, R., Certa, U., Jagasia, R., Freskgård, P. O., … Cowan, C. A. (2015). Generation of vascular endothelial and smooth muscle cells from human pluripotent stem cells. *Nature cell biology*, *17*(8), 994–1003. https://doi.org/10.1038/ncb3205

Peppiatt, C. M., Howarth, C., Mobbs, P., & Attwell, D. (2006). Bidirectional control of CNS capillary diameter by pericytes. *Nature*, *443*(7112), 700–704. https://doi.org/10.1038/nature05193

Pfister, F., Przybyt, E., Harmsen, M. C., & Hammes, H. P. (2013). Pericytes in the eye. In *Pflugers Archiv European Journal of Physiology* (Vol. 465, Issue 6, pp. 789–796). https://doi.org/10.1007/s00424-013-1272-6

Ragelle, H., Dernick, K., Khemais, S., Keppler, C., Cousin, L., Farouz, Y., Louche, C., Fauser, S., Kustermann, S., Tibbitt, M. W., & Westenskow, P. D. (2020). Human Retinal Microvasculature-on-a-Chip for Drug Discovery. *Advanced Healthcare Materials*, *9*(21). https://doi.org/10.1002/adhm.202001531

Ramachandra Bhat, L., Vedantham, S., Krishnan, U. M., & Rayappan, J. B. B. (2019). Methylglyoxal – An emerging biomarker for diabetes mellitus diagnosis and its detection methods. *Biosensors and Bioelectronics*, *133*, 107–124. https://doi.org/10.1016/J.BIOS.2019.03.010

Rangasamy, S., Monickaraj, F., Legendre, C., Cabrera, A. P., Llaci, L., Bilagody, C., McGuire, P., & Das, A. (2020). Transcriptomics analysis of pericytes from retinas of diabetic animals reveals novel genes and molecular pathways relevant to blood-retinal barrier alterations in diabetic retinopathy. *Experimental eye research*, *195*, 108043. https://doi.org/10.1016/j.exer.2020.108043

Reichenbach, A., & Bringmann, A. (2020). Glia of the human retina. *Glia*, *68*(4), 768–796. https://doi.org/10.1002/glia.23727

Roberts, A. C., & Porter, K. E. (2013). Cellular and molecular mechanisms of endothelial dysfunction in diabetes. *Diabetes & vascular disease research*, *10*(6), 472–482. https://doi.org/10.1177/1479164113500680

Roy, S., & Kim, D. (2021). Retinal capillary basement membrane thickening: Role in the pathogenesis of diabetic retinopathy. *Progress in retinal and eye research*, *82*, 100903. https://doi.org/10.1016/j.preteyeres.2020.100903

Runkle, E. A., & Antonetti, D. A. (2011). The blood-retinal barrier: structure and functional significance. In *Methods in molecular biology (Clifton, N.J.)* (Vol. 686, pp. 133–148). https://doi.org/10.1007/978-1-60761-938-3_5

Russ, P. K., Davidson, M. K., Hoffman, L. H., & Haselton, F. R. (1998). Partial characterization of the human retinal endothelial cell tight and adherens junction complexes. *Investigative ophthalmology & visual science*, *39*(12), 2479–2485.

Sahni, A., Sporn, L. A., & Francis, C. W. (1999). Potentiation of endothelial cell proliferation by fibrin(ogen)-bound fibroblast growth factor-2. *The Journal of biological chemistry*, *274*(21), 14936–14941. https://doi.org/10.1074/jbc.274.21.14936

Saint-Geniez, M., Kurihara, T., Sekiyama, E., Maldonado, A. E., & D'Amore, P. A. (2009). An essential role for RPE-derived soluble VEGF in the maintenance of the choriocapillaris. *Proceedings of the National Academy of Sciences of the United States of America*, *106*(44), 18751–18756. https://doi.org/10.1073/PNAS.0905010106

Saker, S., Stewart, E. A., Browning, A. C., Allen, C. L., & Amoaku, W. M. (2014). The effect of hyperglycaemia on permeability and the expression of junctional complex molecules in human retinal and choroidal endothelial cells. *Experimental Eye Research*, *121*, 161–167. https://doi.org/10.1016/J.EXER.2014.02.016

Santos, G. S. P., Prazeres, P. H. D. M., Mintz, A., & Birbrair, A. (2018). Role of pericytes in the retina. In *Eye (Basingstoke)* (Vol. 32, Issue 3, pp. 483–486). Nature Publishing Group. https://doi.org/10.1038/eye.2017.220

Sato, Y., & Rifkin, D. B. (1989). Inhibition of endothelial cell movement by pericytes and smooth muscle cells: activation of a latent transforming growth factor-beta 1-like molecule by plasmin during co-culture. *The Journal of cell biology*, *109*(1), 309–315. https://doi.org/10.1083/jcb.109.1.309

Scanlon P. H. (2017). The English National Screening Programme for diabetic retinopathy 2003-2016. *Acta diabetologica*, *54*(6), 515–525. https://doi.org/10.1007/s00592-017-0974-1
Scanlon, P. H. (2015). Diabetic retinopathy. In *Medicine (United Kingdom)* (Vol. 43, Issue 1, pp. 13–19). Elsevier Ltd. https://doi.org/10.1016/j.mpmed.2014.10.009

Schalkwijk, C. G., & Stehouwer, C. D. A. (2020). Methylglyoxal, a highly reactive dicarbonyl compound, in diabetes, its vascular complications, and other age-related diseases. *Physiological Reviews*, *100*(1), 407–461.

https://doi.org/10.1152/PHYSREV.00001.2019/ASSET/IMAGES/LARGE/Z9J0012029260011.JPEG

Schisano, B., Tripathi, G., McGee, K., McTernan, P. G., & Ceriello, A. (2011). Glucose oscillations, more than constant high glucose, induce p53 activation and a metabolic memory in human endothelial cells. *Diabetologia*, *54*(5), 1219–1226. https://doi.org/10.1007/s00125-011-2049-0

Schlotterer, A., Kolibabka, M., Lin, J., Acunman, K., Dietrichá, N., Sticht, C., Fleming, T., Nawroth, P., & Hammes, H. P. (2019). Methylglyoxal induces retinopathy-type lesions in the absence of hyperglycemia: studies in a rat model. *FASEB Journal*, *33*(3), 4141–4153. https://doi.org/10.1096/FJ.201801146RR

Sefton, A. J., Dreher, B., & Harvey, A. (2004). Visual System. *The Rat Nervous System*, 1083–1165. https://doi.org/10.1016/B978-012547638-6/50033-X

Selvam, S., Kumar, T., & Fruttiger, M. (2018). Retinal vasculature development in health and disease. *Progress in retinal and eye research*, *63*, 1–19. https://doi.org/10.1016/j.preteyeres.2017.11.001

Sernagor, E., Eglen, S. J., & Wong, R. O. L. (2001). Development of Retinal Ganglion Cell Structure and Function. *Progress in Retinal and Eye Research*, *20*(2), 139–174. https://doi.org/10.1016/S1350-9462(00)00024-0

Shamsaldeen, Y. A., Mackenzie, L. S., Lione, L. A., & Benham, C. D. (2016). Send Orders for Reprints to reprints@benthamscience.ae Methylglyoxal, A Metabolite Increased in Diabetes is Associated with Insulin Resistance, Vascular Dysfunction and Neuropathies. In *Current Drug Metabolism* (Vol. 17).

Shimizu, F., Sano, Y., Tominaga, O., Maeda, T., Abe, M. aki, & Kanda, T. (2013). Advanced glycation end-products disrupt the blood-brain barrier by stimulating the release of transforming growth factor-β by pericytes and vascular endothelial growth factor and matrix metalloproteinase-2 by endothelial cells in vitro. *Neurobiology of Aging*, *34*(7), 1902–1912. https://doi.org/10.1016/j.neurobiolaging.2013.01.012

Siemerink, M. J., Klaassen, I., Vogels, I. M., Griffioen, A. W., Van Noorden, C. J., & Schlingemann, R. O. (2012). CD34 marks angiogenic tip cells in human vascular endothelial cell cultures. *Angiogenesis*, *15*(1), 151–163. https://doi.org/10.1007/s10456-011-9251-z
Singh Jaggi, A., Parkash Singh, V., Bali, A., & Singh, N. (2014). Advanced Glycation End Products and Diabetic Complications. *Korean J Physiol Pharmacol*, *18*, 1–14. https://doi.org/10.4196/kjpp.2014.18.1.1

Sinn, R., & Wittbrodt, J. (2013). An eye on eye development. *Mechanisms of Development*, *130*(6–8), 347–358. https://doi.org/10.1016/J.MOD.2013.05.001

Smit-McBride, Z., Nguyen, A. T., Yu, A. K., Modjtahedi, S. P., Hunter, A. A., Rashid, S., Moisseiev, E., & Morse, L. S. (2020). Unique molecular signatures of microRNAs in ocular fluids

and plasma in diabetic retinopathy. *PLOS ONE*, *15*(7), e0235541. https://doi.org/10.1371/JOURNAL.PONE.0235541

Smyth, L. C. D., Rustenhoven, J., Scotter, E. L., Schweder, P., Faull, R. L. M., Park, T. I. H., & Dragunow, M. (2018). Markers for human brain pericytes and smooth muscle cells. *Journal of Chemical Neuroanatomy*, *92*, 48–60. https://doi.org/10.1016/j.jchemneu.2018.06.001

Spuul, P., Daubon, T., Pitter, B., Alonso, F., Fremaux, I., Kramer, I., Montanez, E., & Génot, E. (2016). VEGF-A/Notch-Induced Podosomes Proteolyse Basement Membrane Collagen-IV during Retinal Sprouting Angiogenesis. *Cell reports*, *17*(2), 484–500. https://doi.org/10.1016/j.celrep.2016.09.016

Stebbins, M. J., Gastfriend, B. D., Canfield, S. G., Lee, M. S., Richards, D., Faubion, M. G., Li, W. J., Daneman, R., Palecek, S. P., & Shusta, E. V. (2019). Human pluripotent stem cell-derived brain pericyte-like cells induce blood-brain barrier properties. *Science advances*, *5*(3), eaau7375. https://doi.org/10.1126/sciadv.aau7375

Stone, J. (1988). Chapter 1 The origins of the cells of vertebrate retina. *Progress in Retinal Research*, *7*, 1–19. https://doi.org/10.1016/0278-4327(88)90003-X

Swistowski, A., Peng, J., Liu, Q., Mali, P., Rao, M. S., Cheng, L., & Zeng, X. (2010). Efficient generation of functional dopaminergic neurons from human induced pluripotent stem cells under defined conditions. *Stem cells (Dayton, Ohio)*, *28*(10), 1893–1904. https://doi.org/10.1002/stem.499

Szymborska, A., & Gerhardt, H. (2018). Hold me, but not too tight—endothelial cell–cell junctions in angiogenesis. *Cold Spring Harbor Perspectives in Biology*, *10*(8). https://doi.org/10.1101/cshperspect.a029223

Takahashi, K., & Yamanaka, S. (2006). Induction of pluripotent stem cells from mouse embryonic and adult fibroblast cultures by defined factors. *Cell*, *126*(4), 663–676. https://doi.org/10.1016/j.cell.2006.07.024

Takahashi, K., Tanabe, K., Ohnuki, M., Narita, M., Ichisaka, T., Tomoda, K., & Yamanaka, S. (2007). Induction of Pluripotent Stem Cells from Adult Human Fibroblasts by Defined Factors. *Cell*, *131*(5), 861–872. https://doi.org/10.1016/j.cell.2007.11.019

Tao, C., & Zhang, X. (2014). Development of astrocytes in the vertebrate eye. In *Developmental Dynamics* (Vol. 243, Issue 12, pp. 1501–1510). John Wiley and Sons Inc. https://doi.org/10.1002/dvdy.24190

Thoreson, W. B., & Mangel, S. C. (2012). Lateral interactions in the outer retina. *Progress in Retinal and Eye Research*, *31*(5), 407–441. https://doi.org/10.1016/J.PRETEYERES.2012.04.003

Tóth, A. E., Walter, F. R., Bocsik, A., Sántha, P., Veszelka, S., Nagy, L., Puskás, L. G., Couraud, P. O., Takata, F., Dohgu, S., Kataoka, Y., & Deli, M. A. (2014). Edaravone protects against

methylglyoxal-induced barrier damage in human brain endothelial cells. *PLoS ONE*, *9*(7). https://doi.org/10.1371/journal.pone.0100152

Tout, S., Chan-Ling, T., Holländer, H., & Stone, J. (1993). The role of Müller cells in the formation of the blood-retinal barrier. *Neuroscience*, *55*(1), 291–301. https://doi.org/10.1016/0306-4522(93)90473-s

Trost, A., Lange, S., Schroedl, F., Bruckner, D., Motloch, K. A., Bogner, B., Kaser-Eichberger, A., Strohmaier, C., Runge, C., Aigner, L., Rivera, F. J., & Reitsamer, H. A. (2016). Brain and retinal pericytes: Origin, function and role. In *Frontiers in Cellular Neuroscience* (Vol. 10, Issue FEB). Frontiers Media S.A. https://doi.org/10.3389/fncel.2016.00020

Trost, A., Schroedl, F., Lange, S., Rivera, F. J., Tempfer, H., Korntner, S., Stolt, C. C., Wegner, M., Bogner, B., Kaser-Eichberger, A., Krefft, K., Runge, C., Aigner, L., & Reitsamer, H. A. (2013). Neural Crest Origin of Retinal and Choroidal Pericytes. *Investigative Ophthalmology & Visual Science*, *54*(13), 7910–7921. https://doi.org/10.1167/IOVS.13-12946

van Geest, R. J., Klaassen, I., Vogels, I. M. C., van Noorden, C. J. F., & Schlingemann, R. O. (2010). Differential TGF-β Signaling in Retinal Vascular Cells: A Role in Diabetic Retinopathy? *Investigative Ophthalmology & Visual Science*, *51*(4), 1857–1865. https://doi.org/10.1167/IOVS.09-4181

Vatine, G. D., Barrile, R., Workman, M. J., Sances, S., Barriga, B. K., Rahnama, M., Barthakur, S., Kasendra, M., Lucchesi, C., Kerns, J., Wen, N., Spivia, W. R., Chen, Z., Van Eyk, J., & Svendsen, C. N. (2019). Human iPSC-Derived Blood-Brain Barrier Chips Enable Disease Modeling and Personalized Medicine Applications. *Cell stem cell*, *24*(6), 995–1005.e6. https://doi.org/10.1016/j.stem.2019.05.011

Vinores, S. A. (2010). Breakdown of the Blood–Retinal Barrier. *Encyclopedia of the Eye*, 216–222. https://doi.org/10.1016/B978-0-12-374203-2.00137-8

Wakisaka, M., Yoshinari, M., Yamamoto, M., Nakamura, S., Asano, T., Himeno, T., Ichikawa, K., Doi, Y., & Fujishima, M. (1997). Na+-dependent glucose uptake and collagen synthesis by cultured bovine retinal pericytes. *Biochimica et biophysica acta*, *1362*(1), 87–96. https://doi.org/10.1016/s0925-4439(97)00071-9

Wang, K., Lin, R. Z., & Melero-Martin, J. M. (2019). Bioengineering human vascular networks: trends and directions in endothelial and perivascular cell sources. *Cellular and molecular life sciences : CMLS*, *76*(3), 421–439. https://doi.org/10.1007/s00018-018-2939-0

Wang, Z., Liu, C. H., Huang, S., Fu, Z., Tomita, Y., Britton, W. R., Cho, S. S., Chen, C. T., Sun, Y., Ma, J. X., He, X., & Chen, J. (2020). Wnt signaling activates MFSD2A to suppress vascular endothelial transcytosis and maintain blood-retinal barrier. *Science Advances*, *6*(35), 7457–7485. https://doi.org/10.1126/SCIADV.ABA7457/SUPPL_FILE/ABA7457_SM.PDF

Watson, E. C., Koenig, M. N., Grant, Z. L., Whitehead, L., Trounson, E., Dewson, G., & Coultas, L. (2016). Apoptosis regulates endothelial cell number and capillary vessel diameter but not

vessel regression during retinal angiogenesis. *Development (Cambridge, England)*, *143*(16), 2973–2982. https://doi.org/10.1242/dev.137513

Whitehead, M., Osborne, A., Widdowson, P. S., Yu-Wai-Man, P., & Martin, K. R. (2019). Angiopoietins in Diabetic Retinopathy: Current Understanding and Therapeutic Potential. *Journal of Diabetes Research*. https://doi.org/10.1155/2019/5140521

Wimmer, R. A., Leopoldi, A., Aichinger, M., Kerjaschki, D., & Penninger, J. M. (2019). Generation of blood vessel organoids from human pluripotent stem cells. *Nature Protocols*, *14*(11), 3082–3100. https://doi.org/10.1038/s41596-019-0213-z

Xiang, D. N., Feng, Y. F., Wang, J., Zhang, X., Shen, J. J., Zou, R., & Yuan, Y. Z. (2019). Platelet-derived growth factor-BB promotes proliferation and migration of retinal microvascular pericytes by up-regulating the expression of C-X-C chemokine receptor types 4. *Experimental and therapeutic medicine*, *18*(5), 4022–4030. https://doi.org/10.3892/etm.2019.8016

Yang, A. H. , & Huang, W. (2012). Retinal Vein Occlusion Induced by a MEK Inhibitor - Impact of Oxidative Stress on the Blood-Retinal Barrier. In V. I. Lushchak, & D. V. Gospodaryov (Eds.), Oxidative Stress and Diseases. IntechOpen. https://doi.org/10.5772/36114

Yang, X., Yu, X. W., Zhang, D. D., & Fan, Z. G. (2020). Blood-retinal barrier as a converging pivot in understanding the initiation and development of retinal diseases. *Chinese Medical Journal*, *133*(21), 2586–2594. https://doi.org/10.1097/CM9.0000000000001015

Yao, Y., Du, J., Li, R., Zhao, L., Luo, N., Zhai, J. Y., & Long, L. (2019). Association between ICAM-1 level and diabetic retinopathy: a review and meta-analysis. *Postgraduate Medical Journal*, *95*(1121), 162-168.

Yemanyi, F., Bora, K., Blomfield, A. K., Wang, Z., Chen, J., Yemanyi, F. ;, Bora, K. ;, Blomfield, A. K. ;, Wang, Z. ;, & Chen, J. (2021). Wnt Signaling in Inner Blood–Retinal Barrier Maintenance. *International Journal of Molecular Sciences 2021, Vol. 22, Page 11877*, *22*(21), 11877. https://doi.org/10.3390/IJMS222111877

Yoo, H. S., Shanmugalingam, U., & Smith, P. D. (2021). Harnessing Astrocytes and Müller Glial Cells in the Retina for Survival and Regeneration of Retinal Ganglion Cells. *Cells*, *10*(6), 1339. https://doi.org/10.3390/cells10061339

Zhang, S., Wan, Z., & Kamm, R. D. (2021). Vascularized organoids on a chip: strategies for engineering organoids with functional vasculature. *Lab on a Chip*, *21*(3), 473–488. https://doi.org/10.1039/D0LC01186J

Zhao, Z., Nelson, A. R., Betsholtz, C., & Zlokovic, B. v. (2015). Establishment and Dysfunction of the Blood-Brain Barrier. *Cell*, *163*(5), 1064–1078. https://doi.org/10.1016/J.CELL.2015.10.067

Zheng, Y., Zhang, Y., Barutello, G., Chiu, K., Arigoni, M., Giampietro, C., Cavallo, F., & Holmgren, L. (2016). Angiomotin like-1 is a novel component of the N-cadherin complex

affecting endothelial/pericyte interaction in normal and tumor angiogenesis. *Scientific Reports 2016 6:1*, *6*(1), 1–11. https://doi.org/10.1038/srep30622

Zhong, X., Gutierrez, C., Xue, T., Hampton, C., Vergara, M. N., Cao, L. H., Peters, A., Park, T. S., Zambidis, E. T., Meyer, J. S., Gamm, D. M., Yau, K. W., & Canto-Soler, M. V. (2014). Generation of three-dimensional retinal tissue with functional photoreceptors from human iPSCs. *Nature Communications*. https://doi.org/10.1038/ncomms5047

Statement of contributions

Generation of Functional Vascular Endothelial Cells and Pericytes from Keratinocyte Derived Human Induced Pluripotent Stem Cells

Pars, S., Achberger, K., Kleger, A., Liebau, S., & Pashkovskaia, N. (2021). Generation of Functional Vascular Endothelial Cells and Pericytes from Keratinocyte Derived Human Induced Pluripotent Stem Cells. *Cells*, *10*(1), 74. https://doi.org/10.3390/cells10010074

In this article, a methodology to generate and characterize functional hiPSC-derived endothelial cells and pericytes have been developed. My contribution to this work was the investigation, experimental design, and writing. Endothelial cell and pericyte generation and characterization methodology that is explained in section 3.1.1 and 3.1.2 of this thesis were adapted from this article. Two figures (Fig. 12 and Fig. 16) in the section 3.1 were adapted from Figure 3 and Figure S2 of the aforementioned article, respectively. Regarding Fig. 12, flow cytometry data collection was carried out by FACS Core Facility, FCF Berg (University of Tübingen). Regarding Fig. 16, western blot experiment was done by me and Natalia Pashkovskaia. Except for that, all cell culture experiments and all immunocytochemical stainings in the aforementioned article were carried out by me. Fluorescence image acquisition was done by me and Natalia Pashkovskaia.